# HYDROPHILIC COATINGS OVER $Fe^{3+}$-CARBOXYMETHYL TARA GUM HYDROGEL MICROPARTICLES FOR SUSTAINED DISSOLUTION OF A WATER SOLUBLE DRUG IN GASTROINTESTINAL MILIEU

THESIS SUBMITTED IN THE PARTIAL FULFILLMENT OF THE REQUIREMENTS FOR THE DEGREE OF MASTER OF PHARMACY

IN THE

FACULTY OF ENGINEERING AND TECHNOLOGY

JADAVPUR UNIVERSITY

By

**Pallabita Rakshit**

M. PHARM.

CLASS ROLL NO.: 002211402034

EXAM ROLL NO.: M4PHL24008

REG. NO.: 163676 of 2022-2023

UNDER THE GUIDANCE OF

**Mr. Kaushik Mukherjee**

Division of Pharmaceutics

Department of Pharmaceutical Technology

Faculty of Engineering and Technology

Jadavpur University

Kolkata-700032

2024

DEPARTMENT OF PHARMACEUTICAL TECHNOLOGY

FACULTY OF ENGINEERING AND TECHNOLOGY

JADAVPUR UNIVERSITY

KOLKATA-700032

# CERTIFICATE

This is to certify that **PALLABITA RAKSHIT** (Class Roll No.: 0022211402034, Exam Roll No.: M4PHL24008 and Reg. No.: 163676 of 2022-2023), has carried out the research work on the subject entitled "*HYDROPHILIC COATINGS OVER $Fe^{3+}$-CARBOXYMETHYL TARA GUM HYDROGEL MICROPARTICLES FOR SUSTAINED DISSOLUTION OF A WATER SOLUBLE DRUG IN GASTROINTESTINAL MILIEU*" under my supervision in the Pharmaceutics Research Laboratory in the Department of Pharmaceutical Technology of this university. She has incorporated her findings into this thesis of the same title, being submitted by her, in partial fulfilment of the requirements for the degree of Master of Pharmacy of Jadavpur University. She has carried out this research work independently and with proper care and attention to my entire satisfaction.

Kaushik Mukherjee

Assistant Professor
Dept. of Pharmaceutical Technology
Jadavpur University
Kolkata - 700 032, W.B. India

**Mr. Kaushik Mukherjee**
Assistant Professor
Department of Pharmaceutical Technology
Jadavpur University
Kolkata-700 032

27/8/24

**Prof. (Dr.) Amalesh Samanta**
Head of the Department Technology
Department of Pharmaceutical Technology
Jadavpur University
Kolkata-700 032

Prof. Amalesh Samanta, Ph.D.
Head
Dept. of Pharmaceutical Technology
Jadavpur University, Kolkata, India

Dipak Laha 27.8.24

**Prof. Dipak Laha**
Dean,
Faculty of Engineering and Technology
Jadavpur University
Kolkata-700 032

DEAN
Faculty of Engineering & Technology
JADAVPUR UNIVERSITY
KOLKATA-700 032

# DECLARATION OF ORIGINALITY AND COMPLIANCE OF ACADEMIC ETHICS

I hereby declare that this thesis contains literature survey and original research work by the undersigned candidate, as part of her Master of Pharmaceutical Technology studies. All information in this document have been obtained and presented in accordance with academic rules and ethical conduct. I also declare that as required by these rules and conduct, I have fully cited and referenced all materials and results that are not original to this work.

Name: PALLABITA RAKSHIT

Class Roll No.: 002211402034

Exam Roll No.: M4PHL24008

Registration No.: 163676 of 2022-2023

Thesis title: HYDROPHILIC COATINGS OVER $Fe^{3+}$-CARBOXYMETHYL TARA GUM HYDROGEL MICROPARTICLES FOR SUSTAINED DISSOLUTION OF A WATER SOLUBLE DRUG IN GASTROINTESTINAL MILIEU.

Pallabita Rakshit 27.08.24.

Signature with date

# ACKNOWLEDGEMENT

I deem it a pleasure and privilege to work under the guidance of ***Mr. Kaushik Mukherjee, Assistant Professor, Department of Pharmaceutical Technology, Jadavpur University.*** I express my deep gratitude and regards to my revered mentor for suggesting the subject of this thesis and rendering me his thoughtful suggestions and rational approaches to this thesis work. I am greatly indebted to Mr. Kaushik Mukherjee for his valuable guidance throughout the work that enabled me to complete the work.

I am thankful to the authority of Jadavpur University and Head of the Department, ***Prof. (Dr.) Amalesh Samanta*** for providing all the facilities to carry out this work.

I offer humble gratitude to ***Dr. Tapan Kumar Giri***, (Associate Professor, Department of Pharmaceutical Technology, Jadavpur University) for the support and kindness rendered on me throughout the course of my work.

With a deep sense of thankfulness and sincerity, I acknowledge the continuous encouragement, perpetual assistance and cooperation from my seniors ***Pallabi Dutta***, ***Ankita Dhar and Saban Karmakar***. Their constant support and helpful suggestions have helped me to accomplish this work in time. I am indeed glad to convey cordial thanks to all my labmates ***Riya Hazra, Md Sahil Shanawaz Alam,*** and ***Angita Malakar*** for their continuous help.

I want to thank my parents, ***Mr. Pradipta Rakshit*** and ***Mrs. Pamela Rakshit*** for their constant support, encouragement, and love and their belief in my abilities have been the foundation of my academic journey.

Finally a word of thanks to all those people associated with this work directly or indirectly whose names I have been unable to mention here.

Place: Department of Pharmaceutical Technology, Jadavpur University

Date: 27.08.24

Pallabita Rakshit

**PALLABITA RAKSHIT**

Class Roll No.: 002211402034

Exam Roll No.: M4PHL24008

Registration No.: 163676 of 2022-2023

Department of Pharmaceutical Technology, Jadavpur University

# CONTENTS

# Chapter 1

# INTRODUCTION

# 1. INTRODUCTION

## 1.1. Oral drug delivery:

Oral medications are the most common way to deliver drugs because they offer several benefits, including ease of administration, patient preference, cost-efficiency, and straightforward mass production of oral drug forms. Approximately 60% of approved small-molecule medications are taken orally and about 90% of all pharmaceutical products designed for human use are oral formulations [1]. Patients tend to be more compliant with oral medications compared to other routes like intravenous, subcutaneous, or intramuscular injections, and even compared to inhaled treatments for asthma. Oral drug delivery system offers several benefits, including the ability for self-medication, non-invasive treatment, and ease of administration, which contribute to high patient compliance. Nearly 50% of marketed drugs are administered orally. Oral dosage forms are typically categorised into two main categories based on their physical state: solid forms like powders, tablets, capsules, and liquid forms like solutions, syrups, suspensions and emulsions [2].

## 1.2. Conventional drug delivery system:

Conventional drug delivery systems are the traditional methods for administering medications to patients, utilized widely for centuries. Their primary goal is to achieve therapeutic levels by releasing the drug in a predictable manner. These systems typically release the drug immediately after administration and follow a predictable pharmacokinetic profile (Fig.1.1). The main upsides of this type of drug delivery system include ease of administration, cost-effectiveness, and well-established processes.

### 1.2.1. Disadvantages of the conventional oral dosage form:

Medications with short half-lives must be taken more frequently, increasing the likelihood of missed doses and diminishing patient adherence. The usual peak-and-valley pattern of plasma concentration over time complicates achieving a stable, steady-state condition. The disadvantages of the conventional oral dosage form including [3]:

- Inevitable fluctuations in drug concentration can result in either underdosing or overdosing, as Css (steady-state concentration) values deviate from the desired therapeutic range.
- Drugs having low aqueous solubility in GIT leads to accumulation of the drug.

- Fluctuating drug levels may precipitate adverse effects, particularly in medications with narrow therapeutic indices, whenever overdosing occurs.

To overcome the problem as mentioned above, nowadays conventional dosage forms are rapidly being substituted by novel sustained-release drug delivery systems (SRDDS).

### 1.3. Sustained release drug delivery system:

Sustained-release dosage forms are drug delivery systems intended to provide a sustained therapeutic effect by continuously releasing drugs over an extended period after administrating a single dose (Fig.1.1). The goal is to maintain a steady-state blood level that is therapeutically beneficial and non-toxic for a prolonged duration. Designing the proper dosage form is crucial for achieving and maintaining this goal. Utmost drug bioavailability can be attained by optimizing the rate and extent of drug absorption. Sustained-release dosage forms are taken into consideration as the best method to optimize medication delivery, achieving better control of the therapeutic effect and reducing in vivo fluctuations of drug concentration [4].

#### 1.3.1 Advantages of SRDDS:

SRDDS bears advantages over the conventional dosage forms including [5,6].

- The development of SRDDS aims to decrease dosing frequency, ensuring consistent availability of medication at the treatment site over time, thereby enhancing the therapeutic efficacy of the drug.
- SRDDS reduces the treatment expenses, by minimising the dosing frequency.
- SRDDS can reduce the risk of toxicity that can occur from overdosing with traditional dosing methods.
- This approach can also extend the activity of medications that typically have a short half-life, allowing for longer-lasting effects and potentially improving therapeutic outcomes.

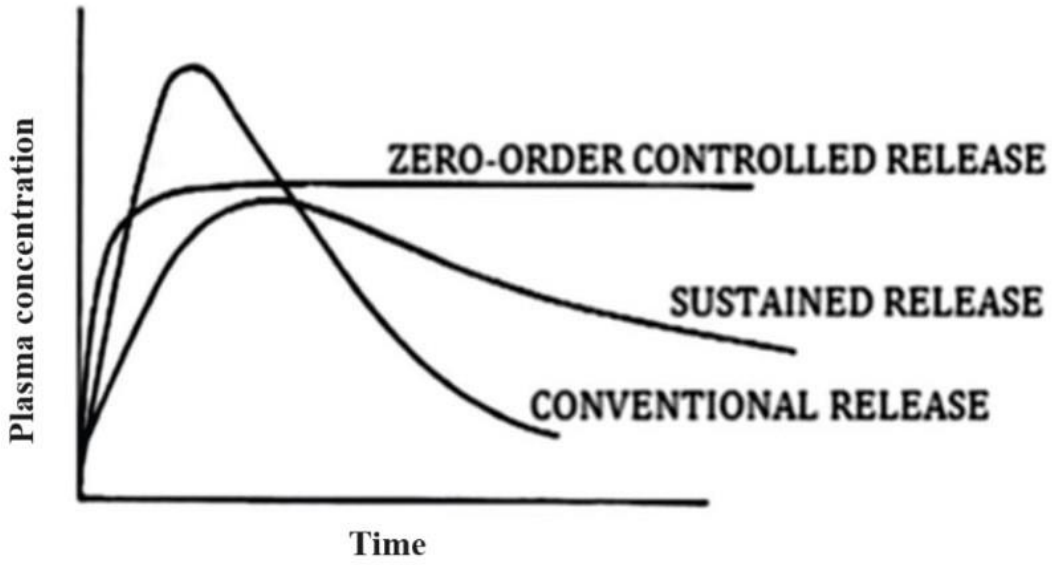


Fig.1.1. Comparative drug plasma level profiles resulting from the administration of conventional, controlled, and sustained-release dosage forms. Conventional dosage forms produce a single, transient burst of the drug. The therapeutic effect lasts as long as the concentration of drugs stays above the minimum effective level.

**1. 3.2 Rationality behind SRDDS:**

The primary purpose of SRDDS (Fig.1.2) is to extend the duration of the drug's action, minimize plasma level fluctuations, improve drug utilization, reduce adverse effects, decrease dosing frequency, and provide uniform drug delivery. These forms achieve their effects by altering the pharmacodynamics and pharmacokinetics of active drug compounds using novel delivery systems or by modifying the molecular structure and physiological parameters of the drug administration route. Sustained drug delivery takes place when a polymer is mixed with a drug or active agent, designed to control the release rate from the material. This release can be predetermined using film-forming polymers and enteric coatings, depending on the application. The terms "controlled release" and "sustained release" are often used interchangeably but represent different processes. Sustained release involves any dosage form that delivers medication over an extended period, providing therapeutic control that can be spatial, temporal, or both. While sustained release systems typically do not achieve zero-order release, they aim to approximate it by delivering the drug in a slow, first-order manner [7,8].

Sustained release drug administration is vital for enhanced treatment, reduced side effects, and patient convenience. It maintains steady drug blood levels, minimizing fluctuations and reducing the need for frequent dosing. These devices often use hydrophilic and lipophilic matrix systems, combining diffusion and erosion processes. Common materials include biocompatible polymers, waxes, and hydrophobic or hydrophilic excipients [9].

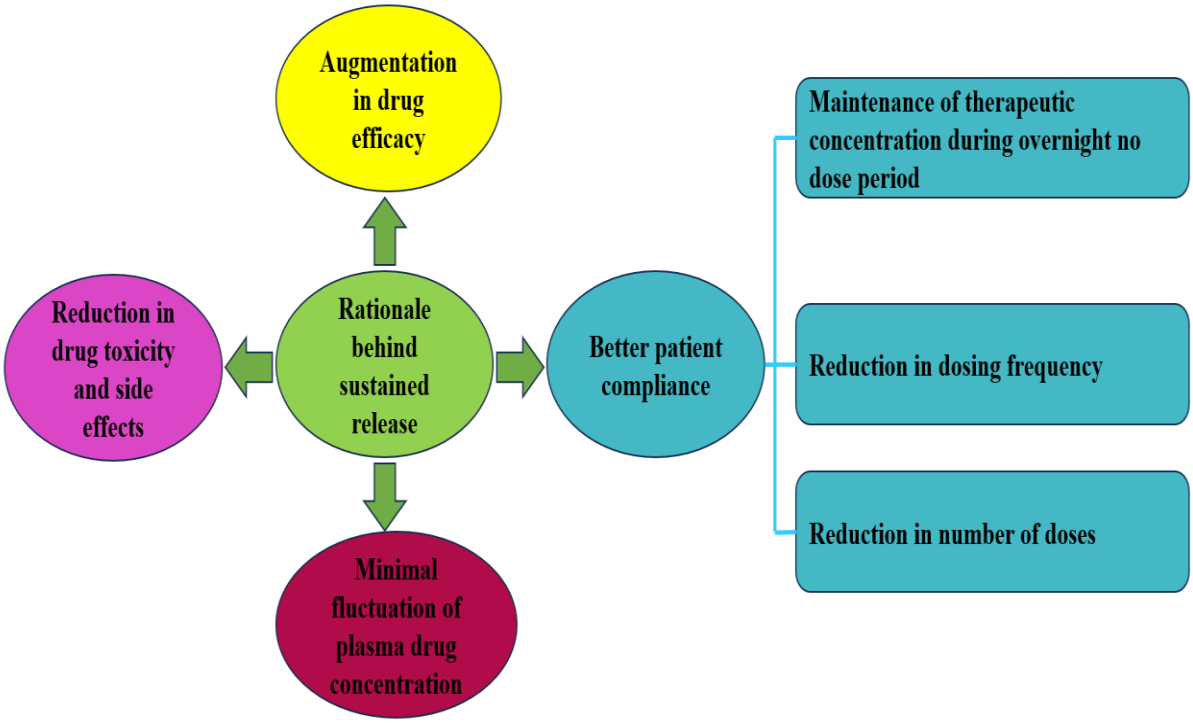


Fig. 1.2. Rationality behind sustained release dosage form.

### 1.4. Hydrogel as SRDDS:

Hydrogels are three-dimensional, hydrophilic polymer networks capable of holding large volumes of water without dissolving. They exhibit rubbery and soft characteristics when swollen, and widely used in biomedical applications such as drug delivery, contact lenses, and tissue expanders due to their mechanical strength and biocompatibility. Hydrogels have found extensive use in drug delivery, providing controlled release of medications. Hydrogels can be chemically, physically, or enzymatically cross-linked. Recently, natural gum-based hydrogels, like those made from chitosan, alginate, gellan gum, and pectin, have gained attention for drug delivery applications due to their biodegradability, biocompatibility, cost effective, and ease of production [10].

### 1.4.1 Natural Hydrogel:

Natural hydrogels are prized for their biocompatibility, biodegradability, low cytotoxicity, and support for cell adhesion and proliferation, making them suitable for biomedical applications. Common natural polymers include collagen, alginate (ALG), hyaluronic acid (HA), and though they often lack strong mechanical properties. These polymers fall into three categories: polysaccharides (e.g., HA, chitosan, ALG), proteins (e.g., collagen, silk, gelatin,), and DNA. Hydrogels are extensively researched for drug delivery, regenerative medicine, wound healing, and tissue engineering. Drug functionalization methods include mixing with reagents before forming the hydrogel or post-loading onto dry hydrogels. Various hydrogel systems have enhanced drug efficacy and reduced cytotoxicity in treating diseases [11].

### 1.4.2 Synthesis of natural hydrogel:

Hydrogels can be synthesized through chemical or physical crosslinking methods (Fig.1.3). Chemical crosslinking creates permanent bonds via techniques such as radical polymerization, grafting, click chemistry, thermo-gelation, and radiation crosslinking. In contrast, physical crosslinking, prevalent in natural hydrogels, forms reversible bonds through self-assembly processes like ionic interactions, hydrogen bonds, or hydrophobic interactions. Despite their instability and rapid decomposition, physically crosslinked hydrogels are popular due to their easier synthesis. Various physical and chemical crosslinking processes are shown in Fig.1.4.

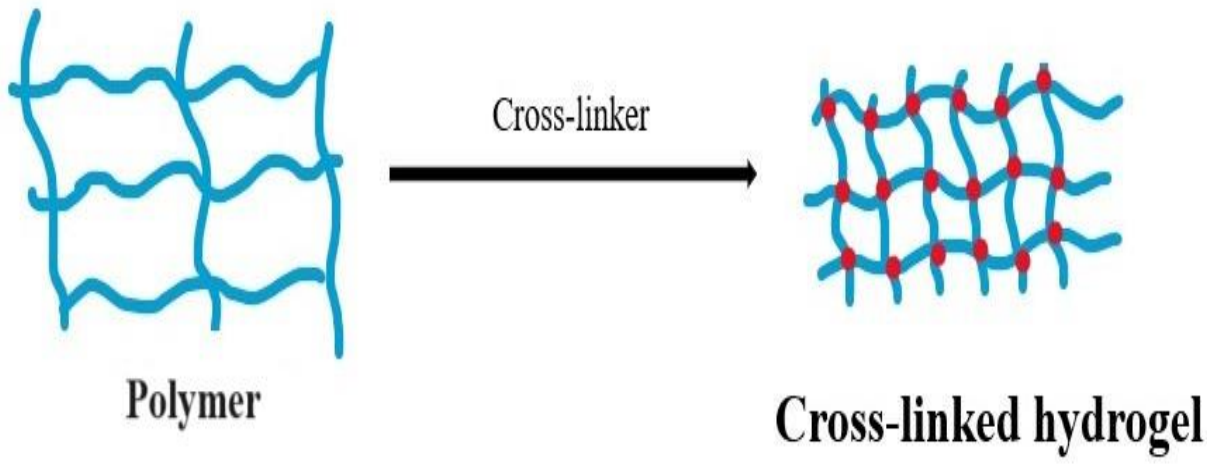


Fig. 1.3. Crosslinking of polymer.

Physical crosslinking methods include:

- **Ionic Interaction:** Counter-ions induce gelation through ionic bond formation, as seen in alginate and chitosan hydrogels.
- **Freeze-Drying:** Polysaccharide-based hydrogels are formed by solubilizing the polymer, freezing, and drying, creating porous structures.
- **Heating/Cooling:** Polymers like carrageenan undergo sol-gel transition through temperature changes.
- **Complex Coacervation:** Oppositely charged polymers form complexes, useful in food processing and drug delivery.
- **Hydrogen Bonding:** Electron-deficient hydrogen atoms bond with electronegative groups, forming hydrogels without additional crosslinkers.

Physical crosslinking can also indused by redusing the pH of a polymer solution which results in to the formation of hydrogen bond [11].

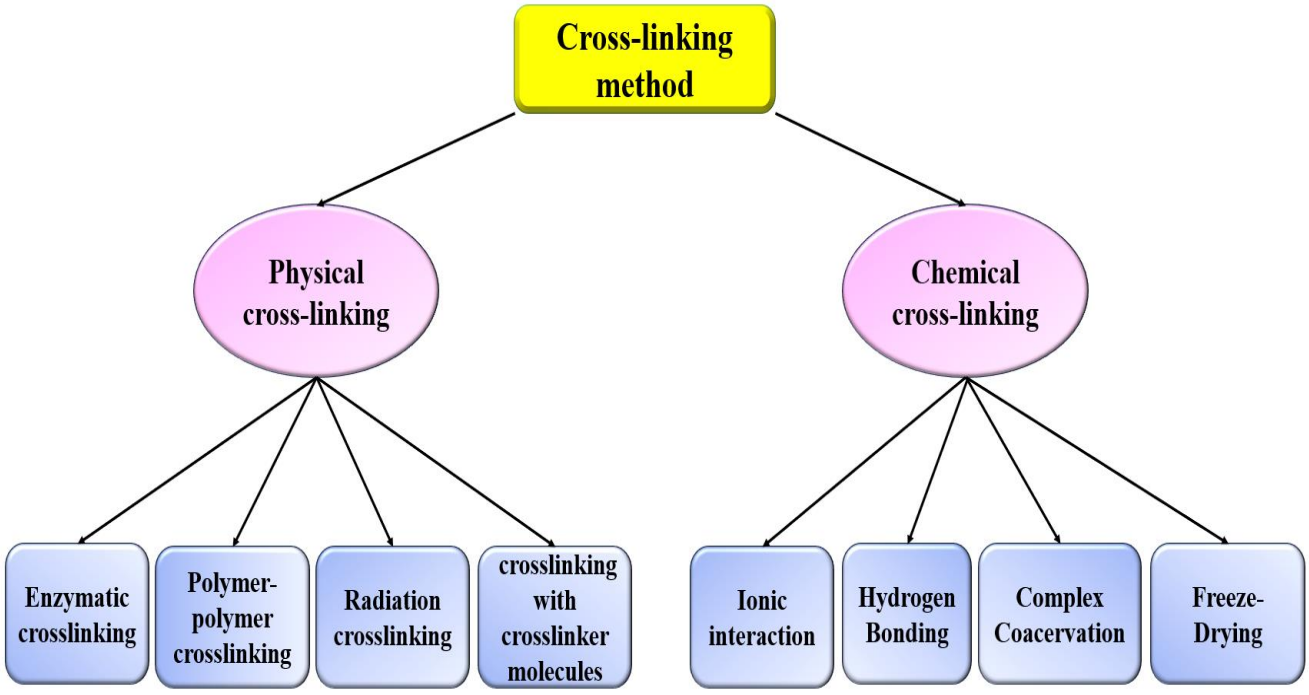


Fig. 1.4. Crosslinking method of hydrogel.

### 1.5. Microparticles as SRDDS:

Microparticles are defined as solid particles or particulate dispersions with sizes ranging from 1 to 1000µm. These particles can encapsulate, entrap, dissolve, or attach a drug within their

matrix. Depending on the preparation method, the resulting products can be microspheres, microparticles, or microcapsules. Microcapsules are characterized by a drug enclosed within a cavity surrounded by a distinct polymer membrane, on the other hand microspheres are matrix systems where the drug is uniformly distributed throughout the particle. In recent developments, biodegradable polymeric microparticles, especially those coated with hydrophilic polymers (like poly(ethylene glycol) (PEG)), have shown promise as drug delivery systems. Known as long-circulating particles, these microparticles can remain in circulation for extended periods, target specific organs, and serve as carriers for DNA in gene therapy. They are also effective in delivering proteins, peptides, and genes [12,13].

### 1.5.1. Advantages of microparticles in DDS:

The particle size and surface characteristics of microparticles can be easily adjusted to enable both active and passive drug targeting following parenteral administration [14].

- These microparticles can control and sustain the release of the drug during transport and at the target site, modifying the drug's organ distribution and clearance to enhance therapeutic efficacy and reduce side effects.
- By selecting appropriate matrix constituents, the controlled release and degradation properties of the particles can be easily modified. High drug loading is possible, and drugs can be introduced without chemical reactions, preserving their activity.
- Site-specific targeting can be accomplished by attaching targeting ligands to the particle surfaces or using magnetic guidance.
- This system is versatile and can be administered through various routes, including oral, parenteral, nasal, and intra-ocular.

### 1.5.2. Hydrogel microparticles in Drug Delivery System:

Hydrogels are formed from macromolecular hydrophilic polymers that arrange into a cross-linked network, capable of absorbing water up to several times their weight and exhibiting swelling behavior. This behavior depends on factors like polymer nature, preparation method, and ingredient concentration. Hydrogels are crucial in nanotechnology, biotechnology, and pharmaceuticals for their unique properties. In smaller forms, they are termed microgels or nanogels, which offer advantages for drug delivery systems (DDS) due to their large surface area and central network for drug insertion. Microgels/nanogels facilitate targeted drug delivery and incorporation of bioactive molecules like drugs, proteins, and DNA. They can also incorporate inorganic nanocrystals for imaging and therapy. Hydrogel microparticles

protect encapsulated drugs from environmental conditions and control drug release over time. The hydrogel structure includes a solid polymeric-network matrix, interstitial fluid, and an ionic phase, formed by physical or chemical cross-linking mechanisms [15].

**1.5.2.1. Drug loading in hydrogel microparticles can be achieved through two main methods:**

- **Post loading:** First, the hydrogel particle matrix is formed, then the drug is absorbed into it. Drug molecules are drawn into the particles via diffusion. The release of drugs occurs through diffusion and the swelling of the hydrogel microparticles.
- **In situ loading:** The drug is mixed with the polymer solution, forming drug-polymer conjugates simultaneously with matrix formation. Drug release from the matrix can occur through diffusion, swelling of the hydrogel, reversible interactions between the drug and polymer, or degradation of labile covalent bonds [16].

**1.5.2.2. Drug release from hydrogel microparticles:**

Drug release from hydrogel microparticles depends on the formulation's composition (polymer type, drug, monomer, initiator, cross-linker), particle size and shape, preparation method, and environmental conditions. Additional influencing factors include [15]:

- Water penetration into particles through pores.
- Wetting of the particle matrix with release media.
- Pore creation by entrapped water.
- Drug and polymer degradation.
- pH changes in the matrix due to polymer degradation.
- Swelling ratio of particles.
- Acidic or basic environment from degradation products.
- Drug amount in the hydrogel matrix.
- Diffusion of drug in the dissolution fluid.
- Hydrostatic pressure in drug delivery devices.
- Pore size changes due to polymer swelling.

**1.5.2.3. Techniques involved in hydrogel microparticles development:**

Various techniques are used to prepare hydrogel microparticles such as [15]

- The ionic gelation method,

- Spray drying dispersion,
- Photopolymerization ionotropic gelation method,
- Free radical precipitation polymerization,
- Inverse emulsion polymerization,
- Free radical polymerization, etc.

### 1.5.3 Applications of hydrogel microparticles in drug delivery:

Various applications of hydrogel microparticles given in table 1.1.

Table. 1.1 Hydrogel microparticles application in drug delivery.

| SL. no | Polymer | Cross-linker | Major observations | References |
|---|---|---|---|---|
| 1 | Chitosan, tamarind seed polysaccharide (IPN) | Glutaraldehyde | • Increasing amount of glutaraldehyde leads to the higher degree of cross-linking which eventually increase the drug entrapment efficiency.<br>• *In-vitro* drug release study of aceclofenac loaded microparticles showed sustained release of drug over 8 h.<br>• The in vivo studies of aceclofenac-loaded microparticles showed sustained anti-inflammatory activity over a prolonged period after oral administration. | [17] |

| | | | | |
|---|---|---|---|---|
| 2 | sodium alginate and HPMC K100 | $CaCl_2$ | • With Increasing concentratio of cross-linker the swelling of the particles was decreased, eventually results in sustained ampicillin sodium release over 24 h.<br>• Increase the amount of HPMC also increase the swelling capacity of the beads due to higher hydrophilicity and beads with HPMC showed 100% drug release at the end of 8 h. | [18] |
| 3 | Carboxymethylated locust bean gum | $AlCl_3$ | • An elevated concentration of $AlCl_3$ concentration leads to a high swelling ratio and increase the glipizide release.<br>• Particles loaded with glipizide showed a prolonged hypoglycemic effect in In-vivo study. | [19] |

| | | | | |
|---|---|---|---|---|
| 4 | Alginate and Carboxymethyl Cellulose | $FeCl_3$ | • Swelling of the hydrogel particles and release of drug from the hydrogel particles decreased with increased $FeCl_3$ concentration due to rigid and compact polymer network.<br>• Increasing concentration of cross-linker leads to decrease free volume space within the polymeric network results in decrease drug entrapment efficiency of the hydrogel particles. | [20] |
| 5 | Starch and calcium alginate | $CaCl_2$ | • Swelling of the beads were decreased with the increasing concentration of $CaCl_2$ because higher degree of crosslinking, which decreases the mesh size of the polymer beads, thereby hindering water molecules from penetrating the bead network. | [21] |

| | | | | |
|---|---|---|---|---|
| | | | • With the increasing concentration of cross-linker the release of chlorpyrifos from the particles decreased because the increased concentration of crosslinkers, reduce the mesh size of the polymer network, limits the diffusion of water molecules into the bead network and hinders the release of chlorpyrifos molecules from the bead into the surrounding medium. | |

## References


[1] M. S. Alqahtani, M. Kazi1, M. A. Alsenaidy, M. Z. Ahmad, Advances in oral drug delivery, Front. Pharmacol. 12 (2021) 618411.

[2] M. M. D. Villiers. Oral conventional solid dosage forms: powders and granules, tablets, lozenges, and capsules, in: T. K. Ghosh, B. R. Jasti, (Eds.), Theory and Practice of Contemporary Pharmaceutics 1st edition, CRC Press (2004) 273-332.

[3] S. Maiti, K. K. Sen, Introductory Chapter: Drug Delivery Concepts. Advanced Technology for Delivering Therapeutics. Intech Open. (2017)1-12.

[4] J. Manish, K. Abhay, Sustained release matrix type drug delivery system: A review, J. Drug Deliv. Ther. 2(6) (2012) 142-148.

[5] A. B. Phad, N. B. Mahale, S. K. Chaudhari, S. K. Salunke, A Sustained Release Drug Delivery System, World J. Pharm. Res. 3(5) (2014)1377-1390.

[6] B. Nagarani, K. K. Ashwin, D. Julapally, A Review on Controlled Drug Delivery System, Int. J. Appl. Pharm. 2 (2014) 1555-1586.

[7] S. Jain, S. K. Yadav, U. K. Patil, Preparation and evaluation of sustained release matrix tablet of furosemide using natural polymers, Res. J. Pharm. Technol. 1(4) (2008) 374-376.

[8] S. Patidar, B. S. Chauhan, and Oral Sustained Release Dosage Form: A review, Journal of Drug Discovery and Therapeutics.1(12) (2013) 9-20.

[9] D. Bikiaris, E. Koutris, E. Karavas, New Aspects in sustained drug release formulations, Recent Pat. Drug Deliv. Formul.1 (2007) 201-213.

[10] A. K. Nayak, Md S. Hasnain, K. Pal, I. Banerjee, D. Pal, Gum-based hydrogels in drug delivery, in: K. Pal, I. Banerjee, K. Majumdar, P. Sarkar, D. Kim, W. P. Deng, N. K. Dubey, (Eds.), Biopolymer-Based Formulations Biomedical and Food, Elsevier Inc, 2020.

[11] M. Dattilo, F. Patitucci, S. Prete, O. I. Parisi, F. Puoci, Polysaccharide-Based Hydrogels and Their Application as Drug Delivery Systems in Cancer Treatment: A Review, J. Funct. Biomater. 14(2) (2023) 55.

[12] R. Langer, J. Folkman, polymers for the sustained release of proteins and other macromolecules, Nature. 263 (1976) 797-800.

[13] J. Moore, The Drug Delivery Outlook to 2005, Business Insights Ltd. 1999.

[14] A. N. Padalkar, S. R. Shahi, M. W. Thube, Microparticles: an approach for betterment of drug delivery system, Int. J. Pharm. Res. Dev. 3(1) (2011) 012.

[15] M. Ahmad, S. M. Rai, A. Mahmood, Hydrogel Microparticles as an Emerging Tool inPharmaceutical Field: A Review, Adv. Polym. Technol. 35(2) (2016) 21535.

[16] M. Silvia, Q. Yue, J. W. Lynne, D. E. Christopher, G.Veronica, J. L. Trevor, M. M. Keith, S. F. John, G. H. Patrick, Self-assembly of ciprofloxacin and a tripeptide into an antimicrobial nanostructured hydrogel, Biomater. 34 (2013) 3678.

[17] S. Jana, A. Saha, A. K. Nayak, K. K. Sen, S. K. Basu, Aceclofenac-loaded chitosan-tamarind seed polysaccharide interpenetrating polymeric network microparticles, Colloids Surf. B Biointerfaces. 105 (2013) 303– 309.

[18] R. S. ÖZAKAR , E. ÖZAKAR, The effect of polymer amount and crosslinker ratio in polymeric hydrogel beads on characterization, Res. Pharm. 25(5) (2021) 653-666.

[19] S. Maiti, P. Dey, A. Banik, B. Sa, S. Ray, S. Kaity, Tailoring of locust bean gum and development of hydrogel beads for controlled oral delivery of glipizide, Drug Deliv.17(5) (2010) 288–300.

[20] B. Y. Swamy, Y. S. Yun, In vitro release of metformin from iron (III) cross-linkedalginate–carboxymethyl cellulose hydrogel beads, Int. J. Bio. Macromol. 77 (2015) 114–119.

[21] A. Roy, J. Bajpai, A.K. Bajpai, Dynamics of controlled release of chlorpyrifos from swelling and eroding biopolymeric microspheres of calcium alginate and starch, Carbohydr. Polym. 76 (2009) 222–231.

# Chapter 2

# LITERATURE REVIEW

## LITERATURE REVIEW

Nie et al. developed bovine serum albumin loaded cellulose-based hydrogel beads using Calcium chloride as a crosslinking agent and the characterization was done by FTIR, SEM, Raman spectroscopy, and XRD analysis [1]. To investigate the impact of calcium ions on bead retention, beads were created with varying $CaCl_2$ concentrations (0, 18, 35, 58, 70, and 80 g/100 mL). Increasing $CaCl_2$ made the beads whiter and harder, as calcium ions crosslinked the dissolved cellulose, enhancing interactions among the polymer chains. X-ray diffraction revealed structural changes with the introduction of $Ca^{2+}$ ions, indicating a new molecular structure for cellulose and modified crystallinity. SEM images showed the formation of regular nanopores at higher $CaCl_2$ levels, with 70% being optimal. Raman spectroscopy confirmed that calcium ions enhanced cellulose crystallinity, with the 481 $cm^{-1}$ peak area indicating the degree of calcification. SEM analysis before and after washing revealed significant shrinkage in hydrogel beads, changing from a slab-like to a nanoporous honeycomb structure, valuable for food, pharmaceutical, and biomedical applications. Experiments with varying calcium concentrations (0–80% $CaCl_2$) showed that mass loss after washing was low at 0–40% calcium, increased to 39% at 70% calcium concentration, and slightly decreased at 80% calcium concentration. The optimal 70% $CaCl_2$ concentration created nanoporous structures, enhancing molecule encapsulation. Water retention diminished over time, disappearing after 120 minutes of washing, resulting in collapsed beads suitable for delivery applications. Bovine serum albumin (BSA) loaded hydrogel beads show BSA release reached 71% after 30 hours, following first-order kinetics, indicating the release rate depends on BSA concentration in the beads. The layered nanoporous network structure found in the beads seems crucial for both the uptake and gradual release of BSA. These beads show potential as effective carriers for delivering substances across various research domains.

Ghawanmeh et al. optimized gum Arab (GA) and carboxymethyl cellulose (CMC) based hydrogel beads (HGB) for delivering anticancer drug 5-fluorouracil (5-FU) [2]. CMC and GA were cross-linked by the $Fe^{3+}$ ion via ionotropic gelation method. SEM images revealed that CMC/GA-hydrogel beads had an oval shape with rough wrinkles and compact ridges due to hydrogen bonding, aiding in controlled drug release. XRD patterns showed that CMC and GA had a semi-crystalline nature, while the placebo CMC/GA-HGB was amorphous. The disappearance of crystalline peaks in the drug-loaded beads suggested that 5-FU was molecularly dispersed. FTIR spectra showed characteristic bands for CMC and GA, indicating various functional groups. A new peak at 1731$cm^{-1}$ in CMC/GA-hydrogel beads suggests

hydrogen bonding with Fe(III). Shifts in CMC/GA/5-FU hydrogel beads spectra indicate successful 5-FU encapsulation. The BET-specific surface area and pore diameter of CMC-hydrogel beads are 0.883 $m^2/g$ and 5.504 nm respectively, but the BET-specific surface area of CMC/GA-hydrogel beads was measured at 6.39 $m^2/g$, with an average pore diameter of 19.984 nm. This indicates that the presence of GA increased both the surface area and pore diameter of the hydrogel beads. Optical microscopy revealed that adding GA to the hydrogel matrix increased the viscosity of the polymer solution, resulting in larger bead sizes and lower density. Drug encapsulation efficiency (DEE) of the hydrogel beads was also optimized, focusing on the impact of key components: CMC, GA, and Fe(III) cross-linker. Using response surface methodology (RSM), optimal ranges for CMC (75-125 mg) and GA (20-120 mg) were determined. Increasing GA up to 40 mg improved DEE to nearly 53%, but further increment of GA, decreases the encapsulation due to enhanced cross-linking and smaller pore size. Similarly, DEE increased with CMC up to 100 mg before declining, indicating optimal levels for higher DEE. Fe(III) cross-linker concentration affected DEE, peaking at 0.2 M, facilitating cross-linking with biopolymers to enhance mechanical properties and drug encapsulation. Excessive Fe(III) concentration, however, led to a rigid network, smaller pores, and reduced drug loading. These findings align with previous reports on Fe(III)'s influence on drug encapsulation and release profiles. Optimal conditions were identified as 100 mg CMC and 40 mg GA for achieving higher DEE. The study examined pH sensitivity in hydrogel beads which is crucial for drug release modulation. Swelling kinetics of CMC-hydrogel beads and CMC/GA-hydrogel beads were studied across various pH ranges. At lower pH, cross-linking limited swelling, aiding in drug release decline in stomach conditions. Higher pH induced ionization, increasing swelling due to repulsion between ionized groups. CMC/GA-hydrogel beads showed higher swelling due to GA's high molecular weight and rich carboxylic groups. In the presence of GA in the matrix, release of 5-FU was sustained in acidic media due to protonation effects but on the other hand at higher pH, drug release increased due to deprotonation and increased electrostatic repulsion. Overall it is concluded that CMC/GA-hydrogel beads could be a promising nanocarrier for the controlled delivery of anticancer drugs.

Sedyakina et al. developed bovine serum albumin (BSA) loaded chitosan microparticles using citric acid as a crosslinking agent [3]. Fourier transform infrared (FTIR) spectroscopy and X-ray diffraction (XRD) validated the ionic interaction between the protonated amine groups in chitosan and the carboxylate ions in the cross-linking agent. Scanning electron microscopy

(SEM) showed that the non-cross-linked microparticles possessed an irregular, wrinkled appearance, whereas the cross-linked particles were spherical and had smooth surfaces. SEM analysis also revealed that all non-cross-linked microparticles had an average diameter of 12.3 µm, while microparticles cross-linked with citric acid showed a reduced diameter size range of 11.2µm to 7.3µm due to the cross-linking effect. Particle size decreased as citric acid concentration increased indicating high cross-linking density. Zeta potential measurements ranged from -15.7 to 12.8mV, suggesting particle aggregation. Cross-linking with citric acid lowered zeta potential values due to surface citrate adsorption, and higher pH levels decreased zeta potential due to changes in surface charge. The erosion behavior of chitosan microparticles in phosphate buffer saline showed that particles with citric acid degraded less (40-56%) compared to the non-cross-linked sample (76%), due to ionic cross-linking. Lower concentrations of cross-linker resulted in reduced erosion, with increased three-dimensional network density. Higher pH decreased erosion due to changes in ionization of the cross-linker, affecting cross-linking density. High-density cross-linking also causes steric hindrance which prevents BSA from penetrating into the polymer matrix and leads to lower BSA encapsulation efficiency. The cumulative release of BSA also depends on the crosslinking density of the chitosan matrix. Release of BSA from a crosslinked matrix is significantly lower than the non-crosslinked matrix. Over all this study demonstrates that the preparation of chitosan microparticles through ionic crosslinking with citric acid is highly dependent on the preparation protocol. Controlling the drug entrapment percentage and release profiles during microparticle preparation is essential and holds the potential for advancing carriers for oral protein and peptide drug delivery.

Rehman et al. developed diclofenac-sodium loaded enteric-coated alginate-based hydrogel beads for colon-targeted drug delivery systems [4]. Hydrogel beads were prepared by adding sodium alginate dropwise into calcium chloride solution. Further, the beads were added into 5% Eudrajit-S solution for coating. Swelling behavior and drug release from the coated and uncoated beads were assessed. The swelling behavior of uncoated Ca-alginate beads and Eudrajit-S coated Ca-alginate was observed at pH levels of 1.2, 6.8, and 7.4. Minimal swelling of uncoated Ca-alginate beads occurred in acidic media (pH 1.2) with no degradation after 24 h. At pH 7.4, beads swelled significantly and began bursting within 2h. due to ion exchange between Ca ions in alginate and Na ions in the buffer. At pH 6.8, stable swelling was noted for up to 4 hours before degradation, influenced by phosphate ions in the buffer. On the other hand, Eudragit-coated beads showed no significant swelling at pH 1.2, but at pH 6.8, they swelled up

to 30% after 7h. At pH 7.4, these coated beads exhibited significant stability and swelling occurred after complete degradation of the coating that is after 4h. The drug release study of uncoated Ca-alginate beads revealed low release at pH 1.2 due to low swelling and solubility of diclofenac sodium. At pH 6.8, drug release reached 68.11% within 4 hours due to the high solubility of sodium alginate. At pH 7.4, the beads burst, releasing all the drug immediately. For Eudragit-coated beads, no drug release occurred in acidic media, minimal release at pH 6.8 after 5h., and 95.16% release at pH 7.4 within a few hours, showing stability and high release in basic conditions, consistent with previous studies using pH-sensitive polymers like Eudragit S-100.

Bhattacharya et al. reported the development of Sodium Carboxymethyl Cellulose (SCMC) and Sodium Carboxymethyl Xanthan (SCMX) Gum-based IPN hydrogel beads for the controlled release of diclofenac sodium (DS) [5]. $AlCl_3$ was used as crosslinking agent. Optical microscope was used to determine the particle size. Particle size, influenced by polymer concentration, gelation time, and $AlCl_3$ concentration, Beads, extruded through a 21-gauge needle into a cross-linking medium, were spherical (1.08-1.42 mm) with narrow size distribution. It is observed that increased cross-linking agent concentration leads to decreased particle size, as $Al^{3+}$ ions formed a gel layer, causing water efflux and bead contraction, resulting in smaller particles. Drug entrapment efficiency (DEE), swelling study and drug release study were also conducted. DEE of IPN beads decreased from 96.96% to 77.45% as the SCMC to SCMXG ratio increased from 1:1 to 2:1, due to higher SCMC solubility causing bead swelling leads to leaching of drug molecules. DEE also decreased with increasing $AlCl_3$ concentration (4-8% w/v) because higher $AlCl_3$ made the beads more rigid, reducing free volume and allowing more $Al^{3+}$ ions to displace the drug. Prolonged exposure in the gelation medium (1h.) further contributed to drug leaching, decreasing DEE. Similar trends were observed in $Al^{3+}$ ion cross-linked carboxymethyl guar gum beads. Drug release from a polymeric matrix is influenced by the swelling behavior of the hydrogel beads. Swelling was measured as water uptake over time and varied with pH levels: low in acidic (pH 1.2) and high in alkaline (pH 7.4) solutions. The –OH groups in the polymers, which cross-link with $Al^{3+}$ ions, remain protonated and unreactive in acidic conditions, leading to minimal swelling. In alkaline conditions, –OH groups ionize, causing electrostatic repulsion and increased swelling. Higher swelling enhances drug release. Conversely, increased $AlCl_3$ concentration and gelation time reduce swelling and drug release due to reduced pore volume and increased rigidity of the polymer matrix. Increasing $AlCl_3$ concentration during bead preparation (4-8% $AlCl_3$) reduced

drug release in both (pH 1.2 and pH 7.4) dissolution media. Higher $AlCl_3$ concentrations rigidify polymeric chains by microvoid contraction, decreasing cumulative drug release. Conversely, lower $AlCl_3$ concentrations result in faster release. Overall the findings suggest that utilizing drug-loaded hydrogel beads could attenuate DS release in acidic conditions and regulate its release in alkaline environments. This approach could aid in reducing the gastric side-effects associated with DS administration.

Rahmani et al. prepared Rivastigmin (RIV) loaded porous hydrogel beads based on gum tragacanth (GT) and graphene oxide (GO), crosslinked by $CaCl_2$ and $BaCl_2$ solution [6]. GT/GO mixture immediately forms spherical beads when dropped into a crosslinking solution. Swelling of the beads, drug loading, and drug release were assessed. The swelling behavior of hydrogel beads is influenced by cross-linker content, type, and the swelling medium's pH. Hydrogels cross-linked with calcium ions exhibit higher swelling (1811%) compared to those with barium ions (1450%) at a 0.15(M) concentration, due to differences in ion size. The swelling capacity increases with the cross-linker amount until excessive cross-linking reduces it. The optimal swelling was found at 0.15(M) for both $CaCl_2$ and $BaCl_2$. Gel content depends on the cross-linker type, with barium showing a slightly higher gel content than calcium due to its higher atomic weight and lower electronegativity. Adding GO nanosheets up to 5 wt% increases swelling due to hydrophilic functional groups, but further increases reduces swelling due to GO aggregation. Swelling is greater at pH 7.4 than pH 1.2, with maximum swelling at pH 7.4 after 24 hours, making these hydrogels suitable for pH-responsive drug delivery systems. The pH in the stomach is acidic (around 1.2) and slightly alkaline in the intestine (pH 7.4). To simulate these conditions, the in vitro release of RIV was tested in 0.1(N) HCl buffer (pH 1.2) and phosphate buffer (pH 7.4). The release of RIV from GT- hydrogel beads containing 5mg GO was significantly faster than from GT-hydrogel beads containing 0mg GO at both pH levels. At pH 1.2, both types of beads released about 50% of the drug after 400 minutes due to lower swelling. However, at pH 7.4, GT-beads containing 5mg GO released 97% of the drug within 240 minutes, while GT-beads containing 0mg GO only released ~50% after 400 minutes. The slower drug release in acidic conditions protects the drug from stomach degradation. These findings suggest that the hydrogel composition and the pH of the medium are crucial for efficient drug release, making these beads suitable for pH-sensitive controlled RIV drug delivery.

Giri et al. developed diltiazem-loaded modified xanthan gum and pectin based hydrogel beads. The beads were prepared by ionotropic crosslinking with $Al^{+3}$ ion and covalent crosslinking

with glutaraldehyde. Beads formed instantly when a drug and SCMX dispersion was extruded into an $Al^{3+}$ solution, but they had poor mechanical strength [7]. To improve this, IPNs were created using SCMX and pectin via ionotropic gelation with $AlCl_3$, forming ionic cross-links. These spherical IPN beads ranged from 669.17 to 1012.67μm in size, decreasing with higher $AlCl_3$ concentration due to rapid hydrogel shrinking. Increased drug loading led to larger bead sizes due to higher interfacial viscosity, preventing smaller droplet formation. Increased concentration of $AlCl_3$ also reduced the drug entrapment efficiency (DEE) from 45.27% to 21.41%, due to thicker gel formation leads to displacement of more drug molecules. The DEE varied from 45.27% to 47.62% with different drug loads and decreased with more GA due to increased cross-link density. These findings align with other studies on similar systems. The drug release behavior of IPN beads was investigated through swelling studies in both pH 6.8 and pH 1.2 buffer solutions. Increasing pH led to increased swelling due to ionization of carboxyl groups in the hydrogel, while higher $AlCl_3$ concentration reduced swelling by increasing cross-linking density. In vitro biodegradation studies revealed slower degradation with higher GA content due to increased cross-linking density, hindering enzyme diffusion. Drug release in both acidic and alkaline media decreased with increasing $AlCl_3$ concentration due to decreased free volume in the polymer matrix. Low drug-loading resulted in faster release due to larger pore fraction, while GA treatment slowed release through covalent acetal linkages. Formulation optimization was based on drug entrapment efficiency (DEE) and t50%. Empirical equation fitting showed Fickian transport in acidic medium and anomalous transport in alkaline medium. Overall, formulations exhibited low drug release in acidic conditions, with increased release in alkaline conditions, depending on cross-linking and drug content. SCMX and pectin blend showed promise for sustained release of DTZ.

Bera et al. prepared gellan gum (GG), Carboxymethyl fenugreek galactomannan (CFG) and calcium silicate (CS) composite beads for glimepiride (GLI) delivery [8]. Zinc chloride, calcium chloride, and aluminium chloride solution were used as crosslinking agents.The bead size was observed within the range from 1.46 ± 0.01 to 1.90 ± 0.04 mm, with larger diameters observed at higher GG:CFG ratios due to more viscous dispersions. Crosslinker types also influenced particle size. $Ca^{+2}$ produces larger beads compared to $Zn^{+2}$ and $Al^{+3}$. The differences are attributed to matrix rigidity and electrostatic attraction. $Al^{+3}$ creating denser gels and smaller particles due to higher cross-linking efficiency. In contrast, $Ca^{+2}$ forms less dense hydrogels, increasing the matrix diameter. Additionally, incorporating CS into the formulation increased bead size, as CS molecules filled the interstitial spaces within the biopolymer

network, preventing inward shrinkage and resulting in larger matrices. The SEM images of the GLI-encapsulating composite beads revealed an approximately spherical shape with notable surface features such as large wrinkles and cracks. The beads had a tight and irregular surface, likely due to interactions between biopolymer chains and CS molecules. CS particles, by incorporating between biopolymer chains, expanded and disrupted the hydrogel network. Small pores or channels on the bead surface were likely formed by water migration and shrinkage during drying, while slight deformations were attributed to differential contraction as water evaporated. The presence of polymeric debris on the surface was linked to the preparation method involving concurrent hydrogel preparation and composite matrix formation. The GLI-loaded formulations exhibited high drug encapsulation efficiency (DEE), ranging from 48.18 ± 1.44% to 96.74 ± 0.59%. This high DEE was due to the rapid formation of a cation-crosslinked polymeric network, which limited drug leakage, and the poor aqueous solubility of GLI, which restricted its outward diffusion. Higher GG: CFG ratio in the polymer blend significantly improved drug entrapment by facilitating the synthesis of compact, rigid matrices with abundant anionic sites for ionotropic crosslinking, thus minimizing drug loss. Matrices crosslinked with $Ca^{+2}$ ions showed higher drug entrapment than those with $Zn^{+2}$ ions, attributed to $Ca^{+2}$ ion's ability to induce faster electrostatic interactions with biopolymer carboxylates, forming a denser coat and preventing drug leakage. The larger diameter of $Ca^{+2}$-crosslinked matrices allowed greater drug (GLI) entrapment and a longer diffusion path, reducing drug leakage. In contrast, $Al^{+3}$ ions, with higher cross-linking density, caused significant water loss and convective drug loss during incubation. CS-modified composite beads significantly enhanced drug entrapment compared to control matrices. This was likely due to CS anchoring GLI molecules through electrostatic interactions and hydrogen bonding, and increased cross-linking density from simultaneous internal and external gelation, which prevented GLI extravasation during preparation. Hydrogel beads exhibited Q8h. (cumulative release at 8 hours) values between 61.94 ± 1.23% and 93.91 ± 1.01%. Delayed GLI release was linked to reduced free volume and increased tortuosity in cation-crosslinked matrices, hindering GLI transport. Drug release was faster in alkaline pH due to the superior ionization of biopolymeric carboxylates and increased solubility of GLI, enhancing diffusivity through the matrices. Higher GG/CFG ration significantly increased drug release at 8 hours due to the ionization of carboxyl groups, loosening the hydrogel network and increasing swelling and drug release rates. $Ca^{+2}$-crosslinked beads showed enhanced drug release compared to $Zn^{+2}$-crosslinked beads, as $Ca^{+2}$ ions form electrostatic bonds that are easily hydrated and broken, while $Zn^{+2}$ ions create resistant covalent-like bonds. $Al^{+3}$ ions made the network rigid and

compact, significantly impeding GLI release. Incorporating CS into formulations altered drug release profiles. Initially, CS molecules delayed drug release by acting as inert fillers. Still, over time, $Ca^{+2}$ ions bound to CS were leached, leading to a breakdown of Si-O-Si linkages, creating hydrophilic channels and significantly increasing drug release. The optimised formulation had the highest drug release profile (Q8h, 93.91 ± 1.01%), enhancing in vivo drug absorption and therapeutic benefits of GLI. Swelling data showed pH-dependent behavior, with lower swelling in acidic conditions (pH 1.2) compared to alkaline medium (pH 6.8) ($p < 0.05$). In acidic environments, protonation of carboxyl groups reduced electrostatic repulsion, limiting water penetration. At higher pH, carboxyl groups ionized, increasing hydrophilicity and network expansion, enhancing water migration and swelling. CS incorporation significantly increased swelling in both media ($p < 0.05$), boosting water uptake and swelling ratio. Biopolymer-CS matrices quickly formed a porous structure and disentangled in swelling medium, increasing drug release rate. The swelling rate and water penetration velocity into the biopolymer-CS matrices were higher than in control matrices. Overall, the composite matrices, which were simply produced without any complicated processes, show great potential for use in controlled delivery of hydrophobic drugs.

Maiti et al. developed ionically crosslinked Carboxymethyl cellulose (CMX) microparticles for sustained delivery of bovine serum albumin (BSA). Surface morphology of the microparticles, drug entrapment efficiency, and BSA release study from the microparticles were carried out [9]. Around 86% of BSA loading in the microparticles was reported. Surface morphology analysis showed that the average diameter of the microparticles increased with the addition of aluminium chloride to the gelation solution. At lower concentrations of aluminium chloride, the microparticles were spherical. However, as the concentration of aluminium chloride increased, the microparticles became irregularly shaped, and surface depressions developed. When CMX gum interacts with the aluminium chloride solution, immediate gelation occurs, forming a gel layer on the microparticle surface. Over time, $Al^{3+}$ ions enter the microparticles while water exits from the core. As water is expelled, the microparticles contract, reducing their size. However, higher aluminium chloride concentrations lead to a thicker, denser gel layer, which limits the movement of $Al^{3+}$ ions and water, resulting in larger microparticles. At high aluminium chloride levels, the gelation is uneven, with a dense gel on the surface but less gelation in the core, causing surface depressions upon drying due to core water evaporation. BSA release from the microparticles was rapid in acidic media (pH 1.2), with approximately 51% of the protein released in 2 hours. In a higher pH solution (6.8), the

release was slightly slower, with 41% of BSA released in the same timeframe. The differences in swelling behavior between acidic and buffer solutions affected the protein release rates, with higher swelling in acidic media resulting in greater protein release compared to the buffer media. The data indicated that $Al^{3+}$ crosslinked CMX beads did not effectively limit BSA release in acidic conditions. To address this, the microparticles were coated with sodium CMX or sodium alginate and crosslinked with calcium ions. The coated microparticles were larger than uncoated ones, with sodium CMX-coated particles being larger than alginate-coated ones. Coated microparticles showed lower BSA entrapment efficiency due to leaching during the coating process, which led to reduced protein retention. BSA release from coated microparticles was significantly lower than from uncoated ones. In acidic solutions, protein release was less from alginate-coated microparticles compared to sodium CMX-coated ones. Sodium alginate forms acid-insoluble calcium alginate in the presence of $Ca^{2+}$ ions, which swells less and is less soluble in acid, resulting in slower BSA release. Conversely, in phosphate buffer (pH 6.8), alginate-coated microparticles released BSA faster than sodium CMX-coated ones, as calcium alginate swells and dissolves rapidly in buffer, while aluminium CMX remains insoluble. This study demonstrates that coated and crosslinked CMX microparticles effectively reduce protein release in acidic conditions while providing sustained release in intestinal conditions, making them suitable for oral protein delivery.

**References**

[1] G. Nie, Y. Zang, W. Yue, M. Wang, A. Baride, A. Sigdel, S. Janaswamy, Cellulose-based hydrogel beads: Preparation and characterization, Carbohydr. Polym. Technol. Appl. 2 (2021) 100074.

[2] A. A. Ghawanmeh, L. L. Tan, G. A.M. Ali, M. A. Assiri, K. F. Chong, Optimization of carboxymethyl cellulose-gum Arab-based hydrogel beads for anticancer drugs delivery, J. Mol. Liq. 393 (2024) 123631.

[3] N. Sedyakina, A. Kuskov, K. Velonia, N. Feldman, S. Lutsenko, G. Avramenko, Modulation of entrapment efficiency and in vitro release properties of BSA-loaded chitosan microparticles cross-linked with citric acid as a potential protein–drug delivery system, Materials 13(8) (2020) 1989.

[4] S. Rehman, N. M. Ranjha, M. R. Raza, M. Hanif, A. Majed, N. Ameer, Enteric-coated Ca-alginate hydrogel beads: a promising tool for colon targeted drug delivery system, Polym. Bull. 78 (2021) 5103–5117.

[5] S. S. Bhattacharya, S. Shukla, S. Banerjee, P. Chowdhury, P. Chakraborty, A. Ghosh, Tailored ipn hydrogel bead of sodium carboxymethyl cellulose and sodium carboxymethyl xanthan gum for controlled delivery of diclofenac sodium, Polym-plast. technol. 52 (2013) 795–805.

[6] Z. Rahmani, R. Sahraei, M. Ghaemy, Preparation of spherical porous hydrogel beads based on ion-crosslinked gum tragacanth and graphene oxide: Study of drug delivery behavior, Carbohydr. Polym. 194 (2018) 34-42.

[7] T. K. Giri, C. Choudhary, A. Alexander, Ajazuddin, H. Badwaik, M. Tripathy, D. K. Tripathi, Sustained release of diltiazem hydrochloride from cross-linked biodegradable ipn hydrogel beads of pectin and modified xanthan gum, Indian J. Pharm. Sci. 75(6) (2013) 619.

[8] H. Bera, S. Mothe, S Maiti, S. Vangad, Carboxymethyl fenugreek galactomannan-gellan gum-calciumsilicate composite beads for glimepiride delivery, Int. J. Biol. Macromol. 107 (2018) 604–614.

[9] S. Maiti, S. Ray, B. Sa, Controlled delivery of bovine serum albumin from carboxymethyl xanthan microparticles, Pharm. Dev. Technol. 14(2) (2009) 165-172.

# Chapter 3

# POLYMER PROFILE

## 3. POLYMER PROFILE

### 3.1 Source:

Tara gum, also known as Peruvian carob, is a white or beige powder produced by milling the seed endosperm of the Caesalpinia spinosa tree, a species native to Peru and widely cultivated in China's Yunnan and Sichuan provinces. Its primary component is galactomannan polysaccharides, which feature a linear backbone of (1-4)-β-D-mannopyranose units linked by (1–6) bonds to α-D-galactopyranose units. Structurally and functionally, tara gum resembles guar and locust bean gums. It has a mannose-to-galactose ratio of 3:1[1-2]. The structure of tara gum is shown in Fig.3.1.

### 3.2 Structure:

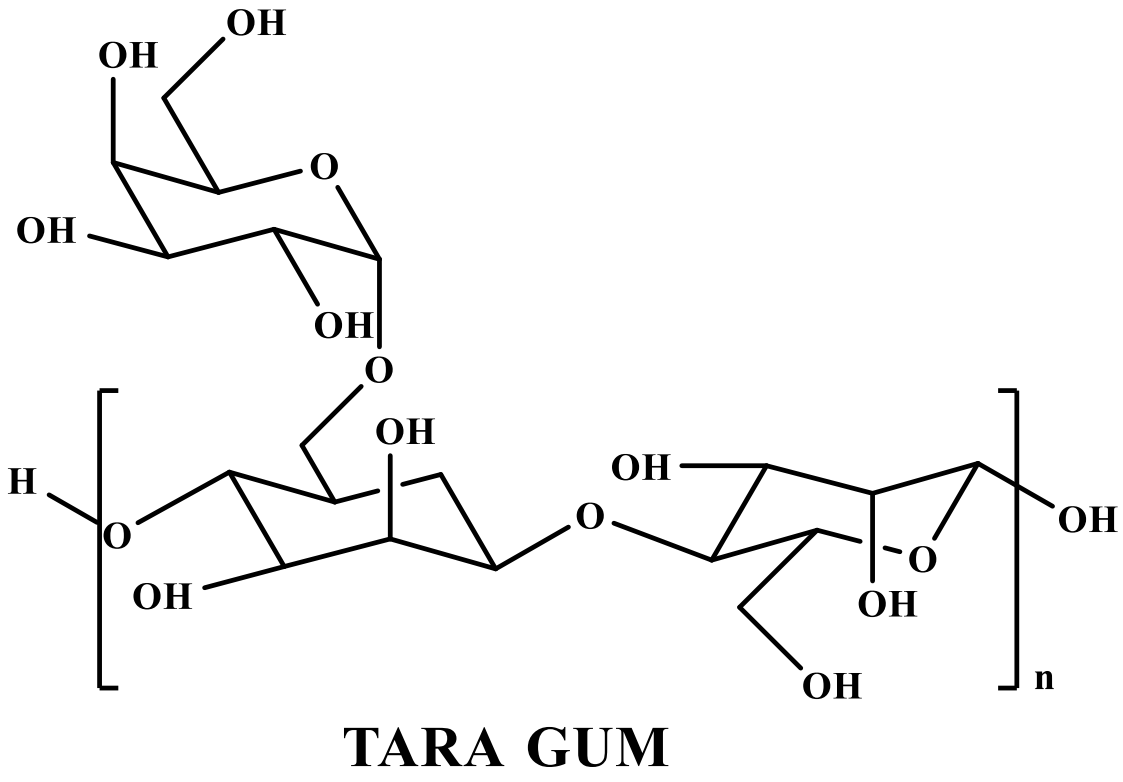


Fig. 3.1. Structure of Tara gum.

### 3.3 Physicochemical properties:

TG is almost soluble in water at room temperature and reaches about 75% of its maximum viscosity potential. When heated to 95 °C and then cooled to 25 °C, it forms opaque, tan-colored sols. These solutions (1% w/v) have viscosities ranging from 300 to 400 cps, depending

on the quality of gum extraction. The viscosities remain stable across a wide pH range at any given shear rate. Tara sols exhibit pseudoplastic rheology. TG solutions quickly gel when crosslinked with specific metal ions. Borax, a well-known cross-linker for galactomannans, binds to cis-hydroxyl groups of either D-galactosyl or D-mannosyl moieties on different chains when the solution pH exceeds 9. Other cross-linkers include multivalent cations such as Chromium (III) and Antimony (III). Gelation in TG solutions can also be induced by intermolecular association, which can be achieved by adding an excess of ethylene glycol or sucrose, or by the freeze-thaw process, as both methods reduce or remove available free water, increasing gum concentration and promoting interaction [3].

**3.4 Toxicological profile:**

The toxicological aspects of tara gum have been thoroughly investigated [4]. It is free of acute and chronic toxic effects and is classified as Generally Recognized As Safe (GRAS). In a 90-day study, rats were fed diets containing 0%, 1%, 2%, or 5% tara gum. At the highest concentration (5%), both male and female rats exhibited reduced body weight, while only males showed this effect at the 2% concentration. Additionally, there was an increase in blood urea nitrogen levels in rats given the 5% solution, although these levels remained within normal ranges. Other parameters such as hematology, urinalysis, and tissue examinations did not show significant differences from the control groups. Reproductive and teratogenicity studies were also conducted with various concentrations of the gum. The fetuses were examined and showed no signs of embryonic or teratogenic effects from tara gum consumption [4].

**3.5 Literature review:**

Mukherjee et al. reported etherified tara gum (CMTG) based hydrogel matrix tablet for sustained delivery of tramadol hydrochloride (TH) [5]. Aluminium chloride ($AlCl_3$) and Calcium chloride ($CaCl_2$) were used as crosslinking solution. The study examined the swelling and erosion behavior of Al-CMTG and Ca-CMTG matrices in acidic media (pH 1.2). The CMTG matrix without cross-linking swelled rapidly, peaking at 381% after 2 hours, and then decreased, showing significant erosion. Introducing $AlCl_3$ reduced swelling and erosion, with higher concentrations (up to 9% w/w) leading to decreased water penetration and a rigid gel layer formation. At 12% $AlCl_3$, erosion increased despite reduced swelling. Similarly, increasing $Ca^{2+}$ ions (up to 12% w/w) in Ca-CMTG matrices decreased swelling and erosion, with further increases (15% w/w) reversing this trend. The Al-CMTG matrices showed lower swelling and erosion compared to Ca-CMTG matrices due to slower water penetration. Visual

assessments confirmed these results, with Al-CMTG matrices forming a more rigid gel layer, retaining their core structure longer than Ca-CMTG and CMTG matrices. The study examined the release of TH from matrices made of carboxymethyl tara gum (CMTG) with and without aluminum chloride ($AlCl_3$) and calcium chloride ($CaCl_2$) as cross-linkers. Matrices showed an initial burst release, followed by a gradual release. Pure CMTG (without crosslinking agent) released 96% of TH in 8 hours. On the other hand adding $AlCl_3$ reduced the release rate; 9% $AlCl_3$ slowed release to 72%, but 12% $AlCl_3$ increased release to 99%. Similar patterns were observed with $CaCl_2$; 12% $CaCl_2$ resulted in a slower release than 15% $CaCl_2$. $AlCl_3$ and $CaCl_2$ cross-linking altered the polymer matrix, creating a dense gel layer that hindered drug diffusion. $Al^{3+}$ ions formed a stronger gel than $Ca^{2+}$ ions due to their higher valency, leading to slower TH release from Al-CMTG matrices compared to Ca-CMTG matrices. Optimal sustained release for Al-CMTG was achieved with 9% $AlCl_3$, while for Ca-CMTG it was 12% $CaCl_2$.Comparing the optimized formulation 9% Al-CMTG matrices to a commercial product (TRD-CONTIN®), both had similar release profiles in acidic media, but the matrices with 9% w/w $AlCl_3/CaCl_2$, had a more sustained release in neutral pH buffer, demonstrating better performance for extended drug release.

Mukherjee et al. reported the effect of intragranular/extragranular semi-IPN hydrogel matrices based on tara gum (TG) and carboxymethyl tara gum (CMTG) for sustained gastrointestinal delivery of a highly water soluble drug Tramadol hydrochloride (TH) [6]. $Al^{+3}$, $Ca^{+2}$ ion were used as crosslinking agent. The release of TH from CMTG matrices cross-linked with either $Al^{3+}$, $Ca^{2+}$, or a combination of both were explored. When CMTG matrices were cross-linked with 9% w/w $Al^{3+}$ , there was a burst release of 22-24% of TH within the first 30 minutes. Over time, the release pattern became uniform. The matrices released 33% and 81% TH at 2 and 10 hours of dissolution study, respectively. Substitution of $Al^{+3}$ ion by $Ca^{+2}$ ion leads to the increment of drug release from 33% to 44% at 2 hours and from 81% to 101% at 10 hours of invitro dissolution study. $Al^{3+}$ ions create a more rigid, viscous gel layer due to their higher cross-linking efficiency compared to $Ca^{2+}$. As $Ca^{2+}$ concentration increased, the gel layer's rigidity decreased, resulting in faster drug diffusion. The Fickian diffusion model indicated that the TH diffusion coefficient increased with higher $Ca^{2+}$ concentrations. Viscosity analysis confirmed that as $Ca^{2+}$ levels increased, the gel layer became less viscous, facilitating faster drug release. For matrices cross-linked with 12% w/w $Ca^{2+}$ , a similar initial burst release of TH was observed. Replacing $Ca^{2+}$ with $Al^{3+}$ in increasing amounts resulted in a more sustained release. After 2 hours, TH release rate was 27% and after 10 hours, it was 75%. These results

clearly depict that formulation with a balanced ratio of $Al^{3+}$ and $Ca^{2+}$ (1:1 at 12% w/w), provided the most sustained release of TH, making it a candidate for further investigation. This was addressed by incorporating TG into the matrix, creating dual cross-linked semi-IPN hydrogel matrices, with increasing TG ratios. The results showed that higher TG content increased both swelling and erosion of the hydrogel, thus enhancing TH release. Overall, the study concludes that modifying the concentration and type of cross-linking ions in hydrogel matrices significantly affects drug release rates, with optimal formulations depending on the desired release profile .

**References**

[1] W. Sittikijyothin, D. Torres, M.P. Gonçalves, Modelling the rheological behaviour of galactomannan aqueous solutions, Carbohydr. Polym. 59(3) (2005) 339-350.

[2] Y. Wu, W. Li , W. Cui , N.A.M. Eskin, H.D. Goff, A molecular modeling approach to understand conformation–functionality relationships of galactomannans with different mannose/galactose ratios, Food Hydrocoll. 26(2) (2012) 359-364.

[3] K. Mukherjee, P. Dutta, H. R. Badwaik, A. Saha, A. Das, T. K. Giri, Food industry applications of Tara gum and its modified forms, Food Hydrocoll. Health. 3 (2023) 100107.

[4] J. F. Borzelleca, B. N. Ladu, F. R. Senti, J. L. Egle Jr, Evaluation of the safety of tara gum as a food ingredient: a review of the literature, J. Am. Coll. Toxicol. 12(1) (1993) 81-89.

[5] K. Mukherjee , P. Dutta , T. K. Giri, Al3+/Ca2+ cross-linked hydrogel matrix tablet of etherified tara gum for sustained delivery of tramadol hydrochloride in gastrointestinal milieu, Int. J. Biol. Macromol. 232 (2023) 123448.

[6] K. Mukherjee, S. Roy, T. K. Giri, Effect of intragranular/extragranular tara gum on sustained gastrointestinal drug delivery from semi-IPN hydrogel matrices, Int. J. Biol. Macromol. 253(5) (2023) 127176.

# Chapter 4

# DRUG PROFILE

## 4. DRUG PROFILE

### 4.1. Introduction:

Acetaminophen, an over-the-counter medication, is commonly used to relieve pain (analgesic) and reduce fever (antipyretic). It differs from other readily available medications like ibuprofen and naproxen, which also address pain and fever but belong to a different pharmaceutical category. Acetaminophen is extensively utilized for managing fever and pain in both children and adults and is available in various forms, including pills, liquids, injectables, and rectal suppositories. Internationally, particularly outside the United States and Canada, acetaminophen is known as **"Paracetamol"** and serves the same purposes. In 1878, scientist Morse synthesized Paracetamol and in 1887, scientist von Mering introduced paracetamol in clinical trials. In 1953, Sterling-Winthrop Co. introduced paracetamol to the market, promoting it as a safer alternative to aspirin, especially for children and individuals with ulcers. However, prolonged use of paracetamol can lead to liver damage [1]. Details about paracetamol is given in Table 4.1. and the structure of the paracetamol shown in Fig.4.1.

Table 4.1 Specifications of Paracetamol [2].

| | |
|---|---|
| Chemical Formula | $C_8H_9NO_2$ |
| Chemical Name | N-(4-Hydroxyphenyl) ethanamide |
| Appearance | White, odorless crystalline powder; forms large monoclinic prisms from water |
| Molecular Weight | 151.16 g/mol |
| Melting Point | 169-170.5°C |
| pH | 5.3 to 6.5 at 25°C |
| Density | 1.293 g/cm³ |
| Stability | Dry, pure paracetamol is stable up to 45°C |
| Dissociation Constant | pKa = 9.0-9.5 |
| Partition Coefficient | 6.237 (octanol/pH 7.2 buffer) |
| Solubility in water | 1:70, 1:20 at 100°C |
| Insoluble in | diethyl ether, petroleum ethers, pentane, and benzene |
| Dosage: | 650-1000 mg every 4-6 hrs as needed |

**4.2 Structure:**

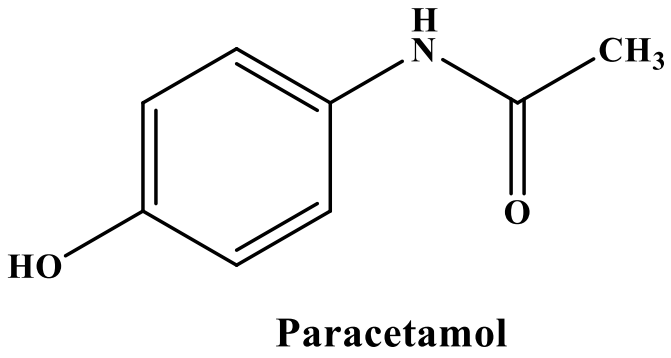


**Paracetamol**

Fig. 4.1. Structure of Paracetamol.

**4.3 Mechanism of action:**

It primarily affects the central nervous system (CNS), raising the pain threshold by inhibiting the COX-1, COX-2, and COX-3 enzymes from producing prostaglandins. Due to its specificity, it minimally inhibits thromboxane synthesis. Unlike NSAIDs, acetaminophen does not inhibit cyclooxygenase in peripheral tissues because it is ineffective in the presence of high peroxide levels found in inflammatory lesions. This explains why acetaminophen is effective in the CNS and endothelial cells, but not in platelets and immune cells, which contain high peroxide levels.

Arachidonic acid is metabolized by the COX family of enzymes into prostaglandin H2, which is then converted into various other pro-inflammatory molecules. Acetaminophen reduces the synthesis of these pro-inflammatory chemicals by lowering the oxidized form of the COX enzyme. The reduced amount of PGE2 lowers the temperature by affecting the thermoregulatory center in the hypothalamus through peripheral vasodilation, sweating, and subsequent heat dissipation [3].

**4.4 Pharmacokinetics:**

After being taken orally, paracetamol is efficiently absorbed from the small intestine. Only about 25% of it binds to plasma proteins, and it is evenly distributed throughout the body. The apparent volume of distribution for paracetamol in humans is approximately 0.9 liters per kilogram of body weight. Paracetamol is primarily metabolized through conjugation with glucuronic acid and sulfates, and these metabolites are quickly eliminated in the urine. The plasma half-life of paracetamol is 2-3h., which coincides with the duration of its pharmacological effects [4].

**4.5 Uses:**

The uses of paracetamol are given below [4]

- Paracetamol is recommended as the first choice analgesic for osteoarthritis.
- One of the best recommended drug to be used as an antipyretic.
- Most commonly used over the counter drug for headaches, mild migration, musculoskeletal pain, etc.

**4.6 Adverse Effects:**

The adverse effects of paracetamol are listed below [5]

- Studies on paracetamol's cardiovascular effects are limited compared to NSAIDs. Some research shows paracetamol may raise blood pressure, potentially increasing heart disease and stroke risks. Observational studies often link long-term use to hypertension, but findings are inconsistent. Further research, including a current trial, is needed to clarify paracetamol's impact on blood pressure.
- Paracetamol is generally considered safer than NSAIDs for patients at risk of GI bleeding. Studies show it causes nausea and dyspepsia but not GI bleeding. However, higher doses (≥2-3 g/day) have been linked to increased GI bleeding risk. Recent studies found significant GI bleeding risk with doses >2 g/day, especially when combined with NSAIDs. Early trials showed no acute GI effects, but more recent research indicates potential occult GI blood loss at high doses. Thus, regular high-dose paracetamol use may pose a significant GI bleeding risk, which is amplified when combined with NSAIDs.
- Paracetamol's safety during pregnancy is debated due to its ability to cross the placenta and differing metabolism in neonates. Large cohort studies found no association between first-trimester use and adverse pregnancy outcomes. However, evidence suggests potential risks of neurodevelopmental disorders, respiratory illness, and reproductive toxicity.
- Use of paracetamol for more than 28 days during pregnancy correlated with issues in gross motor development, communication skills, externalizing and internalizing behavior, as well as increased activity levels, compared to the control group.
- Several studies have explored the potential link between maternal paracetamol use during pregnancy and neurodevelopmental issues in offspring. While some suggest

associations with hyperkinetic disorder, ADHD medications, and ADHD-like behaviors, others find weak links with autistic spectrum disorder. Mechanisms remain unclear, but animal studies suggest changes in brain-derived neurotrophic factor levels. However, these findings are limited by study design and confounding factors, suggesting cautious interpretation is needed regarding paracetamol's impact on neurodevelopment during pregnancy.

### 4.7 Interactions with other drug:

Interactions of paracetamol with other drugs include the following [6].

- Paracetamol increases the risk of bleeding when taken with oral anticoagulants like warfarin and warfarin analogue, possibly by affecting their metabolism.
- Carbamazepine and sulfinpyrazone increase the risk of paracetamol toxicity by enhancing the formation of harmful metabolites in the liver.
- Co-administration of paracetamol with zidovudine may lead to neutropenia or hepatotoxicity, although reports on these effects are inconsistent.
- The interaction between alcohol and paracetamol is particularly concerning. Long-term alcoholics taking paracetamol, even in non-toxic doses, may develop acute toxic liver symptoms, with a worse prognosis compared to non-alcoholics.
- Epileptic patients taking enzyme-inducing anticonvulsants such as phenytoin may experience lower bioavailability of paracetamol.
- Paracetamol enhances the urinary elimination of lamotrigine.
- A single 1000 mg dose of paracetamol has been found to raise the plasma levels of ethinylestradiol by 22%.

### 4.8 Rationality behind choosing Paracetamol as a model drug:

The Pharmacokinetics profile suggests that, to maintain a constant plasma concentration Paracetamol needs to be administered every 3-4 hours interval due to its short plasma half life. Moreover, Paracetamol is well absorbed from the gastrointestinal tract, has low toxicity at therapeutic levels, and a short half-life of about 3 hours, making it suitable for sustained release development.

**4.9 Literature review on Sustained release formulation with Paracetamol:**

Sami et al. reported development of hydrogels based on chitosan guar gum for sustained delivery of paracetamol [7]. A transdermal patch based on chitosan and guar gum was developed and characterized for physicochemical properties, antimicrobial activity, biocompatibility, and cytotoxicity using HeLa cells. Swelling in hydrogels, like those with chitosan, depends on factors like polymer amount and crosslinking. Swelling varies with pH due to protonation of functional groups. Hydrogels with chitosan and guar gum show highest swelling at acidic pH (3.5 g) and decrease at physiological pH (2.25 g) and basic pH (1.18 g). At acidic pH, increased proton concentration aids swelling, while at basic pH, decreased protonation reduces water absorption. This behavior is influenced by the interaction of $NH_2$ and OH groups with protons. The Paracetamol release from CS-GG hydrogel was monitored by measuring absorbance at 250 nm in 0.1 M Tris-Cl pH 7.4. The release follows a diffusion mechanism, where drug molecules diffuse from the polymer network, influenced by hydrogel porosity. A linear trend in Paracetamol release was observed in the buffer, with 3300 µg released within 150 minutes. This sustained release via CS-GG hydrogel suggests its potential for controlled drug delivery applications. Over all the antimicrobial activity, biocompatibility, and cytotoxicity study of the newly formulated transdermal patch of paracetamol proved as safe and novel delivery system.

Almurisi et al. developed paracetamol encapsulated chitosan coated alginate beads to mask the bitterness of paracetamol [8]. This study focused on masking paracetamol's bitterness and investigated the effectiveness of alginate microencapsulation for enhancing its palatability. The process involved optimizing chitosan-coated paracetamol alginate beads using electrospray to produce spherical beads smaller than 1.5mm. The encapsulation efficiency (EE) of the uncoated beads decreased over time, reaching 5 ± 1.32% after 60 minutes. However, chitosan coating significantly boosted EE to between 50% and 76%, depending on the type and concentration of chitosan used. Saturating the gelation bath with paracetamol further increased EE to 99.0 ± 1.1%. Paracetamol release from optimized wet or dry chitosan-coated alginate beads was studied in a gastric simulated buffer of pH 1.2. Chitosan-coated alginate beads typically enhance prolonged drug release in alkaline conditions, but paracetamol, being a highly soluble and permeable drug (Class I BCS), showed rapid release due to its solubility and the micronized nature of the powder. Comparing in vitro release profiles, wet beads and commercial suspension released paracetamol faster in the first 30 minutes compared to dry beads and chewable tablets. The release followed a first-order model and Fickian diffusion.

Wet beads had a release profile similar to the suspension, while dry beads resembled chewable tablets. Taste masking tests conducted in vitro, along with palatability evaluations involving 12 human volunteers, revealed that dry chitosan-coated paracetamol alginate beads were more effective than wet ones at masking taste, performing comparably to marketed paracetamol suspensions and even better in terms of aftertaste. This suggests that alginate microencapsulation with chitosan coating can reduce the need for sweetening and flavoring agents in pediatric formulations, allowing for the creation of dosage forms with fewer undesirable excipients.

**References**

[1] I. M. Iloamaeke, O. K. Iwuozor, Quality assessment of selected paracetamol tablets sold at bridge head market, Onitsha, Nigeria. Br. J. Pharm. Med Res.3(5)( 2018) 8.

[2] I. K. Ogemdi, A Review on the Properties and Uses of Paracetamol, Int. J. Pharm. Chem. 5(3) (2019) 31-35.

[3] M. Ahmed, R. P. Enever, Formulation And Evaluation of Sustained Release Paracetamol Tablets. J Clin Pharm Ther. 6 (1981) 27-38.

[4] K. D. Tripathi, Essentials of medical pharmacology, 6ed., Jaypee brothers medical publishers (P) Ltd., New Delhi, 2008.

[5] J. C. McCrae, E. E. Morrison , I. M. MacIntyre , J. W. Dear and D. J. Webb, Long-term adverse effects of paracetamol –a review, Br. J. Clin. Pharmacol. 84 (2018) 2218–2230.

[6] M. J. Toes, A. L. Jones, L. Prescott, Drug Interactions with Paracetamol, Am. J. Ther. 12 (2005) 56–66.

[7] A. J. Sami, M. Khalid, T. Jamil, S. Aftab, S. A. Mangat, A.R. Shakoori, S. Iqbal, Formulation of novel chitosan guargum based hydrogels for sustained drug release of paracetamol, Int. J. Biol. Macromol. 108 (2018) 324–332.

[8] S. H. Almurisi, Abd A. Doolaanea, M. E. Akkawi, B. Chatterjeed, Md Z. I. Sarker, Taste masking of paracetamol encapsulated in chitosan-coated alginate beads, J. Drug. Deliv. Sci. Technol. 56 (2020) 101520.

# Chapter 5

# AIM & OBJECTIVES

## AIM AND OBJECTIVES

Natural hydrophilic polysaccharides have become highly significant in drug and gene delivery, tissue engineering, and various biomedical applications due to their biocompatibility, biodegradability, affordability, availability, and regulatory approval. These polysaccharides are particularly useful in creating hydrogels, which are hydrophilic, cross-linked, three-dimensional polymer networks capable of retaining large amounts of water or biological fluids without dissolving. The versatility in chemical structure and functional groups of natural polysaccharides makes them ideal for hydrogel formulation.

Hydrogels are employed in various drug delivery systems, such as tablet matrices, microparticles, and microcapsules, where drugs can be dispersed or trapped within the hydrogel network. The release of the drug depends on the hydrogel's rigidity and physicochemical properties, with factors like viscosity, swelling, and erosion playing crucial roles in controlling drug dissolution rates.

Cross-linking is a key technique to control the expansion and rigidity of hydrogel networks. By adjusting the degree of cross-linking, scientists can influence the swellability, viscosity, and erosion characteristics of hydrogels, thus modulating drug release. Cross-linking can be ionic or covalent. Ionic cross-linking, which involves anionic polysaccharides and metal cations in eco-friendly conditions, is mild and reversible. In contrast, covalent cross-linking, which uses organic solvents, is strong and irreversible. The extent of cross-linking can be fine-tuned by altering the reactive functional groups in the polysaccharide structure, the concentration of the cross-linking agent, and the cation's valency in ionic cross-linking.

Based on the above hypothesis, the specific objectives of the research work are:

- Preparation of the standard curve of paracetamol in different medium (pH- 1.2 and pH 7.4 buffer system)
- Synthesis of carboxymethyl Taragum.
- Development, evaluation and optimisation of $Al^{3+}$/ $Fe^{3+}$ cross-linked CMTG core hydrogel microparticles.
- Development, evaluation and optimisation of single cross-link coated core hydrogel microparticles.
- Development, evaluation and optimisation of double cross-link coated hydrogel microparticles.

- Determination of size, volume and viscosity of the hydrogel microparticles.
- Performing the swelling study and *in-vitro* drug dissolution study of the microparticles.
- Determining mean dissolution time of drug release.
- Performing drug release kinetics study.

The overall objective of the research work is to develop and evaluate Borax-$Fe^{3+}$-CMTG hydrogel coated CMTG hydrogel microparticles for sustained gastrointestinal dissolution of water-soluble drug.

# Chapter 6

# ANALYTICAL MONITORING OF DRUG

## 6. ANALYTICAL MONITORING OF PARACETAMOL

### 6.1. Preparation of 0.1 (N) HCl solution (acid solution of pH 1.2)

A total volume of 8.5 ml HCl was carefully measured and added to a volumetric flask initially containing 200 ml of distilled water. Further distilled water was added to reach a total volume of 1000 ml. pH meter (Orion 2-Star, Thermo Scientific, US) was used to adjust the pH of the resulting solution at pH 1.2.

### 6.2. Preparation of 0.2 (M) tri sodium phosphate dodecahydrate (TSP)

76 grams of TSP were measured and placed into a volumetric flask already containing 500 ml of distilled water. Additional distilled water was added to reach a total volume of 1000 ml in the flask.

### 6.3. Preparation of modified phosphate buffer (MPB) solution of pH 7.4

A solution consisting of 200 ml of 0.2 (M) tri-sodium orthophosphate dodecahydrate was introduced into a 700 ml acid solution with a pH of 1.2 to get 900 ml solution with pH 7.4.

### 6.4. Determination of $\lambda_{max}$ of Paracetamol in acid solution of pH 1.2

10 mg of Paracetamol were dissolved in 10 milliliters of pH 1.2 solution, and the volume was increased to 100 milliliters using an acid solution with a pH of 1.2. From this solution, 2 milliliters were taken and diluted to 25 milliliters using an acid solution with a pH of 1.2. The resulting solution was then scanned from 200 to 400 nanometers using a UV Spectrophotometer (UV 2450, Shimadzu, Japan).

### 6.5. Determination of $\lambda_{max}$ of Paracetamol in phosphate buffer (PB) solution of pH 7.4

10 mg of Paracetamol were dissolved in 10 milliliters of pH 7.4 solution, and the volume was increased to 100 milliliters using a phosphate solution with a pH of 7.4. From this solution, 2 milliliters were taken and diluted to 25 milliliters using an phosphate buffer solution with a pH of 7.4. The resulting solution was then scanned from 200 to 400 nanometers using a UV Spectrophotometer (UV 2450, Shimadzu, Japan).

### 6.6. Method development for the estimation of Paracetamol in acid solution of pH 1.2

Precisely, 3 milligrams of Paracetamol were dissolved in 300 milliliters of pH 1.2 solution in a 250 milliliter volumetric flask. Subsequently, aliquots of 1, 2, 3, 4, 5, milliliters were withdrawn from this stock solution and diluted upto 10 milliliters with acid solution.

Absorbance measurements were conducted at 243 nanometers for each dilution. The observations were recorded three times (Table.6.1). The Fig.6.1. show the calibration curve of Paracetamol in pH 1.2 solution.

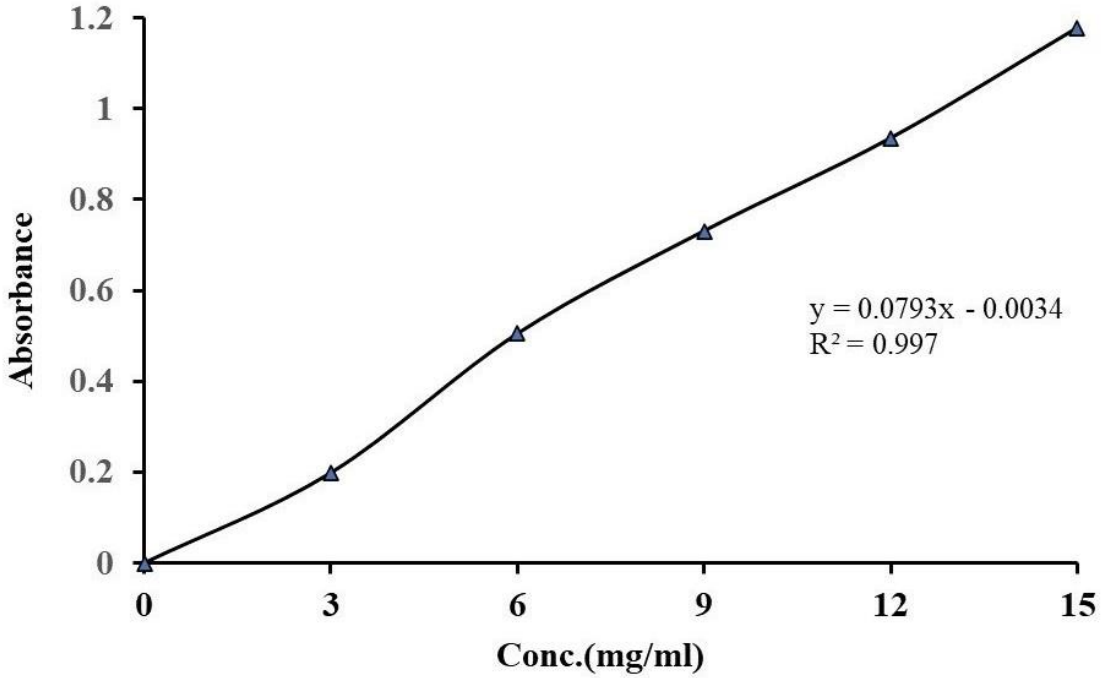


Fig. 6.1. Paracetamol standard curve in pH 1.2.

Table.6.1. Absorbance values in different concentrations of paracetamol in pH 1.2 buffer solutions for the preparation of standard curve.

| Conc. (mg/ml) | Abs.1 | Abs.2 | Abs.3 | Abs.4 | Abs.5 | Abs.6 | Average Abs. |
|---|---|---|---|---|---|---|---|
| 0 | 0 | 0 | 0 | 0 | 0 | 0 | 0 |
| 3 | 0.198 | 0.199 | 0.196 | 0.203 | 0.2 | 0.195 | 0.1985 |
| 6 | 0.504 | 0.504 | 0.505 | 0.504 | 0.506 | 0.506 | 0.5048 |
| 9 | 0.726 | 0.731 | 0.731 | 0.73 | 0.73 | 0.736 | 0.7306 |
| 12 | 0.931 | 0.94 | 0.933 | 0.943 | 0.93 | 0.934 | 0.9351 |
| 15 | 1.169 | 1.179 | 1.18 | 1.181 | 1.179 | 1.178 | 1.1776 |

### 6.7. Method development for the estimation of Paracetamol in PB solution of pH 7.4

Precisely, 3 milligrams of Paracetamol were dissolved in 300 milliliters of pH 7.4 solution in a 250 milliliter volumetric flask. Subsequently, aliquots of 1, 2, 3, 4, 5 milliliters were

withdrawn from this stock solution and diluted upto 10 milliliters with acid solution. Absorbance measurements were conducted at 243 nanometers for each dilution. The observations were recorded three times (Table.6.2). The Fig.6.2. show the calibration curve of Paracetamol in pH 7.4 solution.

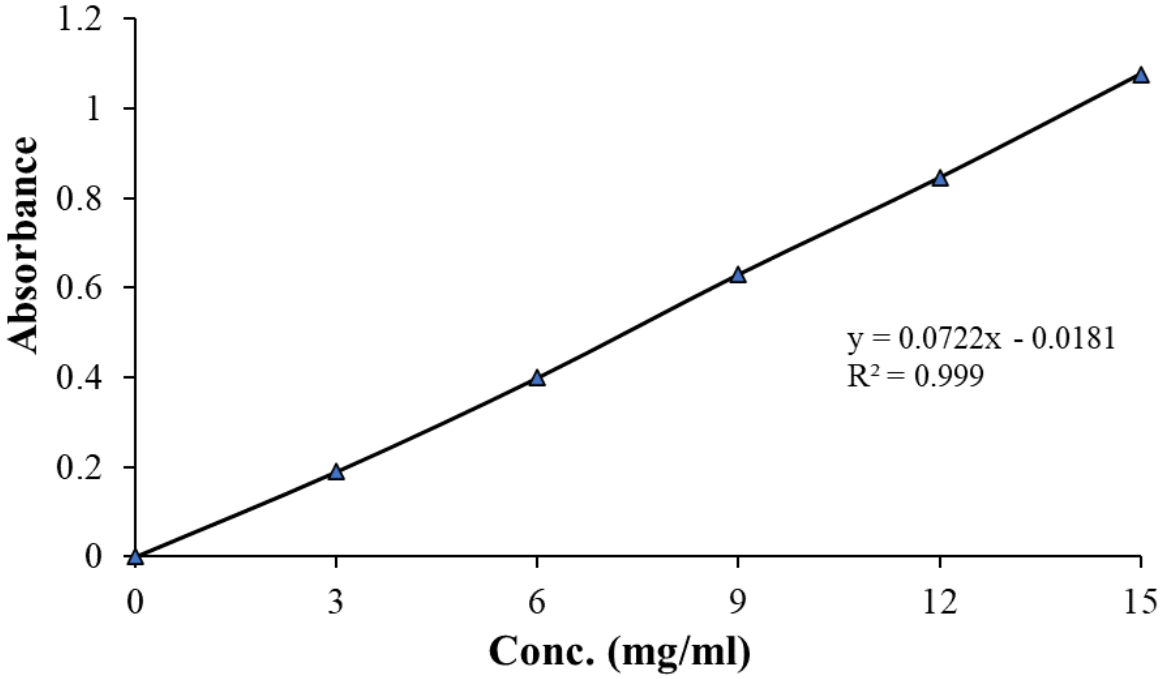


Fig. 6.2. Paracetamol standard curve in pH 7.4.

Table. 6.2. Absorbance values in different concentrations of paracetamol in pH 7.4 buffer solutions for the preparation of standard curve.

| Conc. (mg/ml) | Abs.1 | Abs.2 | Abs.3 | Abs.4 | Abs.5 | Abs.6 | Average Abs. |
|---|---|---|---|---|---|---|---|
| 0 | 0 | 0 | 0 | 0 | 0 | 0 | 0 |
| 3 | 0.197 | 0.189 | 0.186 | 0.184 | 0.19 | 0.191 | 0.1895 |
| 6 | 0.395 | 0.398 | 0.399 | 0.401 | 0.399 | 0.402 | 0.399 |
| 9 | 0.627 | 0.633 | 0.629 | 0.633 | 0.625 | 0.63 | 0.6295 |
| 12 | 0.844 | 0.848 | 0.844 | 0.85 | 0.842 | 0.844 | 0.8453 |
| 15 | 1.079 | 1.077 | 1.075 | 1.079 | 1.078 | 1.07 | 1.0763 |

# Chapter 7

# METERIALS AND METHODS

## 7. MATERIALS AND METHODS

### 7.1. Materials:

Paracetamol (PCL) was procured from Loba Chemie Pvt. Ltd, India. Tara gum was purchased from IAMPURE INGREDIENTS, Chennai, India. Monochloro acetic acid (MCA), Ferric Chloride ($FeCl_{3)}$, Di-Sodium tetra borate, methanol, Sodium hydroxide (NaOH), Aluminium Chloride ($AlCl_3$), hydrochloric acid (HCl), tri-sodium orthophosphate dodecahydrate (TSP) and magnesium stearate were obtained commercially from Merck, Mumbai, India.

### 7.2. Synthesis of carboxymethyl tara gum:

Chemical modification of TG to CMTG was done as per previously published method [1]. Initially, 5 grams of TG were dispersed in freezing deionized water alongside 10 grams of NaOH, allowing complete hydration without agitation. The temperature was then raised to 60°C and sustained. Subsequently, a solution of monochloroacetic acid (1 gram dissolved in 2 ml of water) was gradually introduced with continuous stirring over 30 minutes. Following this, methanol was added to induce precipitation of the carboxymethylated gum. The resulting product underwent washing with 90% v/v methanol solution. After air drying to a constant weight, the material was worked through #72 meshes and stored in desiccators for future applications. The degree of substitution (DS) of CMTG was determined using potentiometric back titration, employing the following equation [2] :

$$DS = 0.162P/(1 - 0.058P)$$

Here, P represents the NaOH required per gram of gum.

### 7.3. Preparation of core hydrogel microparticles:

25% w/w PCL was solubilised in 10 ml distilled water. 3% CMTG was sprinkled to the drug solution with continuous stirring. The resulting uniform CMTG dispersion containing PCL was added dropwise using 22 G flat-tipped needle into a gently stirred aqueous solution of FeCl3 (Table 7.1). After 5 minutes of gelation time the formed microparticles were separated by straining, air dried and kept in desiccators for future use. Preparation of core hydrogel microparticles is depicted in Fig. 7.1.

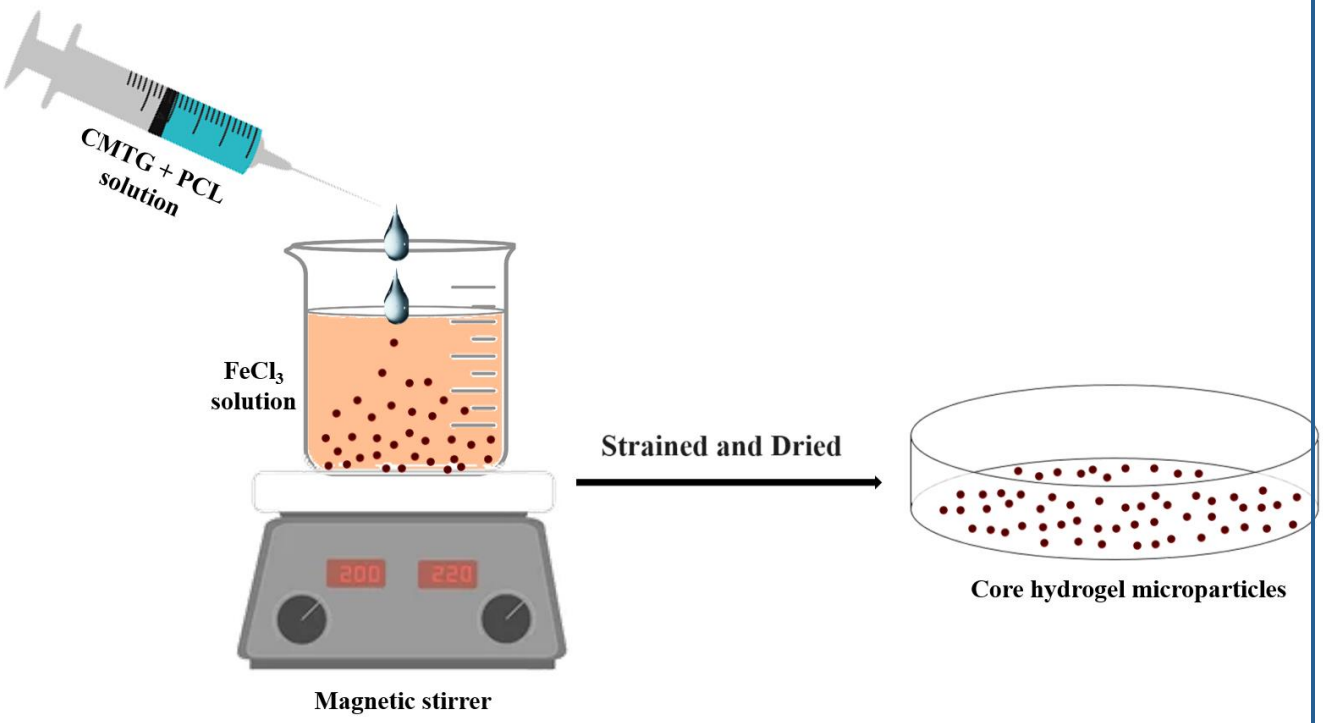


Fig. 7.1. Preparation of core hydrogel microparticles.

### 7.4. Preparation of coated hydrogel microparticles:

Immediately after separation of the core hydrogel microparticles, they were coated with single and double cross-linked CMTG solutions to obtain hydrogel microparticles coated with hydrophilic hydrogel layer (Fig. 7.2). For preparation of the single cross-linked hydrogel coatings over the core hydrogel microparticles, the obtained core hydrogel microparticles were gently soaked in tissue paper to absorb the water from the surface and then sprayed uniformly with CMTG solutions of different concentrations (Table 7.1), then dipped in $FeCl_3$ solutions, kept for 5 minutes and then separated by straining as usual (Fig.7.2A). For preparation of the double cross-linked hydrogel coatings over the core hydrogel microparticles, borax was added in different concentrations into the $FeCl_3$ solutions and the microparticles were kept there for 5 minutes. They were then separated, air dried and kept in desiccators for further use (Fig. 7.2B)

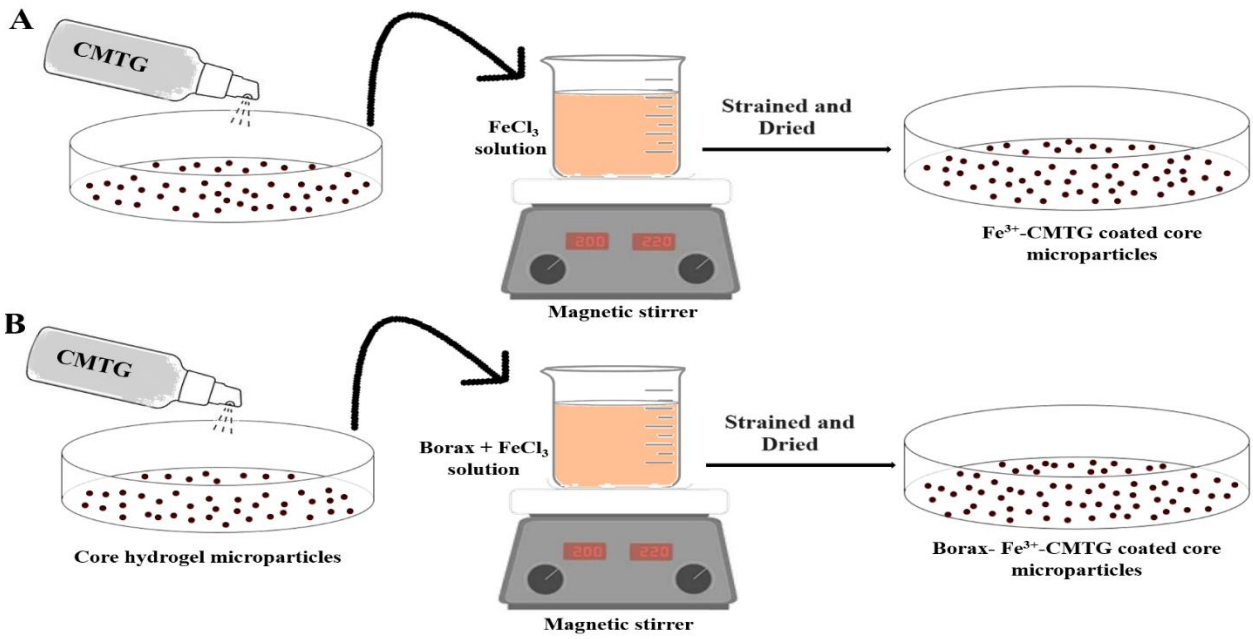


Fig. 7.2. Preparation of coated hydrogel microparticles.

Table 7.1. Composition of hydrogel microparticles.

| | Core microparticles | | | Single cross-link coated | | Double cross-link coated |
|---|---|---|---|---|---|---|
| Formulation code | Conc. of CMTG (% w/v) | Conc. of $AlCl_3$ (% w/v) | Conc. of $FeCl_3$ (% w/v) | Conc. of CMTG (% w/v) | Conc. of $FeCl_3$ (% w/v) | Conc. of Borax (% w/v) |
| F1 | 3 % | 1% | - | - | - | - |
| F2 | 3 % | 2% | - | - | - | - |
| F3 | 3 % | 3% | - | - | - | - |
| F4 | 3 % | - | 1% | - | - | - |
| F5 | 3 % | - | 2% | - | - | - |
| F6 | 3 % | - | 3% | - | - | - |
| F7 | 3 % | - | 3% | 0.5% | 1% | - |
| F8 | 3 % | - | 3% | 1% | 1% | - |
| F9 | 3 % | - | 3% | 1.5% | 1% | - |
| F10 | 3 % | - | 3% | 1.5% | 1.5% | - |
| F11 | 3 % | - | 3% | 1.5% | 2% | - |
| F12 | 3 % | - | 3% | 1.5% | 2% | 0.25% |
| F13 | 3 % | - | 3% | 1.5% | 2% | 0.5% |
| F14 | 3 % | - | 3% | 1.5% | 2% | 0.75% |
| F15 | 3 % | - | 3% | 1.5% | 2% | 1% |

### 7.5. Fourier Transform Infrared (FTIR) analysis:

The FTIR spectrums of TG, CMTG, PCL, and the double cross-linked coated hydrogel microparticle containing PCL was obtained from an FTIR spectrophotometer (RX 1, Perkin Elmer, UK). Sample preparation included blending the samples with potassium bromide and then forming them into pellets using a hydraulic press. The operation range was 4000–400 $cm^{-1}$.

### 7.6. X-ray diffraction (XRD) study:

The X-ray diffraction pattern of PCL, TG, CMTG and the double cross-linked coated hydrogel microparticles containing PCL was performed by X-ray diffractometer (D8, Bruker, Germany) at diffraction angle (2θ) 10–80º and scan speed 5º/min.

### 7.7. Differential scanning calorimetry (DSC) study:

DSC thermograms of PCL, CMTG, and PCL-loaded double cross-linked coated hydrogel microparticles were observed using a DSC (Pyris Diamond TG/DTA, Perkin Elmer, Singapore). The equipment was calibrated using indium as a reference. Samples were enclosed in a sealed aluminum container and subjected to heating from 30ºC to 400°C at an increment of 10°C/min, with a continuous flow of nitrogen.

### 7.8. Estimation of drug entrapment efficiency (DEE):

25 mg microparticles were weighed and immersed in 10 ml of pH 7.4 buffer solution. After 3 hours, the microparticles were crushed using mortar and pestle and were allowed to shake overnight by using mechanical shaker. Then the residue was filtered and transferred in 250 ml of pH 7.4 buffer solution. Following suitable dilution, the samples were analysed with a spectrophotometer (UV 2450, Shimadzu, Japan) at λmax 243 nm. The amount of PCL in the microparticles were then determined from the calibration curve drawn at the respective buffer media. Each DEE estimation was triplicated. The DEE was calculated according to the following equation.

DEE=((Actual amount of drug )/(Theoritical drug loading))×100……(1)

### 7.9. Determination of size of hydrogel microparticles:

The diameter (millimetres, mm) of the hydrogel microparticles was measured with the help of slide calipers (CD-6CSX, Mitutoyo, Japan). Randomly 10 microparticles were taken and the

diameter of each microparticle was recorded and the radius (r) of each microparticle was calculated.

**7.10. Determination of the volume of hydrogel microparticles:**

The volume of blank hydrogel microparticles was determined by using slide calipers (CD-6CSX, Mitutoyo, Japan). The diameter of the completely dry microparticles was measured accurately in mm and then submerged in dissolution media (pH 1.2). Further, the pH was adjusted to pH 7.4 at 2 h. At definite time gap of 2 h, 4 h, 6 h and 7 h the microparticles were meticulously taken out from the dissolution media and the diameter of the microparticles were again precisely measured, following which the microparticles were again submerged to the same dissolution solution. The volume of the microparticles was calculated from the following formula.

$$V=4/3\pi r^3 \ldots\ldots\ldots\ldots\ldots\ldots\ldots\ldots(2)$$

Where, V is the volume of the microparticles with radius r.

**7.11. Swelling study:**

Swelling study of blank microparticles were done in USP type II dissolution machine. The experiment was conducted in pH 1.2 buffer solution (700 ml) for 2 hours and then in pH 7.4 buffer solution (900 ml) for next 6 hours. 15 mg blank microparticles were weighed and sealed in a tea-bag and immersed into dissolution media.[3] Every one-hour interval the tea-bag assembly was taken out, thoroughly blotted with the help of tissue paper, weighed on a digital balance and re-immersed in that same dissolution media. The swelling percentage was determined by using Eq. (3).[4]

$$\% \text{ swelling} = (W_f - W_i)/W_i * 100 \ldots\ldots\ldots\ldots\ldots\ldots\ldots\ldots(3)$$

Where $W_f$ denotes the swollen weight of blank hydrogel microparticles at time t (when it was taken out from dissolution solution) and $W_i$ denotes the weight of microparticles at the beginning.

**7.12. In-vitro PCL dissolution:**

The dissolution of PCL (at 37 ± 0.5℃, 75 rpm) was carried out in a paddle type dissolution machine. 25 mg microparticles were kept in 700 ml of pH 1.2 buffer solution and after 2 hours, the buffer was changed to pH 7.4 by adding 200 ml of TSP solution, for further 10 hours of dissolution study. At hourly intervals, 10 ml of the aliquot was taken from the dissolution

medium and equivalent volume of fresh solution was refilled instantly. The samples were analysed under UV spectrophotometer (UV2450, Shimadzu, Japan) at 243 nm. The amount of PCL dissolution from the microparticles were then determined from the calibration curve drawn at the respective buffer media. Each batch of the dissolution study was triplicated.

**7.13. Release kinetics:**

The PCL release mechanism from the microparticles and the kinetics were determined by using the power law equation Eq. (4).[5]

$$M_t/M_\infty = kt^n \ldots\ldots\ldots\ldots\ldots\ldots\ldots\ldots (4)$$

Where Mt/Mα denotes the portion of PCL dissolved at time t, k is rate constant, n signifies the diffusional exponent. When n = 0.43 it represents Fickian diffusion, 0.43 < n < 0.85 is indicative of anomalous or non-Fickian transport, n = 0.85 stands for case II and values of n > 0.85 represents super case II transport mechanisms [5].

**7.14. Mean Dissolution Time (MDT):**

Eq. (5) is used to determine the MDT (min). The values of k and n were extracted from the power law Eq. 4. [6]

$$MDT=(n/(n+1))\ K^{(-1/n)} \ldots\ldots\ldots\ldots\ldots..(5)$$

**7.15. Determination of viscosity of hydrogel microparticles:**

Dispersions mimicking the microparticle formulations were prepared and the viscosity of the dispersions were measured using viscometer (Modular Compact Rheometer, MCR 102, Anton Paar, Austria).

**7.16. Scanning electron microscopy (SEM) study of hydrogel microparticles:**

The surface microstructures of selected hydrogel microparticles were observed in a scanning electron microscope (SU3800, Hitachi, Japan) at 10 kV voltages. For microscopic analysis, the microparticles were dried, and secured onto stubs and then gold-sputter coated to render them electrically conductive.

**7.17. Statistical analysis:**

ANOVA was carried out in GraphPad Prism (Version 3.0) to calculate the statistical relevance of the data gathered from swelling, DEE, and PCL dissolution studies. The significance of the data was reckoned when $p < 0.05$.

**References**

[1] K. Mukherjee, P. Dutta, T. K. Giri, $Al^{3+}/Ca^{2+}$ cross-linked hydrogel matrix tablet of etherified tara gum for sustained delivery of tramadol hydrochloride in gastrointestinal milieu. Int. J. Biol. Macromol. 2023;232:123448.

[2] H. Gong, M. Liu, J. Chen, F. Han, C. Gao, Zhang B. Synthesis and characterization of carboxymethyl guar gum and rheological properties of its solutions. Carbohydr. Polym. 2012;88:1015–1022.

[3] P. Dutta, K. Mukherjee, T. K. Giri, Methacrylic acid grafted inulin and carboxymethyl cellulose as additives in the development of pH sensitive hydrogel matrix for colon targeting, J. Vinyl Addit. Technol. 2024;1–18.

[4] S. Maity, B. Sa, Ca-carboxymethyl xanthan gum mini-matrices: swelling, erosion and their impact on drug release mechanism. Int. J. Biol. Macromol. 2014;68:78–85.

[5] R. W. Korsmeyer, R. Gurny, E. Doelker, P. Buri, N. A. Peppas, Mechanism of solute release from porous hydrophilic polymers. Int. J. Pharm.1983;15:25–35.

[6] J. E. M¨ockel , B. C. Lippold, Zero-order drug release from hydrocolloid matrices. Pharm. Res. 1993;10:1066–1070.

# Chapter 8

# RESULTS AND DISCUSSION

## 8. RESULT AND DISCUSSION

The synthesis and characterisation of CMTG has been reported in our previous article [1].

### 8.1. Compatibility of PCL in the hydrogel microparticles:

The FTIR analysis of PCL revealed specific vibrational features (Fig.8.1). Notably, peaks were observed at 3325 $cm^{-1}$ indicating stretching vibrations of O–H, peaks at 1653 $cm^{-1}$ was attributed to stretching vibrations of C=O while the N–H amide II bending manifested peak at 1568 $cm^{-1}$. C–N (aryl) stretching was discernible by absorption peaks ranging from 1258 $cm^{-1}$ to 1224 $cm^{-1}$. Moreover, characteristic features of a para-disubstituted aromatic ring is visible at 807 $cm^{-1}$ [2]. Almost similar peaks are found in PCL-loaded hydrogel microparticles which indicates that drug is unreacted in the formulation matrix.

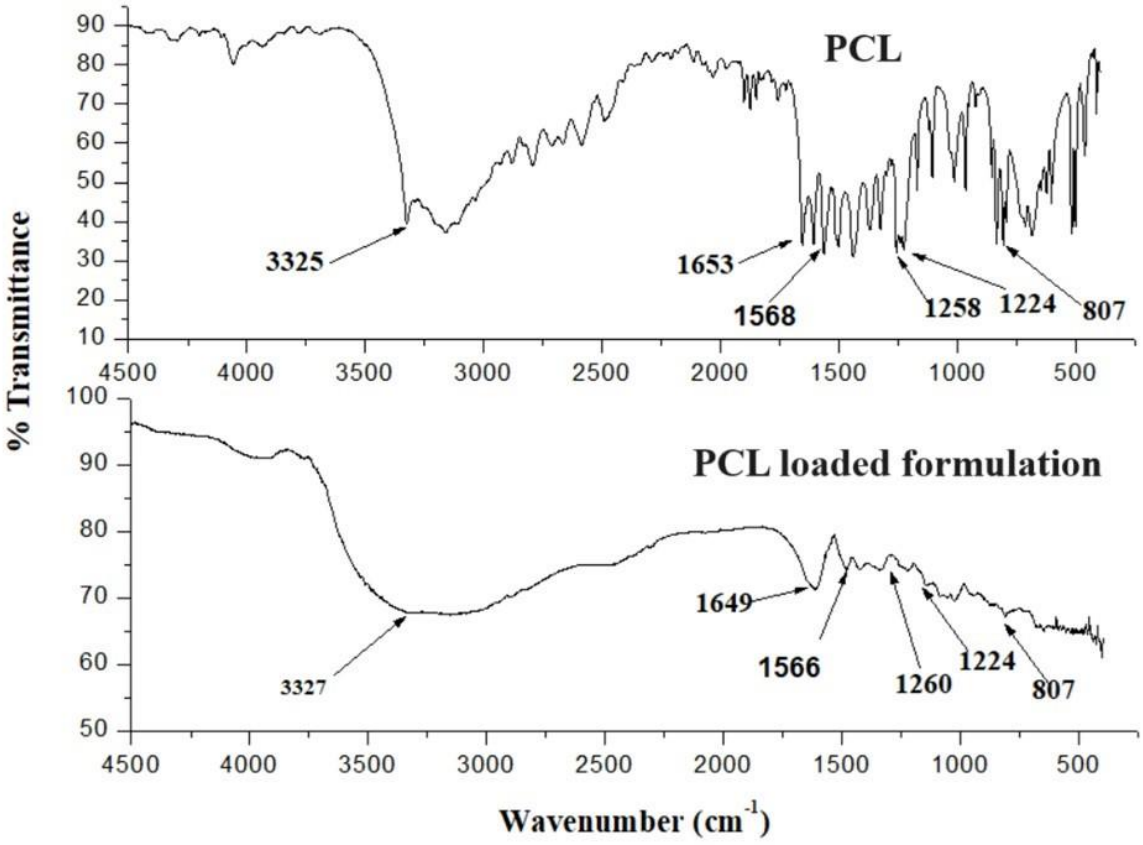


Fig.8.1. FTIR spectra of PCL and PCL loaded formulation.

DSC thermogram of pure PCL and PCL loaded borax-$Fe^{3+}$-CMTG hydrogel microparticles are shown in Fig. 8.2. In the figure, it is observed that paracetamol exhibits a prominent endothermic peak at 183°C which indicates the PCL melting point, along with another endothermic peak at 308°C which likely indicates paracetamol degradation, as reported

previously [3,4]. The PCL loaded hydrogel microparticle displays an endothermic peak at 70℃ due to moisture loss and another exothermic peak starting from 260℃ to 275℃ indicates the decomposition of CMTG. Similar results were found in previous experiment [5,6]. The disappearance of a sharp endotherm of PCL in the DSC thermogram of the PCL containing hydrogel microparticles indicates that PCL was completely dissolved in CMTG matrix and exists as an amorphous solid. Similar result was observed by Bounabi et. al. while formulating PCL loaded poly(2-hydroxyethyl methacrylate) clay composite [7].

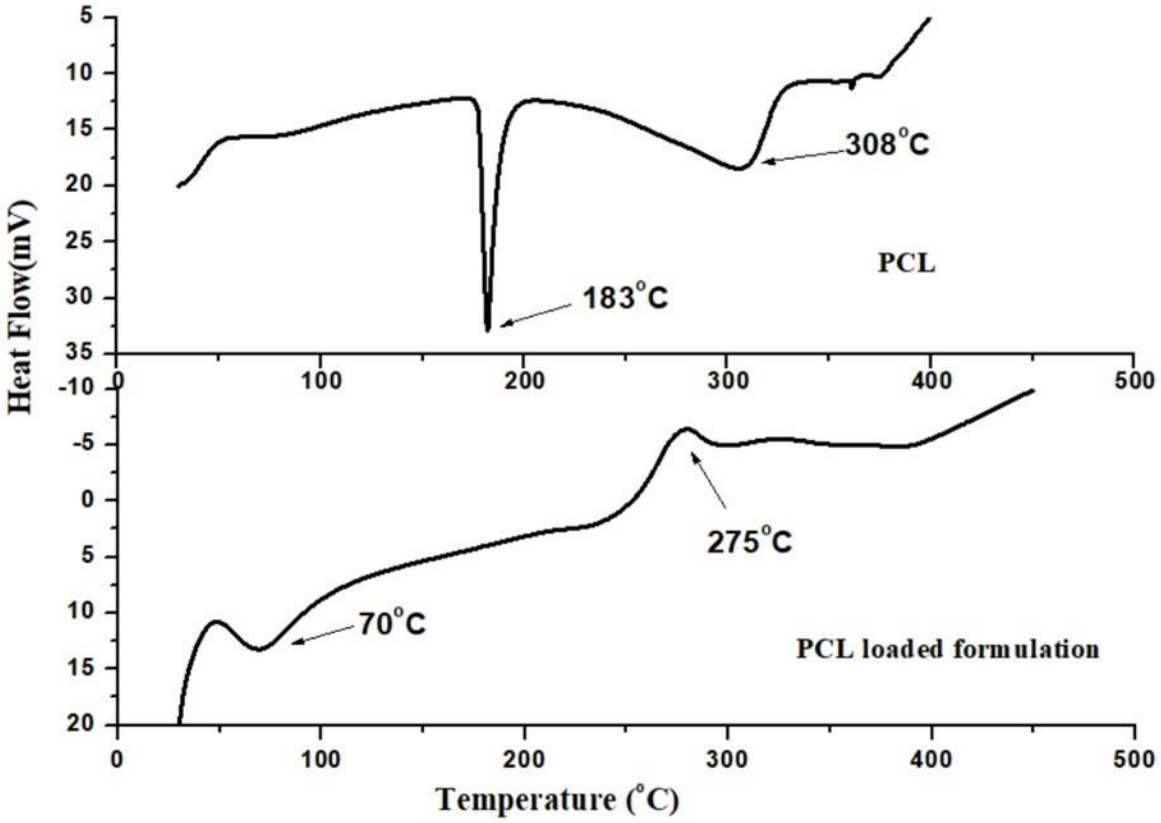


Fig.8.2. DSC thermograms of PCL and PCL loaded hydrogel microparticles.

The XRD pattern of pure PCL and PCL containing borax-$Fe^{3+}$-CMTG hydrogel microparticles are shown in Fig.8.3. For the analysis of pure PCL, X-ray diffraction data was recorded across a range of scattering angles, specifically 15.56, 18.14, 23.45, 24.32, and 26.47º 2θ angle and their intensities are 2601.46, 2120.61, 2191.70, 2756.76 and 1443.29 respectively. Similar XRD pattern of PCL was reported previously [8]. However, in the XRD pattern of the hydrogel

microparticle containing PCL, no such peaks are observed, which indicates the complete conversion of PCL to amorphous form.

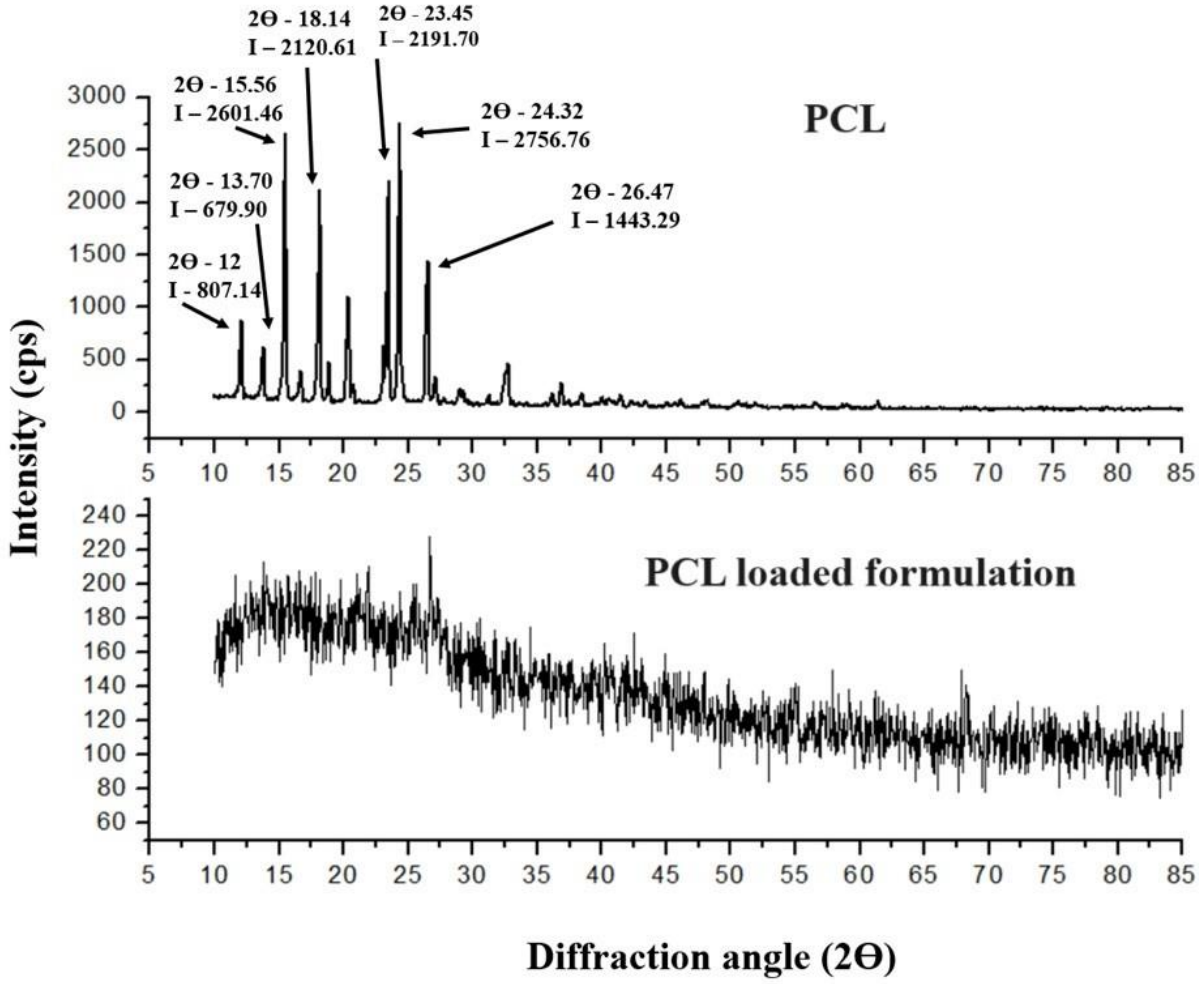


Fig.8.3. XRD pattern of PCL and PCL loaded hydrogel microparticles.

**8.2. Development of hydrogel microparticles:**

The hydroxyl groups (-OH) of TG was substituted with o-carboxymethyl groups under simple, mild alkaline conditions [1]. These carboxymethyl groups can react (cross-link) with mono, di, and trivalent metal ions to form water insoluble hydrogels by the process of ionotropic gelation [9]. The interaction between the carboxymethyl groups and monovalent ions are feeble and mild, and the hydrogel formed is not stable and immediately solubilizes [10]. However, the interaction between di and trivalent metal ions are strong and gives rise to stable hydrogels which are extensively used in the formulation of hydrogel microparticles, microcapsules, and tablet matrices [11].

When CMTG solutions was dropped into sodium chloride solutions of different concentrations using a #22-gauge needle, the cross-linking solution immediately turns turbid and within few seconds again turns clear. This indicated that gelation took place, but was weak and feeble. Similarly, when CMTG solutions (1% w/v- 3% w/v) was dropped separately into barium chloride and calcium chloride solutions (1% w/v-2% w/v), it formed somewhat tail-like and elongated hydrogel which solubilizes within 5-10 min. At 3% w/v concentration of the cross-linking solutions, spherical and isolatable hydrogel microparticles were formed which were stable until separated from the solution. After 5 min of gelation, the spherical hydrogel microparticles were separated from the cross-linking solutions for air drying. However, when the hydrogel microparticles were air dried, it gradually flattened and lost its spherical shape and when fully dried, it took the shape of round disc like structures. CMTG solutions (1% w/v-3% w/v) was then dropped into aluminium chloride solutions (1% w/v- 3% w/v). It immediately formed spherical microparticles which retained its spherical shape not only in the cross-linking solution but also after complete air drying. Based on the above observations, $AlCl_3$ was selected as the cross-linking agent for development of the hydrogel microparticles. Moreover, it seems from visual observation that the hydrogel microparticles became strong and hard with the elevation in the concentration of CMTG solution from 1% w/v to 3% w/v. Beyond the concentration of 3% w/v, CMTG solution became too viscous to be extruded from the #22-guage needle. 3% w/v CMTG solution was thus taken for further development and evaluation.

$Al^{3+}$ cross-linked CMTG hydrogel microparticles were prepared at different concentration of the cross-linking ions (1% w/v $AlCl_3$, F1; 2% w/v $AlCl_3$, F2; 3% w/v $AlCl_3$, F3). PCL loading was 25% w/w of the total polymer and the gelation time was 5 min, in all hydrogel microparticles. $Al^{3+}$ ions imparted significant effects on various parameters of the hydrogel microparticles. Elevation in the $AlCl_3$ concentration decreased the drug entrapment efficiency (DEE) of the microparticles ($p<0.05$) (Table 2). The microparticle size also decreased with the elevation in the concentration of the cross-linking ions ($p<0.05$) (Table 8.1). The *in-vitro* PCL dissolution from $Al^{3+}$-CMTG hydrogel microparticles F1-F3 were conducted in acid solution pH 1.2 for 2 h and then in pH 7.4 until complete dissolution. The results of the dissolution study are shown in Fig.8.4. Elevation in the concentration of the $AlCl_3$ solution from 1% w/v to 3% w/v produced significant changes in the PCL dissolution pattern. The PCL dissolution from the hydrogel microparticles decreased significantly with the elevation in the concentration of the $AlCl_3$ solution ($p<0.05$). The hydrogel microparticles gave a burst PCL dissolution of 82% (F1, containing 1% w/v $AlCl_3$), 72% (F2, containing 2% w/v $AlCl_3$), and 66% (F3,

containing 3% w/v $AlCl_3$) immediately following 30 min of PCL dissolution. The PCL dissolution was gradual and uniform after the burst dissolution. The PCL dissolution from F1 hydrogel microparticles was 94% at the end of 2 h, which decreased to 91% for F2 hydrogel microparticles, and further decreased to 88% for F3 hydrogel microparticles ($p<0.05$). MDT for hydrogel microparticles F1- F3 also increased with the elevation in the concentration of the $AlCl_3$ solution ($p<0.05$) (Table 2).

Table 8.1 Hydrogel microparticles parameters.

| Formulation code | Radius of microparticles (mm) (mean ± SD, n=10) | DEE (%) (mean ± SD, n=3) | MDT (hrs) (mean ± SD, n=3) |
|---|---|---|---|
| F1 | 0.701 ± 0.21 | 48.85 ± 4.75 | 0.53 ± 0.02 |
| F2 | 0.691 ± 0.04 | 46.49 ± 2.46 | 0.68 ± 0.09 |
| F3 | 0.684 ± 0.02 | 39.78 ± 1.67 | 0.88 ± 0.18 |
| F4 | 0.558 ± 0.01 | 46.49 ± 3.27 | 1.08 ± 0.06 |
| F5 | 0.473 ± 0.04 | 43.34 ± 1.68 | 2.01 ± 0.25 |
| F6 | 0.434 ± 0.23 | 42.55 ± 1.28 | 2.51 ± 0.12 |
| F7 | 0.448 ± 0.13 | 42.28 ± 2.04 | 2.71 ± 0.08 |
| F8 | 0.492 ± 0.17 | 41.63 ± 3.84 | 3.07 ± 0.06 |
| F9 | 0.499 ± 0.05 | 42.01 ± 4.16 | 3.58 ± 0.12 |
| F10 | 0.475 ± 0.21 | 41.87 ± 2.45 | 3.78 ± 0.11 |
| F11 | 0.458 ± 0.11 | 41.68 ± 3.53 | 4.76 ± 0.10 |
| F12 | 0.451 ± 0.08 | 40.40 ± 3.88 | 6.25 ± 0.04 |
| F13 | 0.441 ± 0.06 | 41.01 ± 1.52 | 6.60 ± 0.14 |
| F14 | 0.438 ± 0.12 | 41.24 ± 2.24 | 7.05 ± 0.07 |
| F15 | 0.417 ± 0.09 | 41.18 ± 1.21 | 7.40 ± 0.08 |

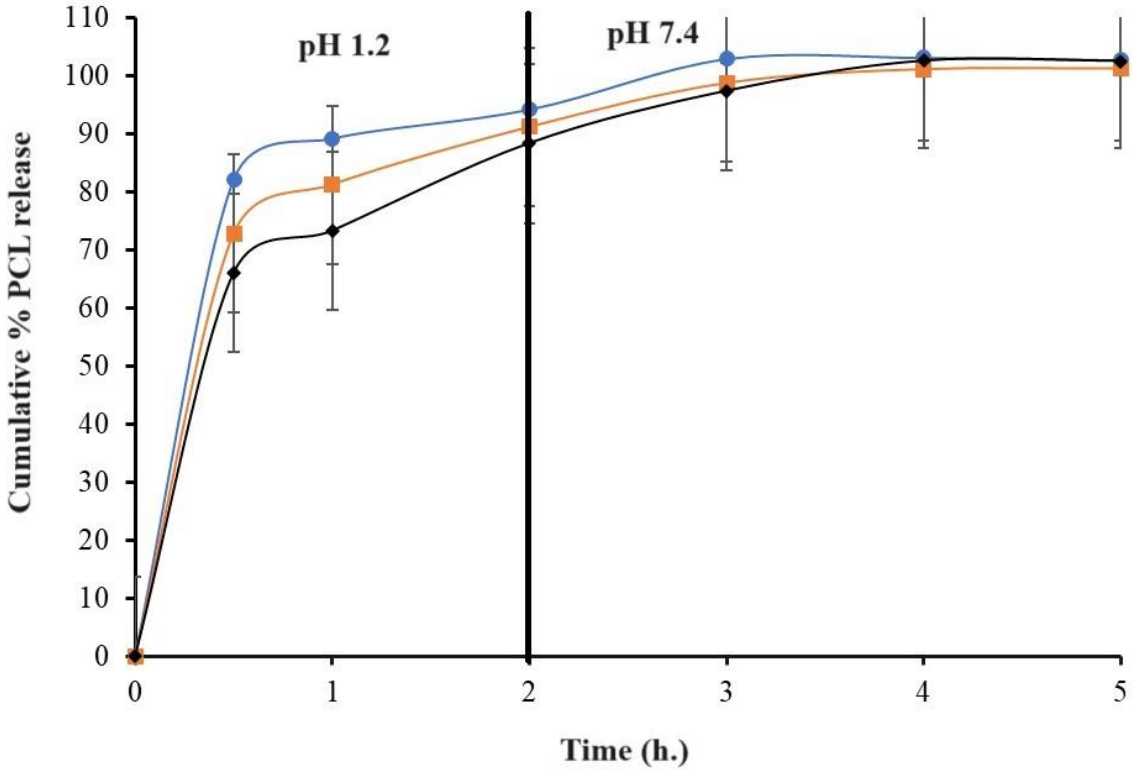


Fig 8.4. *In-vitro* PCL dissolution from $Al^{3+}$ cross-linked hydrogel microparticles. $AlCl_3$ % (w/v): 1% (F1, ● ) , 2% (F2, ■), 3% (F3, ◆), (mean ± S.D ; n=3).

When CMTG solution was dropped into $AlCl_3$ solution, the $Al^{3+}$ ions and the available COOH grours of the CMTG reacted and cross-linked the CMTG polymeric chains. Literature reports identical ionic cross-link between $Al^{3+}$ ions and COOH groups of different anionic polymers for the development of hydrogels [11,12]. This ionic cross-link restricts the mobility of the CMTG polymeric chains and facilitates the growth of thick and highly viscous hydrogel layer [13]. Elevation in the concentration of the $Al^{3+}$ ions elevates the cross-link density and induces superior gel strength [14]. This high gel strength reduces the polymeric chains mesh size and generates a compact and tightly bound gel layer. This is the reason behind decrease in the hydrogel microparticles size with the elevation in the concentration of the $Al^{3+}$ ions. Decrease in the hydrogel microparticles size with the elevation in the concentration of the cross-linking solution have been documented earlier [15]. Elevation in the rigidity and viscosity of the hydrogel microparticles is supposed to decrease the leaching of PCL from the hydrogel microparticles, thereby enhancing the DEE of the hydrogel microparticles with the increase in the amount of the cross-link agent. However, in our case, the DEE was found to decrease with the elevation in the concentration of the cross-linking solution. Similar experiences have been reported by Reddy et.al [11]. They reported that the entrapment efficiency of bovine serum

albumin decreased from 85% to 76% when the concentration of $AlCl_3$ was elevated from 0.08M to 0.16M in $Al^{3+}$-carboxymethyl guar gum microparticles. Identical reports were also reported from $Ca^{2+}$ -gellan gum bead [16]. Elevation in the concentration of $Ca^{2+}$ ions from 1M to 5M proportionately decreased the entrapment efficiency of the drug from 41.77% to 6.22%. It can be expected that as gelation continues water is removed from the microparticles by cationic ion exchange. Therefore, higher cross-link concentration will result in elevated water loss. The water expulsion will result in convective loss of the drug molecules from the microparticles, bringing down the entrapment efficiency of the drug in the hydrogel microparticles [17]. PCL dissolution from the hydrogel microparticles was found to decrease with the elevation in the concentration of the cross-linking solution. The elevation in the gel layer viscosity, compactness, and rigidity with the elevation in the concentration of the cross-linking solution provided greater resistance to the inflow of the dissolution solution into the core of the hydrogel microparticles and outflow of the solubilized PCL from the hydrogel microparticles. This accounted for the decreased PCL dissolution from the hydrogel microparticles with the elevation in the concentration of the cross-linking solution. The PCL dissolution pattern was also verified by the swelling and de-swelling (mass loss) phenomena of the hydrogel microparticles. The results of the swelling and de-swelling phenomena are shown in Fig.8.5. Increase in the concentration of the cross-linking solution from 1% w/v (F1) to 3% w/v (F3), significantly declined the swelling and de-swelling (mass loss) pattern of the hydrogel microparticles ($p<0.05$). Percentage swelling of the hydrogel microparticles F1, F2, and F3 after 30 min of swelling and de-swelling study was 856%, 760%, and 688% respectively. After the immediate burst swelling, the swelling of the microparticles was uniform and increased progressively with time to attain an equilibrium and maximum swelling percentage at 3 h. No change in the swelling pattern was noted when the pH of the dissolution solution was brought to pH 7.4 after 2 h. Percentage swelling of the hydrogel microparticles F1, F2, and F3 after 3 h of swelling and de-swelling study was 1352%, 1258%, and 1192% respectively. Following attainment of the peak swelling percentage, the percentage swelling started to decline and de-swelling or mass loss of the hydrogel microparticles was observed. Surprisingly, the pattern of the de-swelling of the hydrogel microparticles was the reverse of the swelling pattern. The de-swelling pattern was found to bear a direct relationship with the concentration of the cross-linking solution. Percentage de-swelling of the hydrogel microparticles F1, F2, and F3 after 5 h of swelling and de-swelling study was 448%, 488%, and 536% respectively. The swelling and de-swelling phenomena is explained as follows. The chain segments of hydrophilic natural polysaccharides, when placed in aqueous medium, have

a unique property to hydrate and absorb water. [43] Hydration of the chain segments increases the mobility of the polysaccharide chains and brings about relaxation of the chain segments and uncoiling or attainment of straight chain arrangement of the polysaccharide chains [18]. This results in expansion of the polymeric chain network, which is perceived as swelling of the polymer. With time, as more hydration and relaxation of chain segment, and uncoiling of the polysaccharide chains occurs, the polymers swells to attain the maximum swelling capacity. After attainment of the maximum swelling capacity, the branches of the polysaccharide chains start to separate from the main chain which is perceived as erosion or mass loss or de-swelling of the polymer. It is reported that cross-linking of polysaccharide chain segments restricts its mobility and results in the generation of true, highly viscous and rigid hydrogel layer [19]. This rigid hydrogel layer hinders the penetration of water into the core of the polysaccharide chains and thus limits or restricts the swelling of the polymer. Greater the concentration of the cross-linking ions, greater will be the rigidity and viscosity of the hydrogel layer, and lesser will be the swelling of the polymer. This explains the decrease in the swelling of the hydrogel microparticles with elevation in the concentration of the cross-linking ions. The $Al^{3+}$-CMTG hydrogel microparticles attains a maximum swelling capacity at 3 h, after which the swelling declines and de-swelling or mass loss of the microparticles initiates. A highly compact and rigid hydrogel layer will stay intact and will not erode for extended periods of time as compared to a less rigid and compact hydrogel layer [20]. The cross-link density and rigidity of the F3 hydrogel microparticles is more as compared to that of F1 hydrogel microparticles. The de-swelling or mass loss of the F3 hydrogel particle is thus less than that of the F1 hydrogel particle. This is the reason behind the increased percentage swelling (say de-swelling) of the hydrogel microparticles at 5 h. The viscous nature of the hydrogel microparticles was confirmed by analysing the viscosity profiles of hydrogel microparticles F1-F3. The viscosity of the hydrogel microparticles F1-F3 is shown in Fig.8.6. The viscosity of the hydrogel microparticles accentuated with the elevation in the concentration of the $Al^{3+}$ ions. F3 hydrogel microparticles was more viscous as compared to the F1 hydrogel microparticles. The compactness and rigidity of the hydrogel microparticles was verified by observing the SEM surface microstructures of the hydrogel microparticles F1 and F3 (Fig.8.7). The surface microstructure of F1 hydrogel microparticles (Fig. 8.7a) revealed several depressions in its surface which is indicative of lower degree of cross-link density. Kundu et. al. has reported that the surface of $Al^{3+}$- sodium carboxymethyl xanthan hydrogel microparticles had depressions in it and attributed that lower degree of cross-link produced a less rigid matrix which formed depressions when dried [21]. As the concentration of $AlCl_3$ is elevated (F3 hydrogel

microparticles, Fig. 8.7b) the depressions at the surface disappeared and the surface become smooth, compact and dense. Previous literature reports that at elevated cross-link density, the surface of hydrogel matrices is smooth, dense, and compact [22]. The burst PCL dissolution from the hydrogel microparticles F1-F3 was primarily due to the PCL present at the hydrogel particle surface and also due to some PCL dissolution from the superficial layers of the hydrogel particle before the formation of the release retarding viscous hydrogel layer.

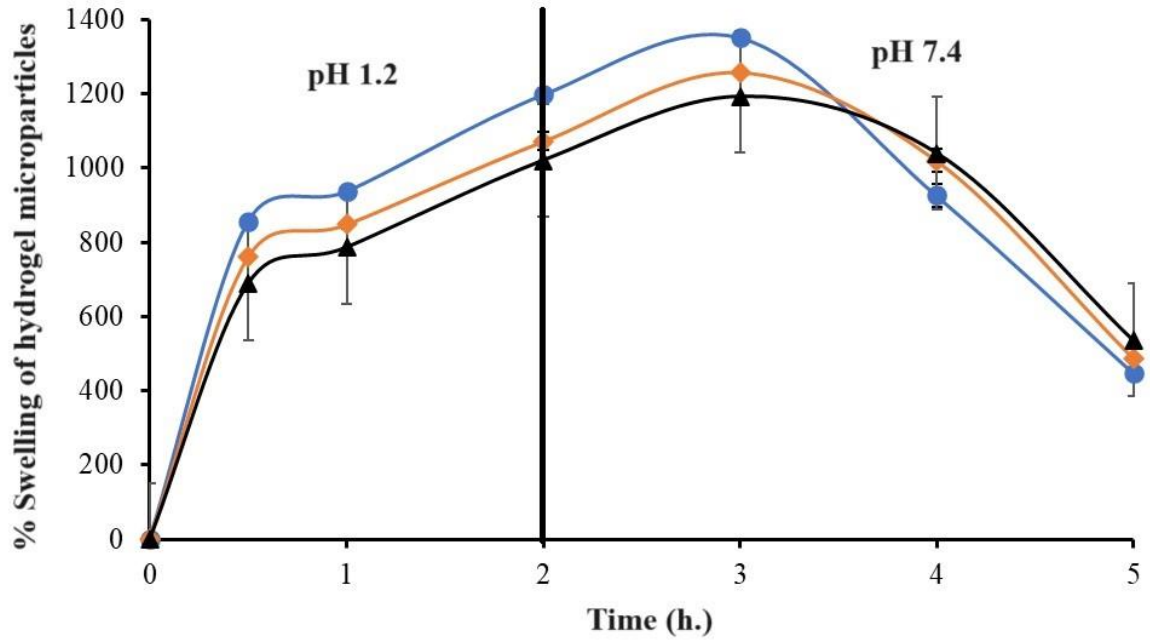


Fig. 8.5. Swelling and de-swelling profile of $Al^{3+}$ cross-linked hydrogel microparticles in acid (pH 1.2) media for 2 h followed by basic (pH 7.4) media up to 5 h. F1 (●), F2 (◆), F3 (▲) (mean ± S.D, n=3)

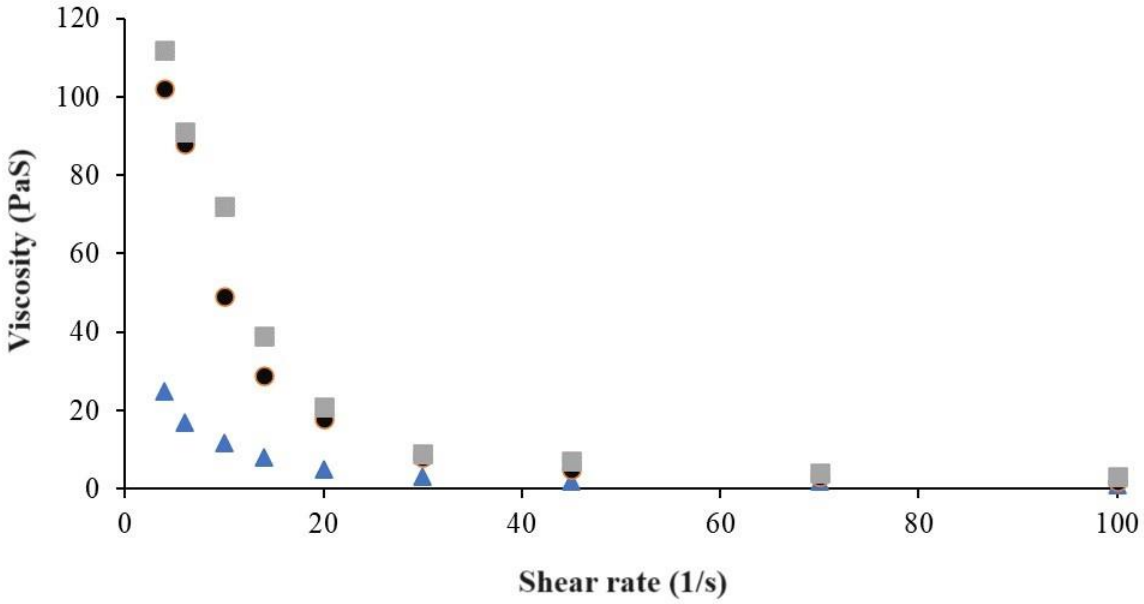


Fig. 8.6. Viscosity profile of $Al^{3+}$cross-linked hydrogel mimicking the formulation of hydrogel microparticles. F1 (▲), F2 (●), F3 (■).

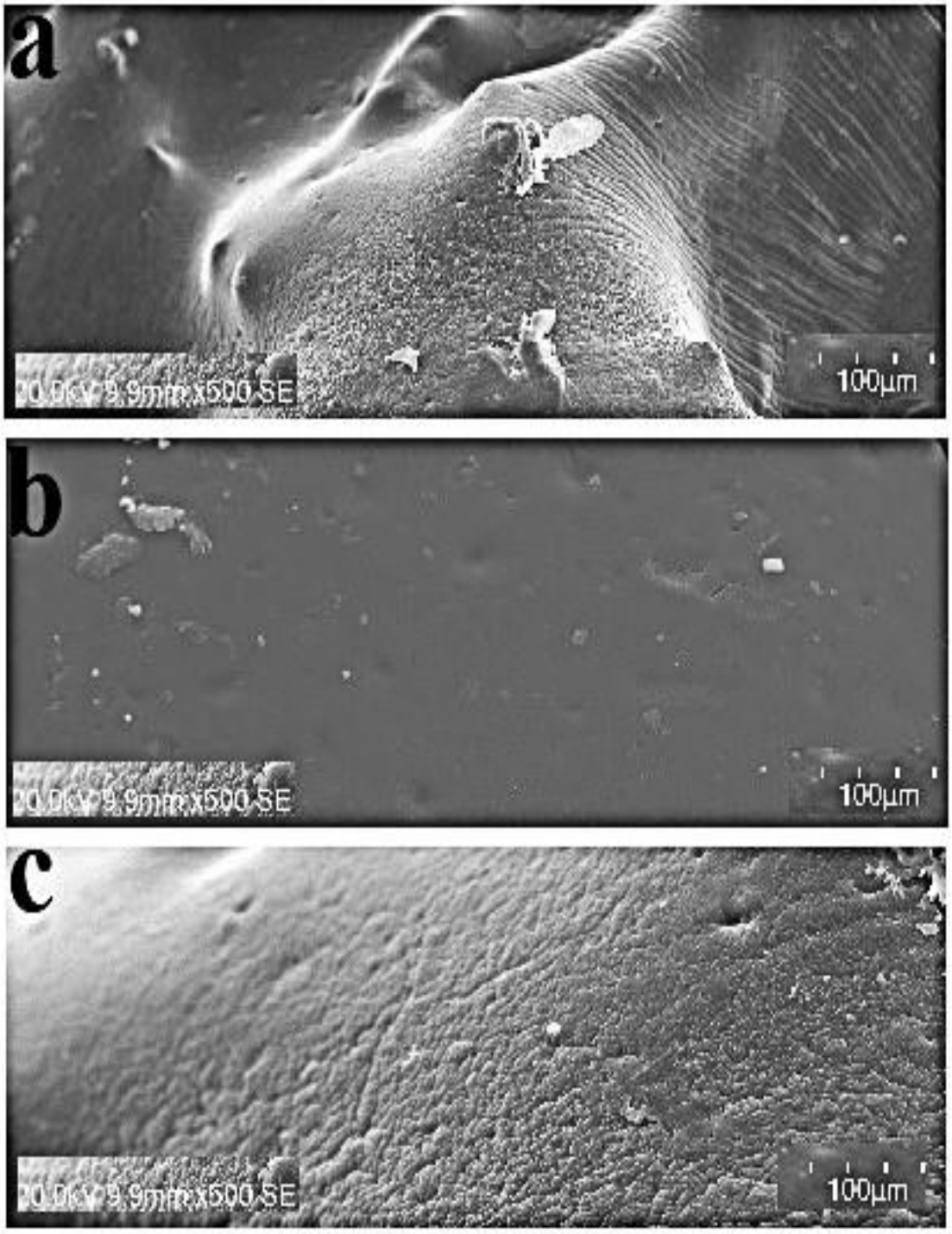


Fig. 8.7. SEM surface microstructures of hydrogel microparticles. F1 (a), F3 (b), F6 (c).

In order to investigate the effect of another trivalent ion on the hydrogel microparticles, $Fe^{3+}$ cross-linked CMTG hydrogel microparticles were developed, keeping the concentration of the CMTG solution at 3% w/v and the concentration of $FeCl_3$ at 1% w/v (F4), 2% w/v (F5), and

3% w/v (F6) respectively. Just like $Al^{3+}$ cross-linked hydrogel microparticles, the DEE decreased with the increase in the concentration of the $Fe^{3+}$ ions ($p<0.05$) (Table 2). The microparticles size also decreased with the elevation in the concentration of the $Fe^{3+}$ ions ($p<0.05$) (Table 2). The *in-vitro* PCL dissolution from hydrogel microparticles F4-F6 also decreased with the elevation in the concentration of the $Fe^{3+}$ ions (Fig.8.8). Burst PCL dissolution of 56% (F4, containing 1% w/v $FeCl_3$), 44% (F5, containing 2% w/v $FeCl_3$), and 42% (F6, containing 3% w/v $FeCl_3$) within 30 min was noticed from the hydrogel microparticles. The PCL dissolution was gradual and uniform after the burst dissolution. The PCL dissolution from F4 hydrogel microparticles was 72% at the end of 2 h, which decreased to 61% for F5 hydrogel microparticles, and further decreased to 51% for F6 hydrogel microparticles in the same time frame ($p<0.05$). At 5 h, the PCL dissolution from F4 hydrogel microparticles was 100%, which decreased to 88% for F5 hydrogel microparticles, and further decreased to 79% for F6 hydrogel microparticles in the same time frame ($p<0.05$). MDT for hydrogel microparticles F4-F6 also increased with the increase in the concentration of the $FeCl_3$ solution ($p<0.05$) (Table 2). The swelling and de-swelling of the F4-F6 hydrogel microparticles also decreased with the elevation in the $Fe^{3+}$ ions concentration (Fig.8.9). Percentage swelling of the hydrogel microparticles F4, F5, and F6 at 30 min was 895%, 712% and 584% respectively, 1263%, 1125%, and 939% respectively at 3 h, and 658%, 693%, and 707% at 6 h respectively.

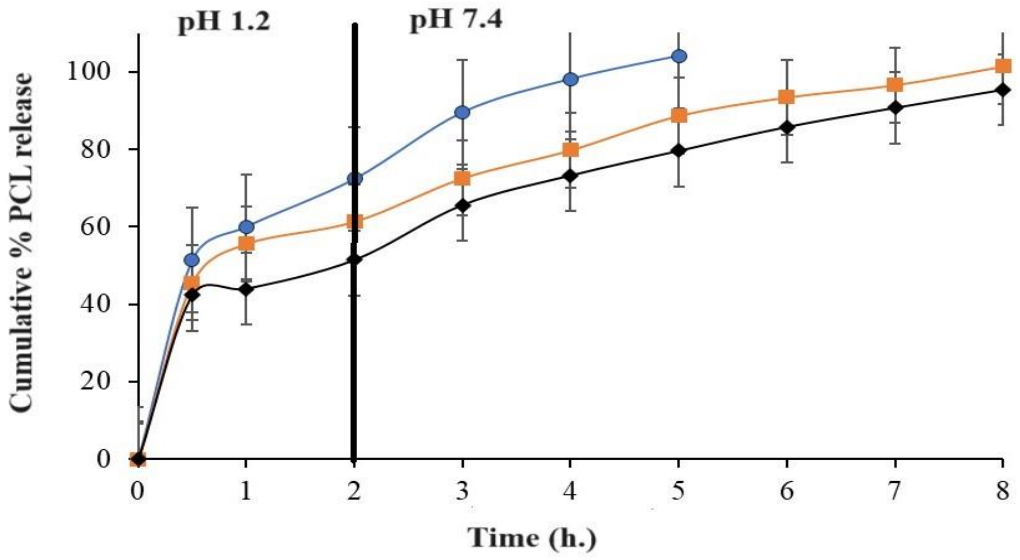


Fig.8.8. *In-vitro* PCL dissolution from $Fe^{3+}$ cross-linked hydrogel microparticles. $FeCl_3$ % (w/v) in microparticles: 1% (F4, ●), 2% (F5, ■), 3% (F6, ◆), (mean ± S.D, n=3)

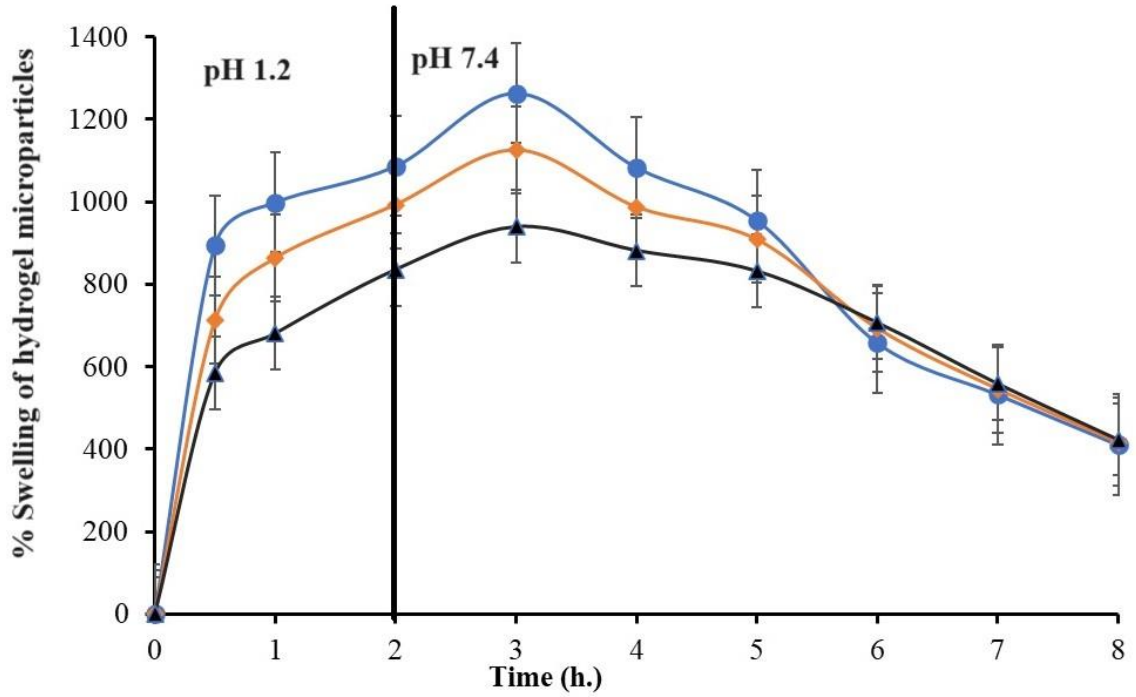


Fig.8.9. Swelling and deswelling profile of $Fe^{3+}$ cross-linked hydrogel microparticles in acid media (pH1.2) for 2 h followed by basic media (pH 7.4) up to 5 h. F4 (●), F5 (◆), F6 (▲). (mean± S. D, n=3).

Similar to $Al^{3+}$ ions, $Fe^{3+}$ ions react with the free COOH groups of the CMTG and cross-links its polymer chains. Elevation in the concentration of the $Fe^{3+}$ ions elevates the cross-link density and produces thicker and stiffer hydrogel microparticles. This decreases the particle size of the hydrogel microparticles F4-F6 with the elevation in the cross-linking ion concentration. Elevation in the concentration of $Fe^{3+}$ ions increases the water loss from the microparticles by cationic exchange which increases the convective loss of the PCL molecules. Augmentation in the concentration of the $Fe^{3+}$ ions produces stiffer, compact and rigid hydrogel microparticles which hinders the swelling, de-swelling and ultimately the PCL dissolution from the hydrogel microparticles. The viscosity of the hydrogel microparticles accentuated with the elevation in the concentration of the $Fe^{3+}$ ions (Fig.8.10). F6 hydrogel microparticles was more viscous as compared to the F4 hydrogel microparticles. The burst PCL dissolution from the hydrogel microparticles F4-F6 was primarily due to the PCL present at the hydrogel particle surface and also due to some PCL dissolution from the superficial layers of the hydrogel particle before the formation of the release retarding viscous hydrogel layer.

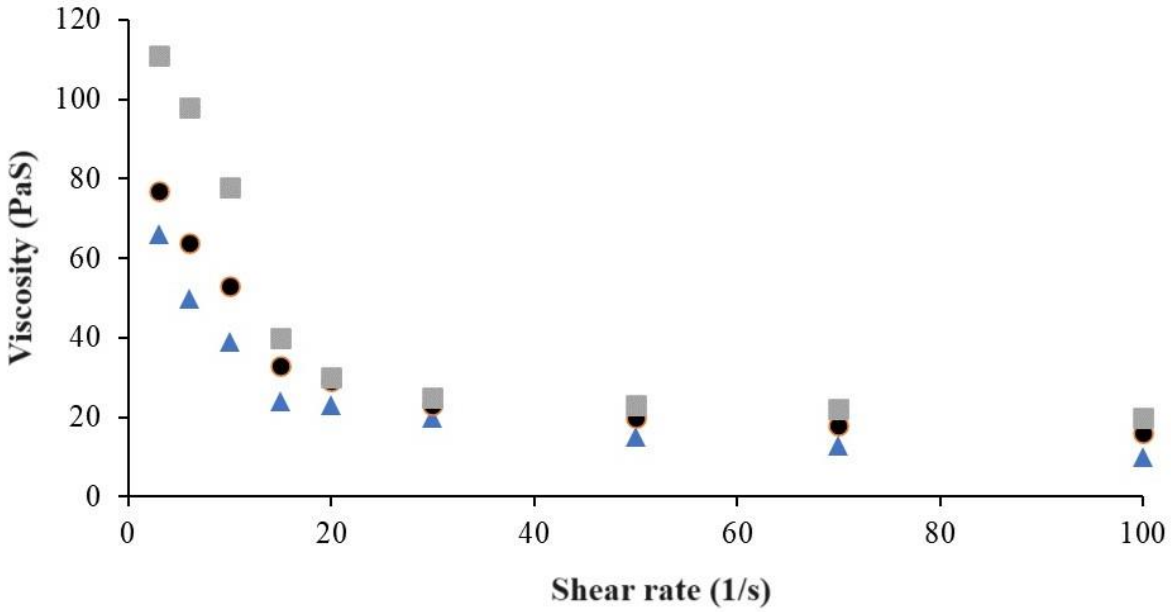


Fig. 8.10. Viscosity profile of $Fe^{3+}$ cross-linked hydrogel mimicking the formulation of hydrogel microparticles. F4 (▲), F5 (●), F6 (■).

Closer look at the swelling and PCL release profiles from the $Al^{3+}$ and $Fe^{3+}$ - CMTG hydrogel microparticles indicated major differences in the swelling and PCL release profiles. The swelling and PCL release from $Fe^{3+}$-CMTG hydrogel microparticles were less at all-time points as compared to the swelling and PCL release from $Al^{3+}$-CMTG hydrogel microparticles. The differences in the swelling and PCL release profiles from CMTG hydrogel microparticles cross-linked with $Al^{3+}$ and $Fe^{3+}$ is explained below. Swelling and drug dissolution from ionically cross-linked hydrogels is dependent on the concentration, valency and ionic radii (size) of the cross-linking ion [23]. Since the concentration and valency of the cross-linking ions are held constant in the hydrogel microparticles, the difference in the swelling and PCL dissolution profiles is created by the differences in the ionic radii of the respective cross-linking ions. Literature reports that the ions having greater ionic radii is able to cross-link more effectively and powerfully as compared to an ion with smaller ionic radii [24]. The ionic radii of the $Fe^{3+}$ ions are greater than the ionic radii of the $Al^{3+}$ ion (Table 3) [25]. $Fe^{3+}$ ions thus occupy greater space between the polysaccharide chains which results in tighter chain arrangements with lesser voids between the polysaccharide chains as compared to the $Al^{3+}$ ions. The above arrangement is illustrated in Fig.8.11. Compact chain arrangement with lesser voids results in decreased entry of water (dissolution solution) into the hydrogel microparticles, which decreases its swelling capacity and PCL release from the hydrogel microparticles. SEM

surface microstructure of the hydrogel microparticles F3 and F6 (Fig.8.7b and 8.7c) also supported the compactness and tighter chain arrangement of the F6 hydrogel microparticles compared to F3 hydrogel microparticles. As discussed earlier, the surface microstructure of F3 hydrogel microparticles is smooth, compact, and dense (Fig.8.7b). The surface microstructure of F6 hydrogel microparticles is even more denser and thick and is severely folded and wrinkled (Fig. 8.7c). This is due to the compact and tighter chain arrangement resulting from larger ionic radii of $Fe^{3+}$ ions. The compact and tighter chain arrangement induced higher cross-link density to the F6 hydrogel microparticles making the surface rough with wrinkles and foldings. Previous literature reports that at high cross-link density the surface of microcapsule is folded and wrinkled [26].

Table 8.2. Ionic radii of $Fe^{3+}$ and $Al^{3+}$ ions.

| Ions | Six coordinated ionic radius (Å) | Four coordinated ionic radius (Å) |
|---|---|---|
| $Fe^{3+}$ | 0.65 | 0.49 |
| $Al^{3+}$ | 0.54 | 0.39 |

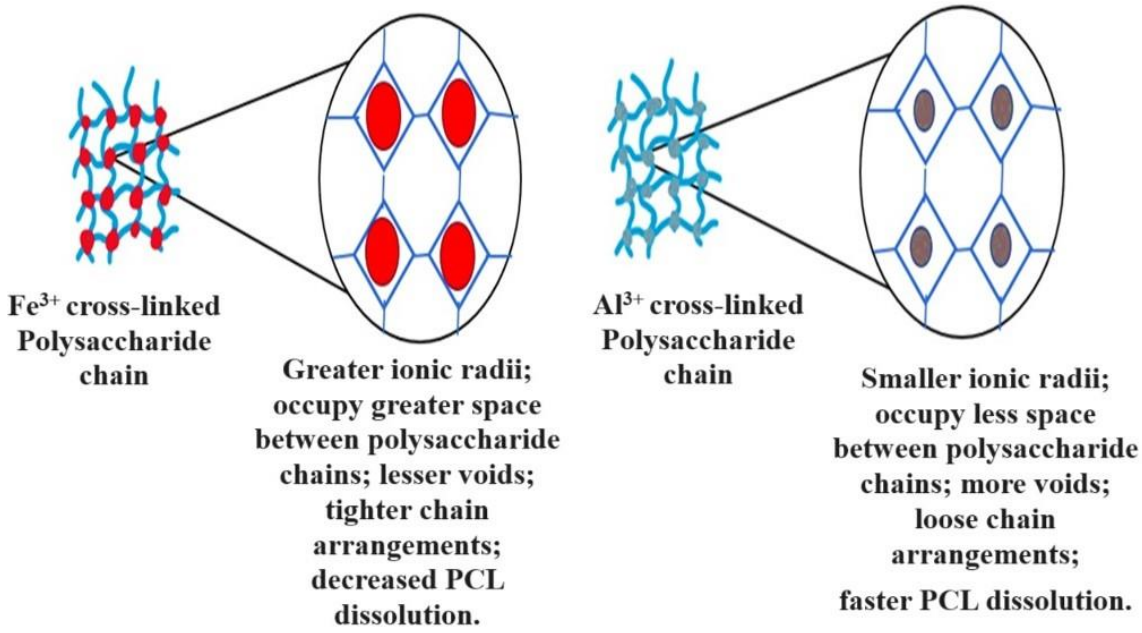


Fig.8.11. Comparison of ionic radii and polysaccharide chain arrangement in F3 and F6 hydrogel microparticles.

F6 hydrogel microparticles gave the most sustained PCL dissolution which extended up to 8 h. Thus, the F6 hydrogel microparticles was chosen for further experimentations and optimizations with an objective to get a more sustained PCL dissolution profile. Hydrophilic hydrogel coatings over F6 hydrogel microparticles were done. F6 hydrogel microparticles following 5 min of gelation was taken out of the gelation solution, gently tapped with tissue paper to soak the surface water and then uniformly sprayed with CMTG solutions (0.5% w/v-1.5% w/v), and then transferred to 1% w/v $FeCl_3$ solution and kept for 5 min to effect gelation and hardening. Accordingly, cross-linked coated hydrogel microparticles F7-F9 were prepared, where the concentration of the CMTG solution was 0.5% w/v (F7), 1%w/v (F8), and 1.5%w/v (F9), and the concentration of the cross-linking gelation solution $FeCl_3$ was 1% w/v. Beyond the concentration of 1.5%w/v CMTG, the solution become too thick and viscous to be uniformly sprayed over the core F6 hydrogel microparticles.

Cross-linked coating over the core F6 hydrogel microparticles produced significant changes in the hydrogel microparticles. The size of the cross-linked coated hydrogel microparticles was significantly more than the core hydrogel microparticles ($p<0.05$) (Table 2). The burst PCL dissolution associated with the core hydrogel microparticles got significantly reduced in case of cross-linked coated hydrogel microparticles. Burst PCL dissolution decreased in the following fashion: F6 (42%)>F7(38%)>F8(25%)>F9(11%). After the burst PCL dissolution, PCL dissolution from the coated hydrogel microparticles was uniform and gradual (Fig.8.12). Increase in the concentration of the coating CMTG solution from 0.5% w/v (F7) to 1.5% w/v (F9), significantly decreased the PCL dissolution from the coated hydrogel microparticles. PCL dissolution from the coated hydrogel microparticles decreased in the following manner: after 2 h - F6 (66%)>F7(48%)>F8(42%)>F9(30%), after 4 h - F6 (73%)>F7(69%)>F8(64%)>F9(48%), and after 6 h of PCL dissolution - F6 (86%)>F7(84%)>F8(81%)>F9(66%). MDT of hydrogel microparticles F7-F9 also increased significantly ($p<0.05$) (Table 2).

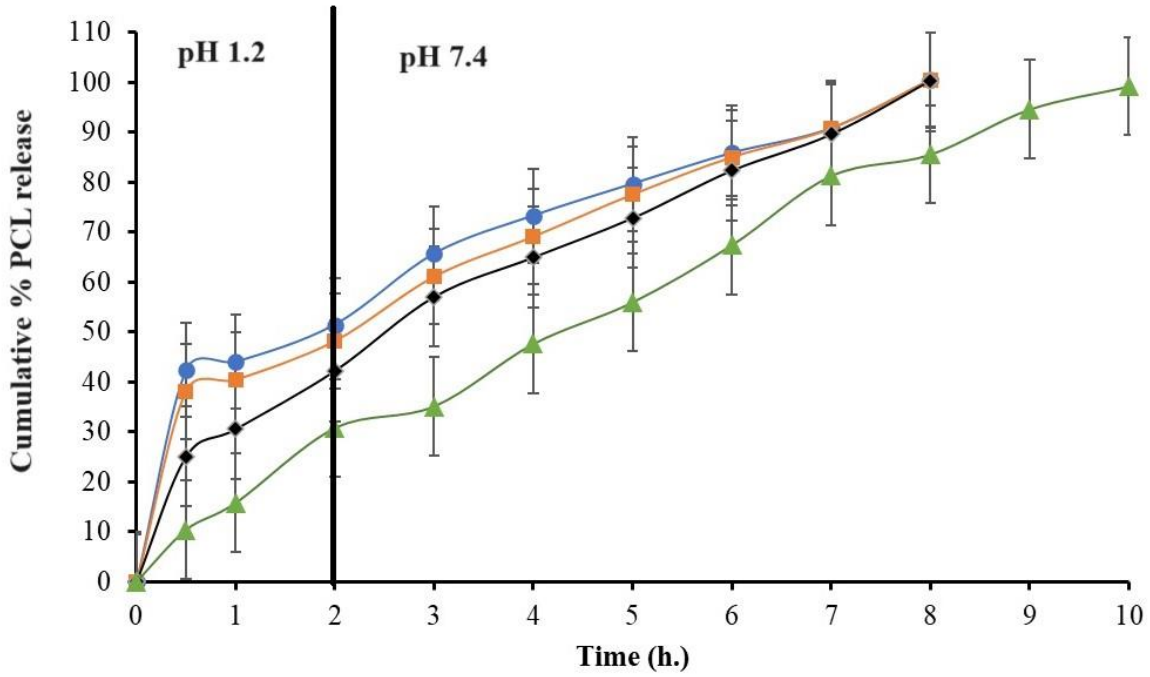


Fig.8.12. *In-vitro* PCL dissolution from single cross-link coated hydrogel microparticles. CMTG % (w/v) in coating: 0% (F6, ●), 0.5% (F7, ■), 1% (F8, ◆), 1.5% (F9, ▲), and $FeCl_3$ % (w/v) : 1%; (mean ± S.D, n=3).

The increase in the size of the coated hydrogel microparticles is due to the formation of additional coating layer over the core hydrogel microparticles. The burst PCL dissolution from the core hydrogel microparticles was primarily due to the PCL present at the surface of the core hydrogel microparticles. The surface of the coated hydrogel microparticles is bereft of any PCL and is composed of the cross-linked coated hydrogel layer, which accounts for the decrease in the burst PCL dissolution from the coated hydrogel microparticles. The decrease in PCL dissolution from the coated hydrogel microparticles with the increase in the concentration of the coating CMTG solution is explained below. As stated, hydrophilic natural polysaccharides when placed in aqueous medium, have a unique property to hydrate, absorb water and swell. The swollen layer is principally a thick and viscous layer of the polymer generated by simple entanglement of the polysaccharide chains [13]. This viscous layer has sufficient strength to form an obstruction which can prevent the ingress and egress of water (dissolution solution). The viscosity of this layer is proportional to the polymer concentration [20]. Increase in the polymer concentration will increase the viscosity of the gel layer, which will accentuate the barrier effect of the viscous layer. In case of coated hydrogel microparticles F7-F9, the concentration of the CMTG solution is gradually increased from 0.5 % w/v to 1.5 % w/v. This

might have increased the viscosity of the coating layer, which have accounted for the decreased ingress of the dissolution solution to the PCL loaded core hydrogel microparticles and egress of the dissolved PCL from the core hydrogel microparticles. The above observation was ascertained by analysing the viscosity of solution mimicking the composition of the coating layer. The viscosity profiles of the cross-linked CMTG coating layer is shown in Fig.8.13. Increase in the concentration of the CMTG solution led to an increase in the viscosity of the coating layer. This decreased the PCL dissolution from the coated hydrogel microparticles F7-F9 (Fig.8.12).

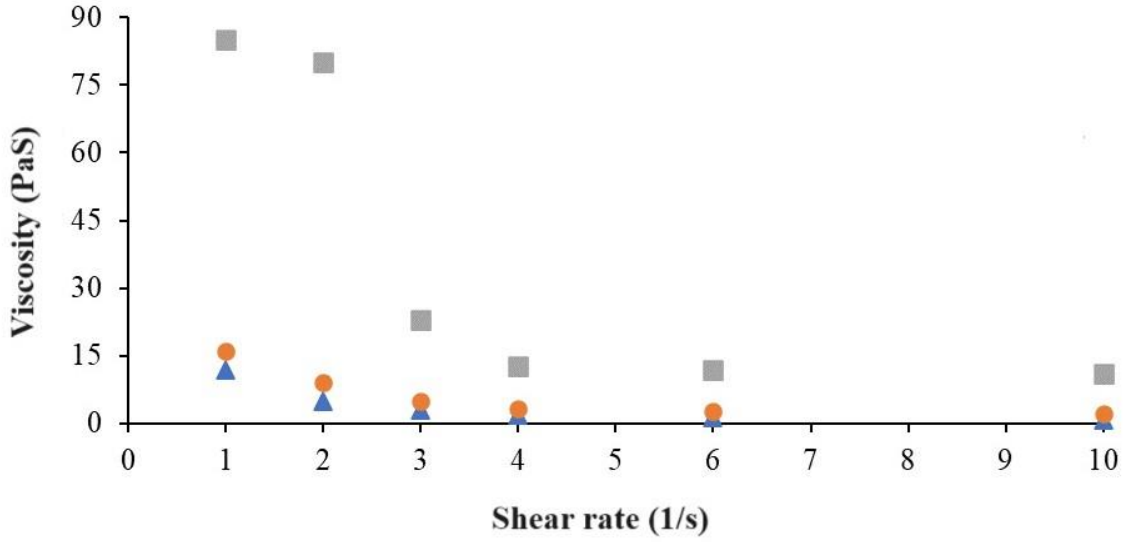


Fig. 8.13. Viscosity profile of single cross-linked CMTG coating layer mimicking the single cross-linked hydrogel microparticles. F7 (▲), F8 (●), F9 (■).

The coated (1.5% w/v CMTG; 1% w/v $FeCl_3$) F9 hydrogel microparticles gave the most sustained PCL dissolution profile extending up to 10 h. The effect of the concentration of the $FeCl_3$ on the coating hydrogel layer of the hydrogel microparticles were examined by varying the concentration of the $FeCl_3$ at a fixed concentration of CMTG solution (1.5% w/v). Hydrogel microparticles F10 (1.5% w/v $FeCl_3$) and F11 (2% w/v $FeCl_3$) were prepared and its effect on the PCL dissolution was investigated. Increase in the concentration of the $FeCl_3$ solution decreased the size of the hydrogel microparticles ($p<0.05$) (Table 2). The burst PCL dissolution from the coated hydrogel microparticles is significantly reduced with the increase in concentration of the $FeCl_3$ solution (Fig.8.14). Burst PCL dissolution (30 min) decreased in the following fashion: F9 (11%)>F10(8%)>F11(6%). After the burst PCL dissolution, PCL dissolution from the coated hydrogel microparticles was uniform and gradual. Increase in the

concentration of the $FeCl_3$ solution from 1% w/v (F9) to 2% w/v (F11), significantly decreased the PCL dissolution from the coated hydrogel microparticles. PCL dissolution from the coated hydrogel microparticles decreased in the following manner: after 2 h – F9 (30%)>F10(27%)>F11(22%), after 5 h – F9 (57%)>F10 (54%)>F11(50%), and after 8 h of PCL dissolution – F9 (85%)>F10(81%)>F11(79%). MDT of hydrogel microparticles F9-F11 also increased significantly ($p<0.05$) (Table 2).

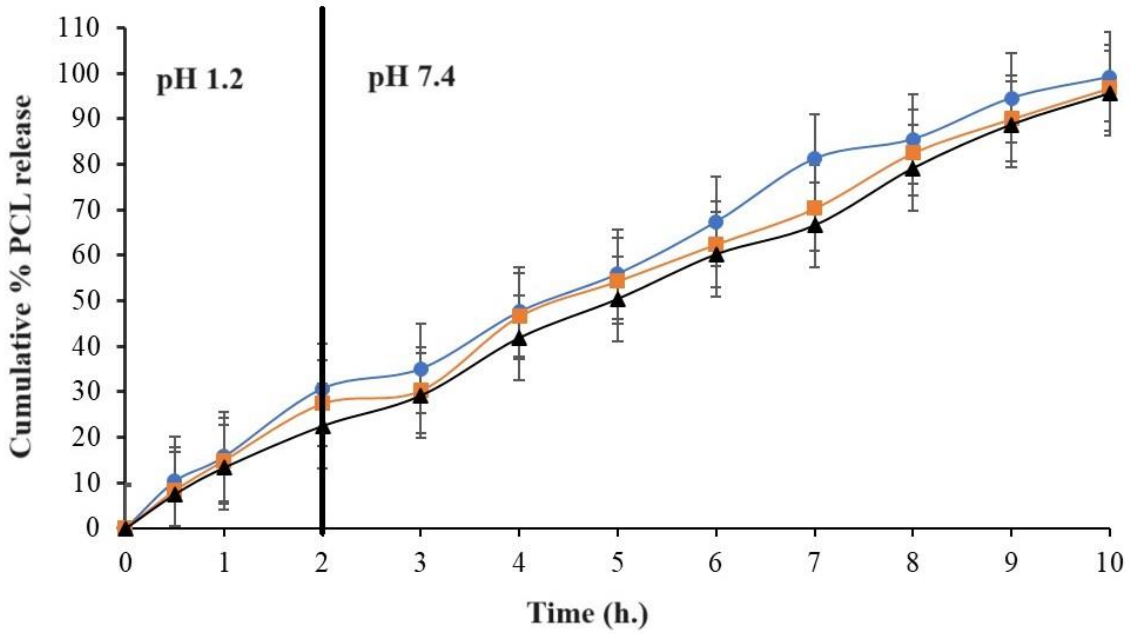


Fig. 8.14. *In-vitro* PCL dissolution from single cross-link coated hydrogel microparticles. CMTG %(w/v ): 1.5 and $FeCl_3$ % (w/v) in coating : 1% (F9, ●), 1.5% (F10, ■), 2% (F11, ▲); (mean ± S.D, n=3).

Elevation in the concentration of the $FeCl_3$ solution (1% w/v, F9 to 2% w/v, F11) at a fixed concentration of the CMTG solution, provided a greater amount of the $Fe^{3+}$ ions to cross-link with the carboxyl groups of CMTG. This elevated the cross-link density of the coating layer of the hydrogel microparticles and made the hydrogel network more compact and tight. This might have decreased the particle size of the hydrogel microparticles with the elevation in the concentration of the $FeCl_3$ solution (Table 2). Increase in the cross-link density of the hydrogel coating layer may have also elevated the viscosity of the coating layer. The increased viscosity of the coating layer provided greater resistance to the ingress of the dissolution solution to the PCL laden core hydrogel microparticles and egress of the dissolved PCL to the dissolution solution. This might have decreased the rate of PCL dissolution from the coated hydrogel microparticles. Analysis of the viscosities of the solutions mimicking the composition of the

coating solution also indicated that the elevation in the concentration of the $FeCl_3$ enhanced the viscosity of the coating layer (Fig.8.15). Beyond the concentration of 2% w/v $FeCl_3$, the viscosity of the coated hydrogel microparticles is so much increased that the coated hydrogel microparticles in the $FeCl_3$ solution is sticking with each other and forming a single lump like mass.

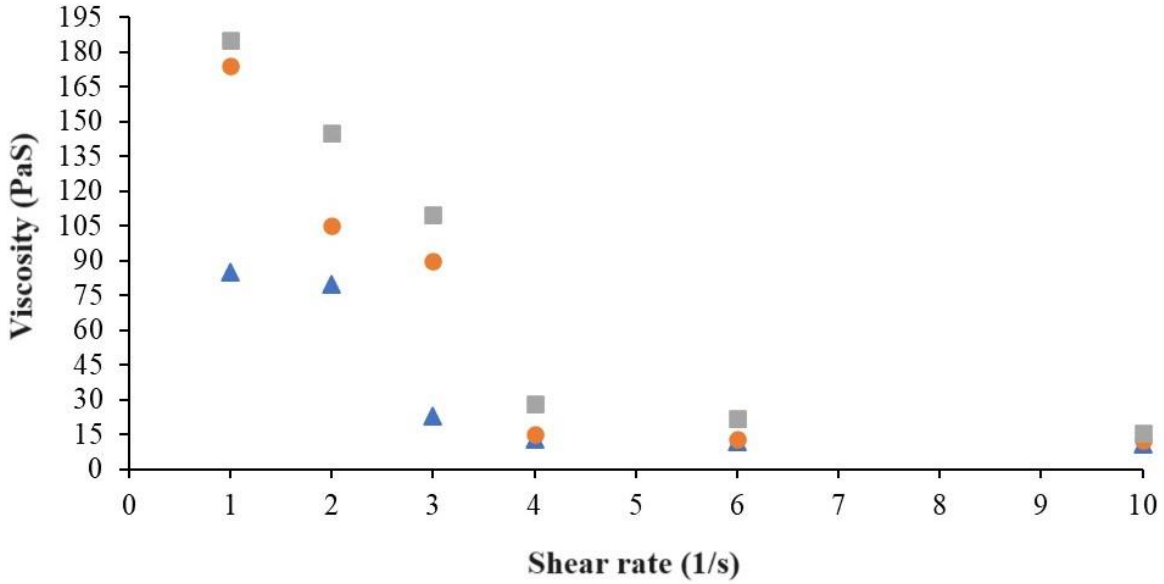


Fig. 8.15. Viscosity profile of single cross-linked hydrogel mimicking the formulation of hydrogel microparticles. F9 (▲), F10 (●), F11 (■).

F11 hydrogel microparticles coated with 1.5% w/v CMTG and 1.5% w/v $FeCl_3$ gave the longest PCL dissolution, extending beyond 10 h. F11 hydrogel microparticles were selected for further optimizations. The DS of the synthesised CMTG was 0.84 [1]. It indicates that some of the OH groups of TG has been substituted while some are free and can take part in different cross-link process. Borax is a well-known cross-linker for TG solutions and is known to cross-link with the OH groups of different polymers [27, 28]. Borax ($Na_2B_4O_7.10H_2O$) readily dissociates in aqueous solutions to give rise to boric acid and the tetra hydroxyl borate ion $[B(OH)^-_4]$ . The tetra hydroxyl borate ion is highly reactive and can instantaneously cross-link with up to 4 OH groups of the polymer chains to form hydrogels [29]. The mechanism of cross-linking with borax is illustrated in scheme 1. The borax cross-linked hydrogels have been widely used for drug delivery [27,28, 30,31].

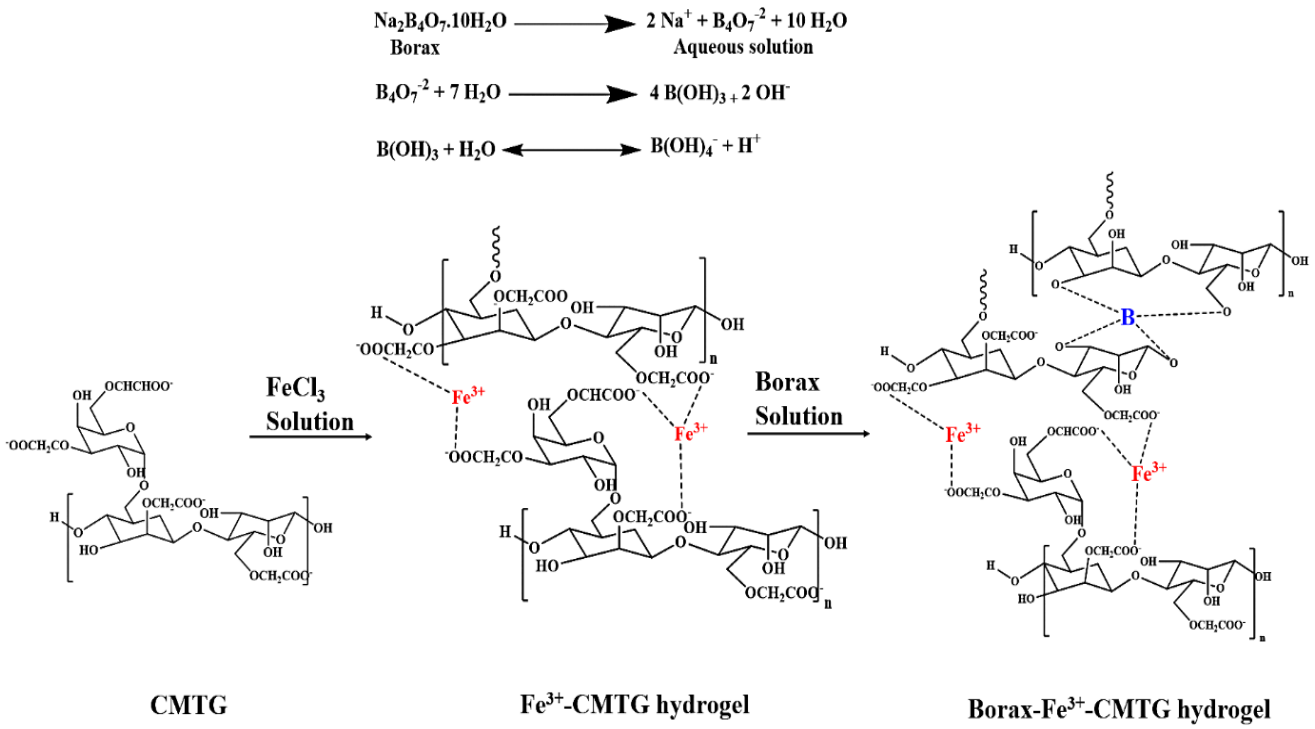


Scheme.8.1. Mechanism by which borax cross-link with CMTG.

$Fe^{3+}$ cross-linked coated hydrogel microparticles F11 was further cross-linked with borax with an objective to cross-link the free OH groups of CMTG and produce a double cross-linked coated hydrogel microparticles. The double cross-link was done with a motive to further densify and impart rigidity to the coating hydrogel layer so that PCL dissolution is further sustained. Accordingly, double cross-linked coated hydrogel microparticles were formulated with 0.25% w/v (F12), 0.50% w/v (F13), 0.75% w/v (F14), and 1% w/v (F15) borax respectively. Borax exerted significant changes to the double cross-linked coated hydrogel microparticles. The size of the microparticles was further significantly decreased as the concentration of borax solution was increased ($p<0.05$) (Table.2). Burst PCL dissolution was also significantly reduced with the increase in the concentration of the borax solution. Burst PCL dissolution after 30 min was decreased in the following pattern: F11(6%)> F12(5%)>F13(4%)>F14(3.5%)> F15%(2.2%) (Fig.8.16). PCL dissolution was uniform and gradual after the burst dissolution and decreased with the increase in the concentration of the borax solution in the following way: after 2 h- F11(22%)> F12(14%)>F13(10%)>F14(8%)> F15%(6%), after 5 h- F11(50%)> F12(39%)>F13(30%)>F14(23%)> F15%(19%), and after 10 h- F11(96%)> F12(81%)>F13(78%)>F14(72%)> F15%(66%). MDT of hydrogel microparticles F12-F15 also increased significantly ($p<0.05$) (Table2).

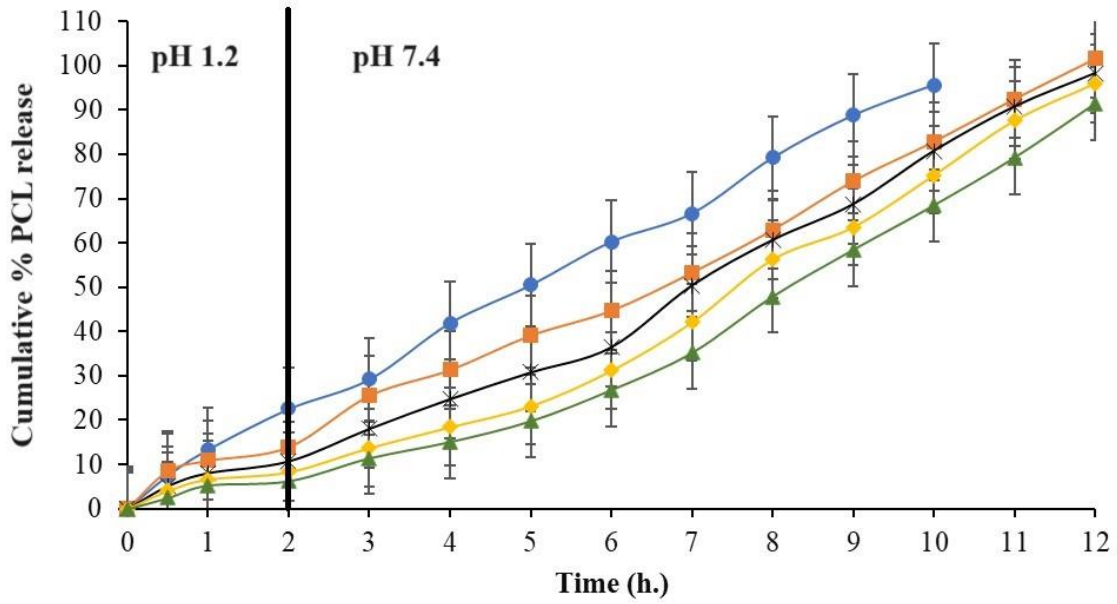


Fig.8.16. *In-vitro* PCL dissolution from double cross-link coated hydrogel microparticles. In coating CMTG : 1.5% (w/v) ; $FeCl_3$ : 2% (w/v). Borax % (w/v) in coating: 0% (F11, ●), 0.25% (F12, ■), 0.5% (F13, ✱), 0.75% (F14, ◆), 1% (F15, ▲); (mean ± S.D, n=3).

Elevation in the concentration of the borax solution (0.25% w/v, F12 to 1% w/v, F15) at a fixed concentration of the CMTG solution, provided a greater amount of the $B(OH)^-_4$ ions to cross-link with the OH groups of CMTG. This elevated the cross-link density of the coating layer of the hydrogel microparticles and made the hydrogel network more compact and tight [20]. This might have decreased the particle size of the hydrogel microparticles with the elevation in the concentration of the borax solution. Increase in the cross-link density of the hydrogel coating layer may have also elevated the viscosity of the coating layer. The increased viscosity of the coating layer provided greater resistance to the ingress of the dissolution solution to the PCL laden core hydrogel microparticles and egress of the dissolved PCL to the dissolution solution. This decreased the rate of PCL dissolution from the coated hydrogel microparticles. Analysis of the viscosities of the solutions mimicking the composition of the coating solution also indicated that the elevation in the concentration of the borax enhanced the viscosity of the coating layer (Fig.8.17). The rigidity and compactness of the double cross-linked coated hydrogel microparticles was further verified by analysing the change in volume of the double cross-linked hydrogel microparticles with time. As stated earlier, hydrophilic natural polysaccharides have a unique property to hydrate, absorb water and swell. The swelling of the hydrogel microparticles is associated with the increase in volume of the hydrogel microparticles. A compact and rigid hydrogel layer will absorb less water (dissolution

solution), will swell less and thus the volume will also be less. Increase in the borax concentration made the hydrogel layer more rigid and compact which is perceived by the decrease in the volume of the hydrogel microparticles (Fig.8.18). The volume of the double cross-linked hydrogel microparticles decreased in the following way: after 2 h- F11(0.463 $mm^3$)> F12(0.437 $mm^3$)>F13(0.420 $mm^3$)>F14(0.386 $mm^3$)> F15%( 0.335 $mm^3$), after 4 h- F11(0.542 $mm^3$)> F12(0.517 $mm^3$)>F13(0.489 $mm^3$)>F14(0.437 $mm^3$)> F15%( 0.373 $mm^3$), and after 6 h- F11(0.633 $mm^3$)> F12(0.619 $mm^3$)>F13(0.575 $mm^3$)>F14(0.539 $mm^3$)> F15%( 0.498 $mm^3$). Beyond the concentration of 1% w/v borax, the viscosity of the coated hydrogel microparticles is so much increased that the coated hydrogel microparticles in the cross-linking ($FeCl_3$ and borax) solution is sticking and agglomerating with each other and forming a single lump like mass.

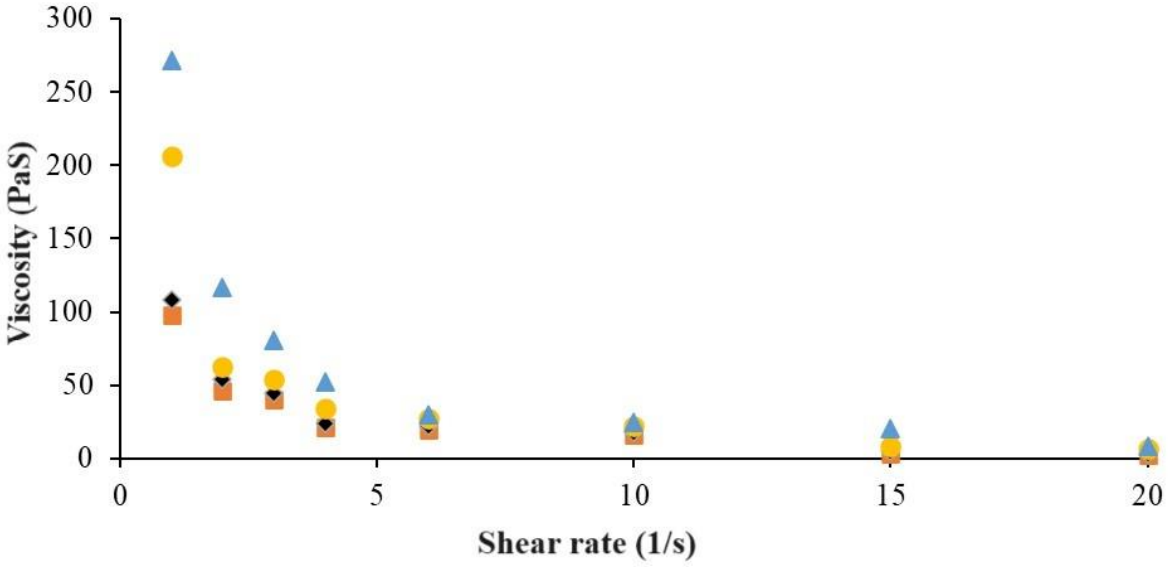


Fig.8.17. Viscosity profile of double cross-linked hydrogel mimicking the formulation of hydrogel microparticles. F12 (■), F13 (◆), F14 (●), F15 (▲).

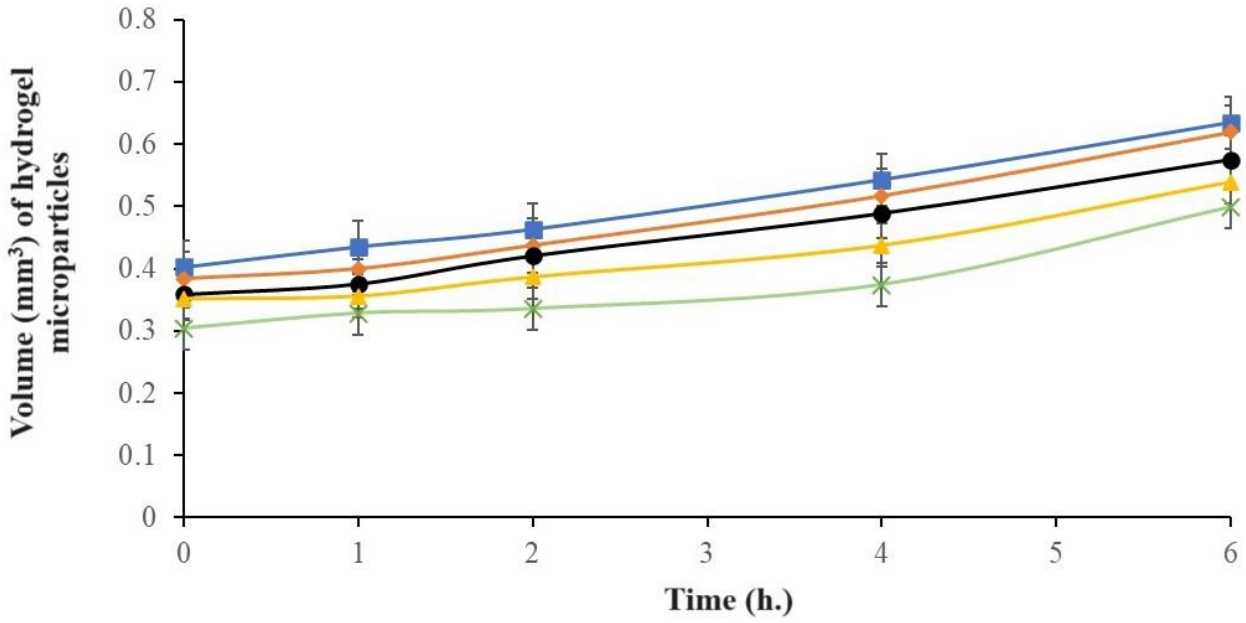


Fig. 8.18. Changes in the volume ($mm^3$) of the hydrogel microparticles at different time points in acid (pH 1.2) solution for 2 h followed by basic (pH 7.4) buffer till 6 h. F11 (■ )F12 (◆ ), F13 (●), F14 (▲), F15 (×). (mean ± S.D,n=3).

### 8.3. Drug release kinetics

The PCL release mechanism has been shown in Table 4. The PCL release from the uncoated and coated hydrogel microparticles followed zero order kinetics, indicating that PCL dissolution is independent of its concentration in the microparticles [32]. The PCL release (till 60%) from the coated and uncoated obeyed the power law equation. The PCL release from uncoated hydrogel microparticles F1-F6 followed the Fickian diffusion model ($r^2$ values 0.840-1.00) as indicated by the values of "n", the release exponent. This indicates that PCL dissolution from F1-F6 hydrogel microparticles was primarily by diffusion of the PCL from the hydrogel microparticles. Literature reports that for water soluble drugs, diffusion is the primary mechanism of drug dissolution [33]. Single cross-link coating of the hydrogel microparticles (F7-F11) shifted the PCL release mechanism from diffusion to anomalous transport ($r^2$ 0.879-0.995). This indicated that both swelling and diffusion are the controlling mechanism of PCL dissolution from the hydrogel microparticles. The swelling of the coating layer promoted the entry of the dissolution fluid to the core of the hydrogel microparticles and allowed the diffusion of the PCL through the hydrogel microparticles. Dual cross-linking of the coating layer (F12-F15) further shifted the PCL dissolution mechanism to super case II mechanism ($r^2$ 0.908-0.955), indicating that erosion/mobility of the polymeric chains dictated

the PCL release mechanism. Literature reports that drug dissolution mechanism from chemical cross-linking of the polymeric chains is primarily by erosion of the polymeric chains [34].

Table.8.3. Release mechanism parameters of PCL from hydrogel microparticles.

| Formulation code | Zero-order | First order | Release exponent (n) | Co-relation coefficient ($r^2$) |
|---|---|---|---|---|
| F1 | 0.9736 | 0.9275 | 0.1247 | 0.9202 |
| F2 | 0.9764 | 0.9558 | 0.1636 | 0.9905 |
| F3 | 0.9819 | 0.9646 | 0.2457 | 0.995 |
| F4 | 0.9759 | 0.8252 | 0.2197 | 1 |
| F5 | 0.967 | 0.964 | 0.215 | 0.9626 |
| F6 | 0.9859 | 0.8222 | 0.2311 | 0.84 |
| F7 | 0.9942 | 0.8121 | 0.4512 | 0.8791 |
| F8 | 0.9913 | 0.7941 | 0.4712 | 0.9752 |
| F9 | 0.9909 | 0.8041 | 0.75 | 0.9921 |
| F10 | 0.9944 | 0.8612 | 0.8017 | 0.9901 |
| F11 | 0.9982 | 0.8629 | 0.8272 | 0.9955 |
| F12 | 0.9917 | 0.7181 | 0.7506 | 0.9558 |
| F13 | 0.9682 | 0.7433 | 0.8837 | 0.9086 |
| F14 | 0.9648 | 0.7817 | 0.9665 | 0.9361 |
| F15 | 0.9524 | 0.7804 | 1.0536 | 0.9535 |

**References**

[1] K. Mukherjee, P. Dutta, T. K. Giri, $Al^{3+}/Ca^{2+}$ cross-linked hydrogel matrix tablet of etherified tara gum for sustained delivery of tramadol hydrochloride in gastrointestinal milieu. Int. J. Biol. Macromol. 2023;232:123448.

[2] S.H. Almurisia, A. B. D. Doolaanea, M. E. Akkawic, B. Chatterjeed, Md Z. I. Sarker, Taste masking of paracetamol encapsulated in chitosan-coated alginate beads. J. Drug Deliv. Sci. Technol.56 (2020) 101520.

[3] J. Sibik, M. J. Sargent, M. Franklin, J. A. Zeitler, Crystallization and phase changes in paracetamol from the amorphous solid to the liquid phase. Mol. Pharmaceutics.11 (2014) 1326–1334.

[4] G. G. G. Oliveira, A. Feitosa, K. Loureiro, A. R. Fernandes, E. B. Souto, P. Severino, Compatibility study of paracetamol, chlorpheniramine maleate and phenylephrine hydrochloride in physical mixtures. Saudi Pharm. J. 25 (2017) 99–103.

[5] M. B. Santos, C. H. C. dos Santos, M. G. de Carvalho, C. W. P. de Carvalho, E. E. Garcia-Rojas, Physicochemical, thermal and rheological properties of synthesized carboxymethyl tara gum (Caesalpinia spinosa). Int. J. Biol. Macromol. 134 (2019) 595–603.

[6] C. W. Vendruscolo, C. Ferrero, E. A. G. Pineda, J. L. M. Silveira, R. A. Freitas, M. R. Jim´enez-Castellanos, T. M. B. Bresolin, Physicochemical and mechanical characterization of galactomannan from Mimosa scabrella: effect of drying method. Carbohydr. Polym.76 (2009) 86–93.

[7] L. Bounabi, N. B. Mokhnachi, N. Haddadine, F. Ouazib, R. Barille, Development of poly(2-hydroxyethyl methacrylate)/clay composites as drug delivery systems of paracetamol. J Drug Deliv Sci Technol. 33 (2016) 58e65.

[8] A. Saha, K. Mukherjee, B. Ghosh, T. K. Giri, Grafted tamarind kernel polysaccharide based Al3þ cross-linked hydrogel matrices for sustained release of drug in the gastrointestinal milieu. Adv. Pharm. J.2 (2024) 100022.

[9] H. Mahmoud, A. Elella, H. M. Abdallah, H. Gamal, E. B. Moustafa, E. S. Goda, Rational design of biocompatible IPNs hydrogels containing carboxymethyl starch and trimethyl chitosan chloride with high antibacterial activity. Cellulose. 29 (2022) 7317–7330.

[10] J. Patel, S. Maiti, N. S. H. N. Moorthy, Repaglinide-laden hydrogel particles of xanthan gum derivatives for the management of diabetes, Carbohydr. Polym. 287 (2022) 119354.

[11] T. Reddy, S. Tammishetti, Gastric resistant microbeads of metal ion cross-linked carboxymethyl guar gum for oral drug delivery, J. Microencapsul. 19(3) (2002) 311–318.

[12] K. Mukherjee, T. Kundu, B. Sa, Al 3+ ion cross-linked matrix tablets of sodium carboxymethyl cellulose for controlled release of aceclofenac: Development and in-vitro evaluation, Der. Pharm. Lett. 4(6) (2021) 1633-1647.

[13] J. Collett, C. Moreton, (Eds.), M. E. Aulton in: Pharmaceutics: The Science of Dosage Form Design, 2nd ed. Churchill Livingstone: 2002.

[14] S. Maiti, S. Ray, B. Sa, Controlled delivery of bovine serum albumin from carboxymethyl xanthan microparticles, Pharm. Dev. Technol. 14 (2009) 165-172.

[15] R. J. Babu, S. Sathigari, M. T. Kumar, J. K. Pandit, Formulation of controlled release gellan gum macro beads of amoxicillin, Curr. Drug Deliv. 7 (2010) 36–43.

[16] B. N. Singh, K. H. Kim, Effects of divalent cations on drug encapsulation efficiency of deacylated gellan gum, J. Microencapsul. 22(7) (2010) 761–771.

[17] S. Maiti, S. Ranjit, R. Mondol, S. Ray, B. Sa, Al+3 ion cross-linked and acetalated gellan hydrogel network microparticles for prolonged release of glipizide. Carbohydr. Polym. 85 (2011) 164–172.

[18] J. Ostrowska-Czubenko, M. Gierszewska, M. Pieróg, pH-responsive hydrogel membranes based on modified chitosan: water transport and kinetics of swelling, J. Polym. Res. 22 (2015) 153.

[19] A. Nokhodchi, A. Tailor, In situ cross-linking of sodium alginate with calcium and aluminum ions to sustain the release of theophylline from polymeric matrices, IL Farmaco.59 (2004) 999–1004.

[20] K. Mukherjee, S. Roy, T. K. Giri, Effect of intragranular/extragranular tara gum on sustained gastrointestinal drug delivery from semi-IPN hydrogel matrices, Int. J. Biol. Macromol. 253 (2023) 127176.

[21] T. Kundu, K. Mukherjee, B. Sa, Hydrogel beads composed of sodium carboxymethyl xanthan and sodium carboxymethyl cellulose for controlled release of aceclofenac: effect of formulation variables, Res. J. Pharm. Technol. 5(1) (2012) 103–113.

[22] S. Kaity, J. Issac, A. Ghosh, Interpenetrating polymer network of locust bean gum-poly (vinyl alcohol) for controlled release drug delivery, Carbohydr. Polym. 94 (2013) 456–467.

[23] S. Jana, P. Das, S. K. Nandi, Ionotropic cross-linking of biopolymers for drug delivery in wound management, In: A. K. Nayak, Md. S. Hasnain, (Eds.), Ionotropic Cross-Linking of Biopolymers Applications in Drug Delivery, Elsevier (2024) 619-641.

[24] S. K. Bajpai, S. Sharma, Investigation of swelling/degradation behaviour of alginate microparticles crosslinked with $Ca^{2+}$ and $Ba^{2+}$ ions, React. Funct. Polym. 59 (2004) 129–140.

[25] N. Pathak, S. K. Gupta, K. Sanyal, M. Kumar, R. M. Kadama, V. Natarajana, Photoluminescence and EPR studies on Fe3+ doped ZnAl2O4: an evidence for local site swapping of Fe3+ and formation of inverse and normal phase, Dalton Trans. 43 (2014) 9313–9323.

[26] R. V. Kulkarni, B. S. Mangond, S. Mutalik, B. Sa, Interpenetrating polymer network microcapsules of gellan gum and egg albumin entrapped with diltiazem–resin complex for controlled release application, Carbohydr. Polym. 83 (2011) 1001–1007.

[27] G. P. Asnania, J. Bahekar, C. R. Kokare, Development of novel pH–responsive dual crosslinked Hydrogel microparticles based on Portulaca oleracea polysaccharide-alginate-borax for colon specific delivery of 5-fluorouracil, J Drug Deliv Sci Technol. 48 (2018) 200–208.

[28] N. Zohreh, N. Karimi, S. H. Hosseini, C. Istrate, C. Busuioc, Fabrication of a magnetic nanocarrier for doxorubicin delivery based on hyperbranched polyglycerol and carboxymethyl cellulose: An investigation on the effect of borax cross-linker on pH-sensitivity, Int. J. Biol. Macromol. 203 (2022) 80–92.

[29] C. Liu, F. Lei, P. Li, K. Wang, J. Jiang, A review on preparations, properties, and applications of cis-ortho-hydroxyl polysaccharides hydrogels crosslinked with borax, Int. J. Biol. Macromol. 182 (2021) 1179–1191.

[30] F. A. Sana, S. Khoshbakht, A. F. Azarbayjani, New approach to treat methicillin resistant Staphylococcus aureus with the application of boric acid, J Drug Deliv Sci Technol. 67 (20220 103006.

[31] P. Matricardi, I. Onorati, T. Coviello, F. Alhaique, Drug delivery matrices based on scleroglucan/alginate/borax gels. Int. J. Pharm. 316 (2006) 21–28.

[32] S. Adepu, S. Ramakrishna, Controlled Drug Delivery Systems: Current status and future directions. Molecules.26 (2021)5905.

[33] M. L. Bruschi, Mathematical models of drug release. In: Strategies to Modify the Drug Release From Pharmaceutical Systems. Elsevier (2015) 63–86.

[34] D. L. A. Sitta, M. R. Guilherme, E. P. Silva, A. J. M. Valente, E. C. Muniz, A. F. Rubira, Drug release mechanisms of chemically cross-linked albumin microparticles: Effect of the matrix erosion. Colloids Surf. B Biointerfaces.122 (2014) 404-413.

# Chapter 9

# SUMMARY AND CONCLUSION

**SUMMARY:**

First of all synthesis of carboxymethyl tara gum (CMTG) was done by dispersing tara gum (TG) in freezing deionized water with NaOH, and heat at 60°C. Then monochloroacetic acid was added to the TG-NaOH dispersion. The mixture was stirred for 30 minutes, followed by methanol-induced precipitation. The product was washed with 90% methanol, air-dried, and stored after passing through #72 mesh. The degree of substitution (DS) of CMTG was investigated in previous research work. After synthesis of CMTG, core hydrogel microparticles were prepared by dissolving 25% w/w PCL in water, adding 3% CMTG, and dropping into $FeCl_3$ solution from 22G needle. The microparticles were air-dried and stored for further evaluation and optimization. For single cross-linking coating, core microparticles were sprayed with CMTG solutions, dipped in $FeCl_3$, and air-dried, on the other hand for double cross-linked coatings involved addition of borax to the $FeCl_3$ solution. The size, volume, viscosity, swelling, and in-vitro PCL dissolution of the microparticles were measured. Release kinetics and mean dissolution time (MDT) were calculated using power law equations. After carboxymethylation, the carboxymethyl groups of TG can cross-link with metal ions to form water-insoluble hydrogels via ionotropic gelation. The interaction between CMTG and monovalent, divalent and trivalent ions was investigated in this project work. When CMTG solutions were added to sodium chloride solutions of varying concentrations, weak and unstable gels formed. Dropping CMTG solutions into barium chloride and calcium chloride solutions resulted in somewhat stable, tail-like hydrogels, but they dissolved within 5-10 minutes. At higher concentrations (3% w/v) of these solutions, spherical and stable hydrogel microparticles formed, which maintained their shape until separated from the solution. However, air drying these particles caused them to flatten. On the other hand, when CMTG solution was dropped into aluminum chloride solutions, resulted in spherical microparticles that retained their shape even after air drying. Consequently, $AlCl_3$ was chosen as the cross-linking agent for further development of the hydrogel microparticles. Increasing the concentration of CMTG solution from 1% w/v to 3% w/v resulted in stronger and harder microparticles. Beyond 3% w/v, the CMTG solution was too viscous to be extruded from a #22-gauge needle.

$Al^{3+}$ cross-linked CMTG hydrogel microparticles were prepared using different concentrations of $AlCl_3$ (1%, 2%, and 3% w/v). The drug entrapment efficiency (DEE) and microparticle size decreased with increasing AlCl3 concentration. In vitro PCL dissolution studies in acid solution (pH 1.2) for 2 hours followed by pH 7.4 until complete dissolution showed that increasing $AlCl_3$ concentration significantly reduced PCL dissolution. Higher $AlCl_3$ concentrations

resulted in less PCL being released initially and more gradual release over time. The interaction between $Al^{3+}$ ions and CMTG's carboxyl groups restricts the mobility of the polymer chains, forming a dense and rigid hydrogel layer. Higher $Al^{3+}$ concentrations increased cross-link density, producing more compact microparticles and reducing their size. Despite the expectation that higher cross-linking would increase DEE, it actually decreased from 48.85±4.75 to 39.78±1.67, likely due to water loss during gelation causing convective loss of the drug molecules. The swelling and de-swelling behavior of the hydrogel microparticles also supported the findings on PCL dissolution. Increased cross-linking decreased swelling and de-swelling, as the rigid hydrogel layer restricted water penetration. The surface microstructures observed via SEM revealed that higher $AlCl_3$ concentrations resulted in smoother, denser, and more compact microparticles.

For comparison, another trivalent ion was investigated. $Fe^{3+}$ cross-linked CMTG hydrogel microparticles were also developed. Similar to $Al^{3+}$, increasing $Fe^{3+}$ concentration reduced DEE and microparticle size. PCL dissolution from these microparticles was lower than that from $Al^{3+}$ cross-linked microparticles at all time points, due to the larger ionic radii of $Fe^{3+}$, which created a tighter polymer chain arrangement with fewer voids, reducing water ingress and PCL release. SEM images confirmed the compactness and rigidity of $Fe^{3+}$ cross-linked microparticles, which showed dense and wrinkled surfaces.

To achieve more sustained PCL release profile, hydrophilic hydrogel coatings were applied to $Fe^{3+}$ cross-linked microparticles. Coated microparticles showed significantly reduced burst PCL dissolution and more gradual release. With increased CMTG and $Fe^{3+}$ concentration in coating leading to decreased PCL dissolution. The coated microparticles had increased size due to the additional coating layer. The coating's viscosity, which increased with polymer concentration, further impeded PCL dissolution. The size of coated microparticles increased due to the additional layer, and burst PCL dissolution decreased with higher coating CMTG concentrations. The coated microparticles provided sustained PCL release up to 10 hours.

The optimised $Fe^{3+}$ cross-linked coated hydrogel microparticles (F11) were further cross-linked with borax to form double cross-linked coated hydrogel microparticles, aiming to cross-link the free OH groups of CMTG and enhance the rigidity and density of the hydrogel layer to sustain PCL dissolution. These double cross-linked microparticles were formulated using varying concentrations of borax. As the borax concentration increased, the microparticle size significantly decreased ($p<0.05$). Consequently, burst PCL dissolution reduced significantly,

with F11 showing 6% burst dissolution after 30 minutes, while F15 showed only 2.2%. The gradual dissolution of PCL was observed to decrease with increasing borax concentration. The mean dissolution time (MDT) of double cross-linked microparticles also increased significantly. Higher borax concentrations led to more $B(OH)_4^-$ ions cross-linking with the OH groups of CMTG, increasing the cross-link density, making the hydrogel network more compact and decreasing particle size. The increased cross-link density also elevated the viscosity of the coating layer, providing more resistance to the ingress of the dissolution solution and the egress of dissolved PCL, thereby slowing the rate of PCL dissolution. Viscosity analysis indicated that higher borax concentrations increased the coating layer's viscosity. The rigidity and compactness of the double cross-linked microparticles were further verified by analyzing their volume changes over time. More rigid hydrogel layers absorbed less water and swelled less, reducing the microparticle volume: after 2 hours (F11: 0.463 $mm^3$, F15: 0.335 $mm^3$), after 4 hours (F11: 0.542 $mm^3$, F15: 0.373 $mm^3$), and after 6 hours (F11: 0.633 $mm^3$, F15: 0.498 $mm^3$). Beyond 1% w/v borax concentration, the viscosity increased so much that the microparticles began to stick and agglomerate, forming lumps.

The PCL release mechanism indicated zero-order kinetics, meaning PCL dissolution was independent of its concentration in the microparticles. The release obeyed the power law equation up to 60% release. Uncoated hydrogel microparticles (F1-F6) followed the Fickian diffusion model, where PCL dissolution was primarily due to diffusion. Single cross-link coating (F7-F11) shifted the release mechanism to anomalous transport, indicating both swelling and diffusion-controlled PCL dissolution. Double cross-linking (F12-F15) further shifted the release mechanism to super case II transport, where erosion/mobility of polymeric chains dictated PCL release, aligning with literature reports that drug dissolution from chemically cross-linked polymeric chains is primarily driven by polymer erosion.

## CONCLUSION:

Double cross-link coated hydrogel microparticles were developed for sustained dissolution of hydrophilic drug PCL. The effects of Al3+ / Fe3+ ions on swelling and erosion, viscosity and cumulative % PCL release from the core hydrogel microparticles were investigated. An increase in the concentration of the cross-linking ions leads to the increment of the viscosity of the hydrogel microparticles that eventually results in a decrease in swelling and erosion of the microparticles and cumulative % PCL release. At the same concentration of cross-linking ions, PCL release from Fe3+-CMTG microparticles was significantly slower than Al3+-CMTG microparticles because Fe3+-CMTG microparticles had greater cross-linking density, produce more rigid surface as compared to Al3+-CMTG microparticles. The optimized Fe3+-CMTG hydrogel microparticle sustained PCL release up to 8 h and was selected for single cross-link coating with Fe3+ - CMTG. Single cross-link coated hydrogel microparticles extend the cumulative % release of the PCL up to 10 h. Further the microparticles were subjected to double cross-link coating. Double cross-link coating was done by both ionic cross-linking (Fe3+ ion) and chemical cross-linking (borax). Double cross-linking coated microparticles extend the cumulative % release of the PCL up to 12 h. PCL release from the hydrogel microparticles followed zero-order kinetics. Diffusion was the primary mechanism of PCL release from Fe3+-CMTG hydrogel microparticle. The single cross-link coated hydrogel microparticle followed an anomalous PCL transport mechanism while the double cross-linking of the coated microparticles exhibit super case II mechanism, indicating that erosion/mobility of the polymeric chains dictated the PCL release mechanism. Overall the investigation suggests that the borax and Fe3+ coated Fe3+-CMTG hydrogel microparticles can be used for sustained dissolution of water soluble drug.